UNIVERSITEIT
AMSTERDAM

VU Research Portal

Fluorescent probes and their local environment studied under high-resolution conditions
Bader, A.N.

2005

document version
Publisher's PDF, also known as Version of record

Link to publication in VU Research Portal

Fluorescent probes and their local environment studied under high-resolution conditions

VRIJE UNIVERSITEIT

Fluorescent probes and their local environment studied under
high-resolution conditions

ACADEMISCH PROEFSCHRIFT

ter verkrijging van de graad Doctor aan
de Vrije Universiteit Amsterdam,
op gezag van de rector magnificus
prof.dr. T. Sminia,
in het openbaar te verdedigen
ten overstaan van de promotiecommissie
van de faculteit der Exacte Wetenschappen
op dinsdag 22 november 2005 om 13.45 uur
in het auditorium van de universiteit,
De Boelelaan 1105

door

Arjen Nicolaas Bader

geboren te Amstelveen

promotor: prof.dr. C. Gooijer
copromotor: dr. F. Ariese

Contents
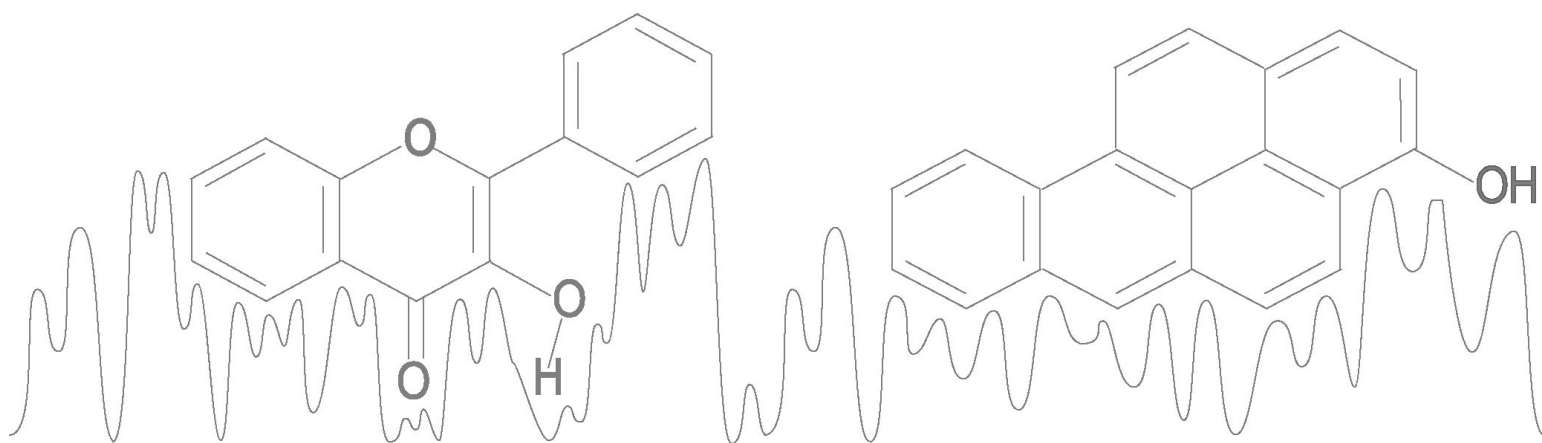
CHAPTER 1

General introduction

This thesis deals with environment sensitive fluorescent probes that are studied under high-resolution conditions. Such probes combine high detection sensitivity with the sensing of various microscopic (or better, nanoscopic) properties in their immediate surrounding. This topic continues to receive wide attention in the literature from a variety of research fields such as biological membranes, vesicles, proteins, nucleic acids, polymers, solid surfaces, surfactant solutions, etc [1-6]. Probes are available that are sensitive to e.g. the polarity, the pH or the viscosity of a solvent. Such local information is seldomly accessible by other techniques.

So far, fluorescence probing studies have almost exclusively been conducted at room temperature, that is, under conditions where the excitation and emission spectra are dominated by inhomogeneous band broadening; the bandwidths are typically not better than 10-20 nm, and the underlying vibrations are hardly resolved. In the present study a novel approach is followed: fluorescent probes are studied under high-resolution conditions in frozen matrices at cryogenic temperatures. Under these circumstances the inhomogeneous contributions are greatly reduced, and line widths are typically ca. 0.1 nm, some hundredfold narrower than under conventional conditions [7-11]. Obviously the influence of the local micro-environment on such spectra requires a special discussion, because the effects can be disentangled far more precisely. Furthermore, unlike at room temperature the environmental effects are not obscured by reorientation phenomena.

This Introduction will start with a basic description of the fluorescence phenomenon. Secondly, the environment sensitivity (that all fluorescent compounds have to some extent) will be discussed. Next, the concepts of the two high-resolution fluorescence techniques that are used in the thesis will be briefly explained. In Section 1.4 the scope of this thesis will be outlined: how can high-resolution fluorescence spectroscopy be used to elucidate the photophysical processes occurring within specific (dual wavelength) fluorescent probes, and how can we obtain more information on the probe's environment. This Chapter ends with an overview of the main conclusions and a discussion of future trends.

1.1 General features of fluorescence

Molecular spectroscopy deals with transitions between molecular states, accompanied by absorption or emission of electromagnetic radiation. In fluorescence, the wavelength region of relevance ranges from the ultraviolet (200 to 400 nm), to the visible (400 to 750 nm) although for exceptional compounds also transitions in the near-infrared play a role. The corresponding transitions involve changes in electronic and vibrational energies; in the condensed phase molecular rotations do not show up in the spectra.

In Fig. 1A the phenomenon of fluorescence is illustrated with a simplified Jablonski energy diagram, in which several singlet electronic states (S_0 to S_n) and some associated vibrational states of the molecule are depicted. It should be noted that triplet electronic states are left out of this discussion.

As a result of the Boltzmann distribution, most molecules will exist in the lowest electronic and vibrational state (ground state, S_0). Let us assume that upon absorption of a photon in the UV or visible range, the molecule is excited to one of the vibrational levels of a higher electronic state. Since this is far from the equilibrium situation, the molecule wants to return to its original state. To this end, the excess vibrational energy is lost via collisions with the surrounding solvent molecules, i.e., transferred as heat to the solvent. Transitions to a lower electronic state take place via internal conversion of electronic energy to vibrational energy, and subsequent vibrational relaxation as described above. This way the molecule relaxes to the lowest vibrational level of the S_1 state. This state is metastable: it has a lifetime on the nanosecond timescale. Most often also further decay to one of the vibrational levels of the ground state occurs via non-radiative pathways, but fortunately, for some compounds this transition can also occur via the emission of a photon. This phenomenon is called fluorescence. The ratio of the rate of fluorescence relative to the summed rates of all radiative and non-radiative decay processes is defined as the fluorescence quantum yield. More information about the basic principles of fluorescence can be found in various textbooks [3,4,12,13].
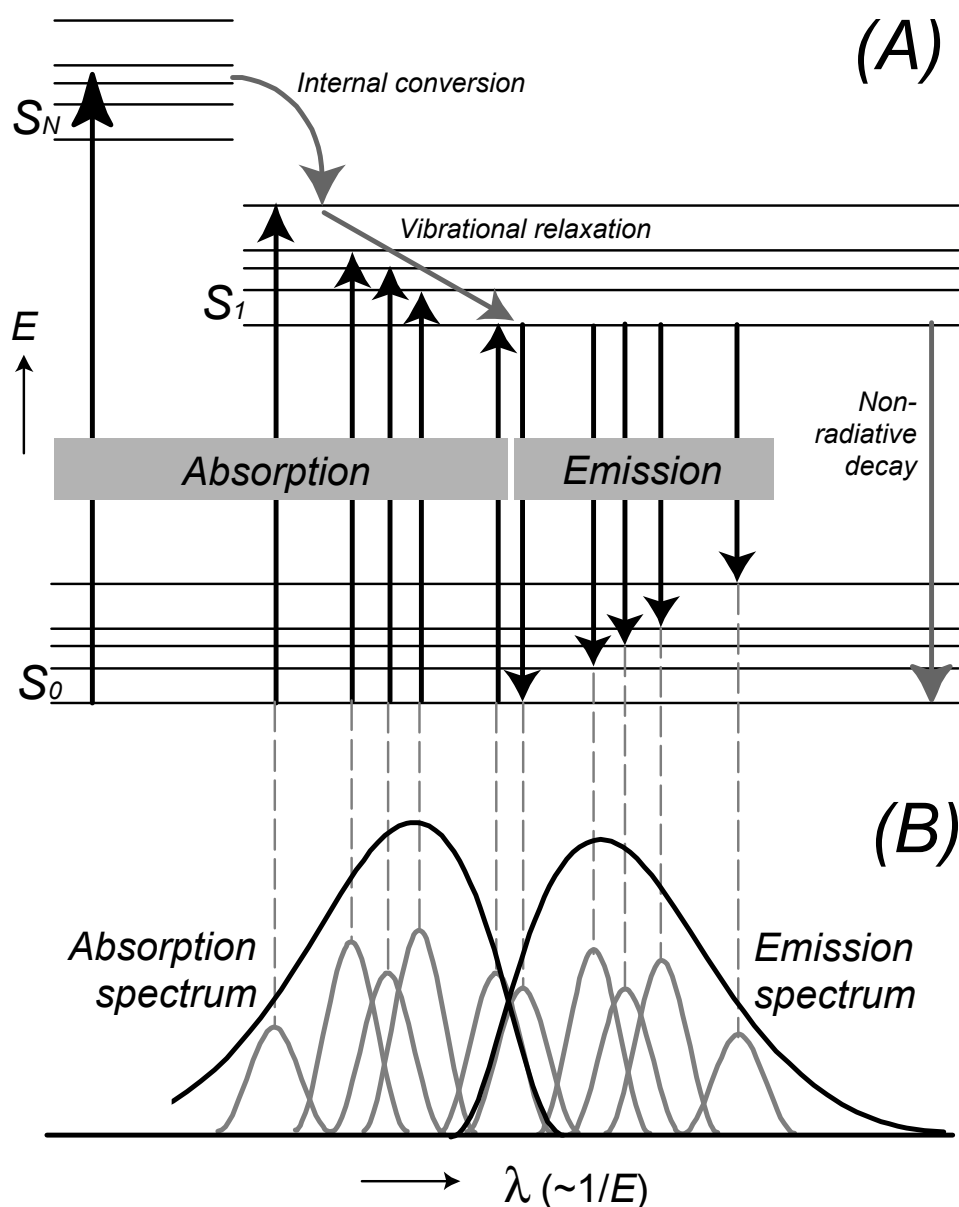
Figure 1: *Jablonski diagram illustrating the concept of fluorescence (A) and the corresponding spectra (B). the black arrows correspond to radiative transitions (left-hand side: absorption, and right-hand side: fluorescence). The gray arrows correspond to non-radiative decay (internal conversion and vibrational relaxation). Only five vibrational levels are shown.*

Similar to absorption, most fluorescence transitions result in a change of both electronic and vibrational energy (referred to as vibronic transitions). The dotted lines between Figures 1A and B illustrate how these vibronic transitions correspond with the typical fluorescence spectra of a compound ("fluorophore") in solution. The emission spectrum is a plot of the intensity of the fluorescence as a function of the emission wavelength after excitation at a fixed wavelength. The excitation spectrum is a plot of the intensity of the fluorescence

emission observed at a fixed wavelength as a function of the excitation wavelength. The excitation spectrum is therefore similar to the UV/Vis absorption spectrum of the fluorophore. In Figure 1B, absorption bands corresponding with $S_0 \rightarrow S_2$ transitions or higher are left out of consideration, although (part of) these transitions usually show up in the absorption and excitation spectra as well.

It should be noted that in Fig. 1B no sharp lines are depicted because in general an ensemble of fluorophores in solution is studied. Each individual molecule has its own energy difference between the electronic states because of its particular interaction with the surrounding solvent molecules. It other words: due to the (continuously changing) solvent environment, the well-defined vibronic transitions of a fluorophore are inhomogeneously broadened in conventional, condensed-phase molecular spectroscopy. Circumventing such broadening effects will be a crucial aspect of this thesis.

The interaction with the solvent does not only cause broadening; it can also induce spectral shifts in the spectrum if the solute-solvent interactions are not identical for the different electronic states. Suppose for instance that the molecule in the S_1-state has a larger electrical dipole moment than in the S_0-state. In a polar solvent the S_1 state will be more stabilized than the ground state. As a result, upon increasing the solvent polarity a red shift in fluorescence emission should be expected (provided that the required reorganization of the surrounding solvent molecules can be achieved within the lifetime of the excited state). Thus, spectral changes provide information on the nature of the solvent environment. This will be discussed in more detail in Chapter 1.2.

So far we have considered fluorescence (excitation and emission) spectra in the wavelength domain. It should be emphasized that for probing purposes the time domain also offers many interesting options. Normally, in condensed matrices fluorescence emission starts from the lowest vibrational level of the S_1 state and the fluorescence lifetime τ observed shows the depopulation of this particular state, via both radiative and non-radiative pathways. Typical fluorescence lifetimes are of the order of a few nanoseconds. In the simplest situation (a single emitting species) the fluorescence intensity I(t) follows a monoexponential decay:

$$I(t) = I_0 \cdot e^{-t/\tau} \qquad\qquad [1]$$

More complicated situations are encountered if there are more (simultaneously) emitting states and/or if one is dealing with an inhomogeneous distribution of fluorophores (for instance in different environments). Since solute-solvent interactions will affect τ, also lifetime measurements can be utilized for probing purposes.

Various fluorescence based methods are used for studying fluorescent compounds in complex (often biological) systems. The major advantages of using fluorescence for this purpose are the following. First, compared to other detection techniques fluorescence is very sensitive. Secondly, fluorescence is selective because not all compounds will fluoresce and those compounds that are fluorescent will have different excitation and emission spectra. This can also improve the sensitivity: interferences from other compounds are low or might be reduced by choosing the appropriate excitation and emission wavelengths. Therefore, the background in fluorescence is often low and fluorescent molecules can be easily detected even in complex systems. Furthermore, it should be realized that fluorescence processes will take place within a short period of time (of the order of nanoseconds), after which the molecule returns to its original state, i.e., the process as such is non-destructive for both the fluorophore and its environment. Fluorescence probing therefore offers the possibility of following dynamic processes; excited state processes can be studied at the lifetime of emission, whereas slower processes can be followed by studying the changes in fluorescent properties over time.

Fluorescence applications are of course not limited to compounds that are natively fluorescent; a compound of interest can also be labeled with a fluorophore. Those labels are called (fluorescent) probes. In biological applications, these probes can be attached to, e.g., proteins or DNA [5,14]. The major application of these probes is in fluorescence microscopy, where an image of the fluorescence emission from these probes is monitored, so that information on the location of the probes within e.g. a cell can be obtained [14]. The application range of fluorescent probes can be expanded to labels that are solvent dependent. This means that some fluorescent probes can also provide information on their local environment. Studying such environment sensitive probes and how the interaction with their environment affects the high-resolution fluorescence spectra will be the subject of this thesis.

1.2 Solvent dependency in fluorescence spectra

As noted above, the environment sensitivity of fluorescence spectra can be due to various solvent parameters and is referred to as solvatochromism [15]. Fluorescent probes have been developed that yield information on local physical and structural parameters (polarity, microviscosity, molecular mobility) as well as local chemical parameters (pH, ion concentration). [1-4,14]. The most common type of probe shows solvent polarity dependence. Unfortunately, this property is difficult to define and even more difficult to quantify [15-17]. The polarity of a solvent can be described using parameters such as dielectric constant, permanent dipole moment and refractive index. When calculating solute/solvent interactions, these parameters are often regarded as macroscopic bulk properties of the environment. In reality, however, solute/solvent interactions take place on a molecular level, where only a limited number of solvent molecules are involved and these can have preferential orientations around the solute. Furthermore, these parameters only consider nonspecific interactions, e.g. Coulomb forces between dipolar molecules or ions, or polarization forces arising from dipoles induced by nearby molecules. Specific interactions, e.g. interactions due to H-bonding or via electron pairs, can also have significant effects. For pragmatic reasons, the polarity of a solvent is therefore suggested to be defined as the total solvation power of a solvent [15].

Quantification of the solvent polarity is difficult. In practice, it is often achieved empirically by studying the solvatochromism of carefully selected environment-sensitive probes [15,17]. Using this approach, a number of solvent polarity scales have been proposed. For example, simple single-parameter approaches like the $E_T(30)$ scale which have been applied successfully [15]. More accurate and broadly applicable is a multi-parameter approach like the one suggested by Kamlet and Taft [18]. Their linear solvation energy relationship includes three UV/vis spectroscopically derived solvent parameters: π^* (a measure of the dipolarity and polarizability of the solvent), α (H-bond donor acidity, "the ability of a solvent to donate a proton") and β (H-bond acceptor basicity, "the ability of a solvent to accept a proton").
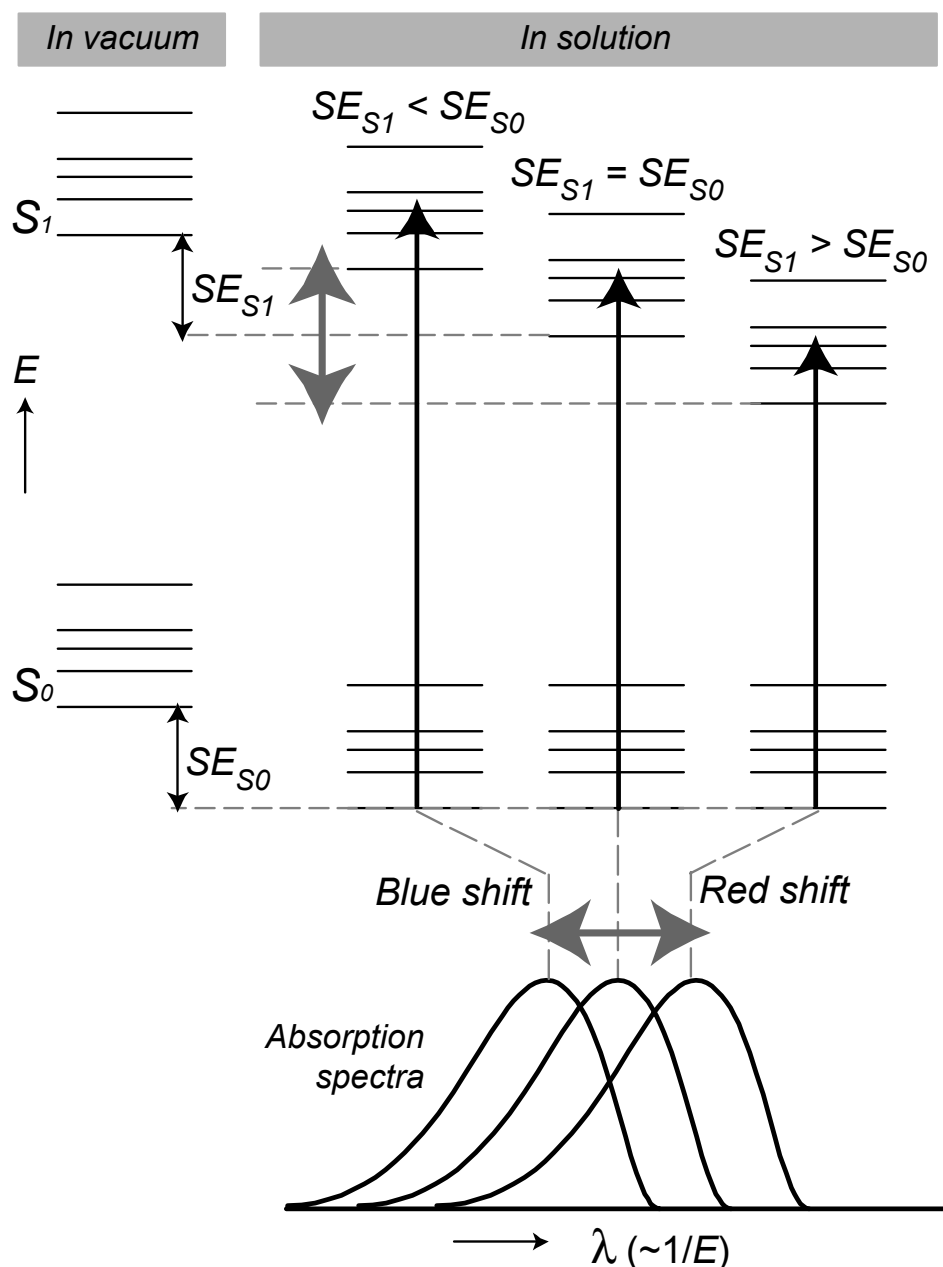
Figure 2: *Jablonski diagram illustrating the origin of blue and red shifts in absorption (top) and the resulting spectrum (bottom). SE is the stabilization energy.*

It should be realized that the solvent dependencies observed in absorption spectroscopy have a different origin than those observed in emission [15,16]. This is related to the fact that excitation occurs to a Franck-Condon state, i.e., a state in which the excited molecule still has the conformation and solvent orientation as in the ground state situation. This is no longer the optimal situation since the electronic state configuration has different chemical and physical properties. In general, the amount of stabilization energy in the Franck-Condon state will be different from that in the ground state situation. This will result in a solvent-dependent shift

in the absorption spectrum, as shown in Figure 2. If there is less stabilization in the Franck-Condon state, the energy difference between the S_0 and S_1 will increase compared to the situation in vacuum and a blue shift will be observed in the absorption spectrum. Conversely, more stabilization in the Franck-Condon state will result in a red shift.

In emission, the solvent shift depends on more factors and requires a more extensive discussion. After excitation, several excited state processes can take place before the metastable fluorescent state is reached. Some of these processes are dependent on the solvent. They can be categorized by the effect they have on the spectrum.

1. Solvent-induced changes in the **<u>intensity</u>** of the fluorescence spectrum. These effects are most often due to quenching [3,4]. When a solvent causes (partial) quenching of the fluorescence, it provides an alternative pathway for the decay from the lowest vibrational level of the first excited state of the fluorophore. As a result, the lifetime of this state will be shortened, the relative probability of radiative decay is reduced (lower fluorescence quantum yield) and thus less fluorescence will be observed. In general, quenching can be more accurately studied in the time domain, because – contrary to changes in fluorescence intensity - lifetime reductions are concentration independent.

2. Solvent-induced changes in the **<u>shape</u>** of the fluorescence spectrum. For probing purposes this offers great advantages: quantification of spectral changes is easily achieved by determining the intensity ratio between two wavelength ranges [6]. An example is the occurrence of an excited state intramolecular proton transfer (ESIPT) reaction in 3-hydroxyflavone (3HF) and its derivatives. Whereas in the electronic ground state one exclusively deals with the neutral molecule, in the excited state intramolecular proton transfer becomes probable. In some solvents, this reaction takes place on a timescale similar to fluorescence. As a result, the excited-state fluorophore can be present in two distinct conformations, a "normal" form and a spectrally shifted tautomeric form. The ratio between these two forms depends on the rate of this solvent dependent ESIPT reaction. Therefore, such compounds can be used as ratiometric probes. Based on this proton transfer reaction a class of environment sensitive probes has been developed. This will be the subject of Chapter 2 and will be introduced in Chapter 1.3.1.
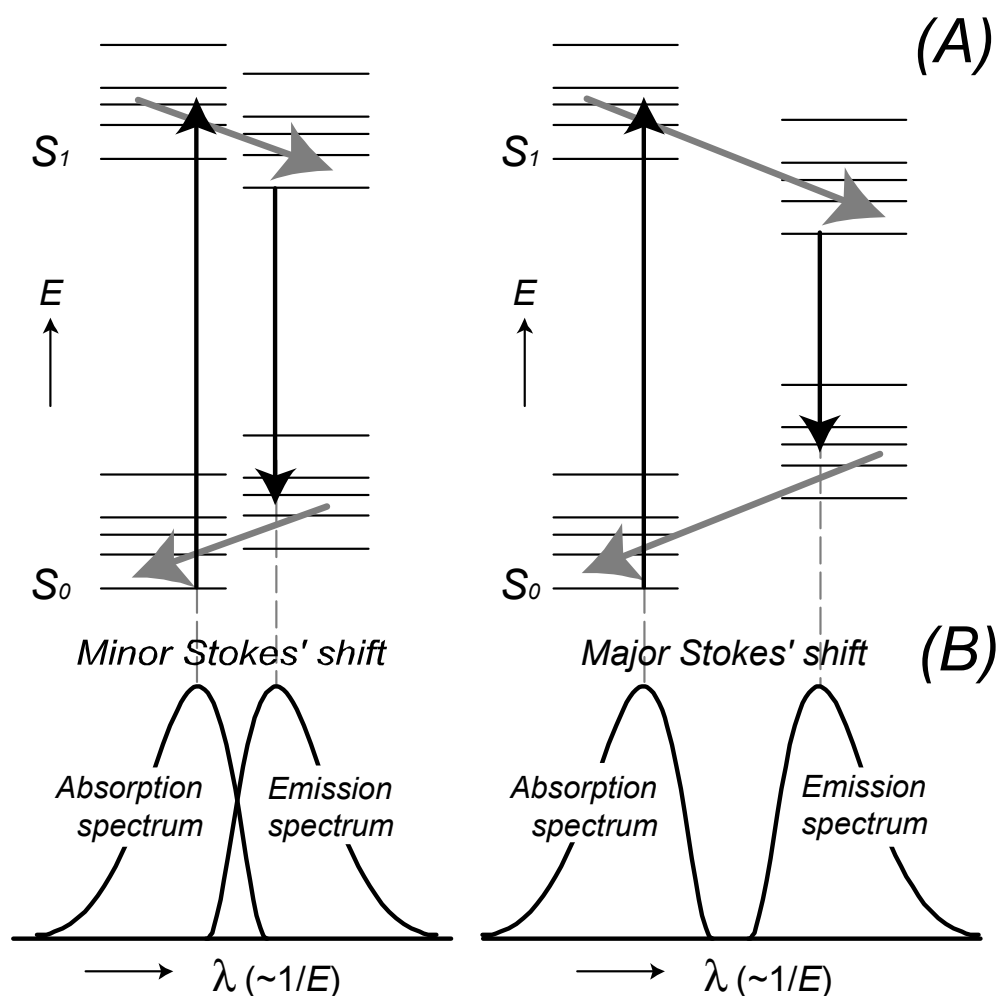
Figure 3: *Jablonski diagram illustrating reorientation effects (A) and the resulting Stokes' shift in the spectra (B).*

3. Solvent-induced **wavelength shifts**. Spectral shifts are by far the most often studied parameters to quantify solvatochromism [1,3,4,15,16]. Shifts in emission spectra are often due to solvent reorientation, as illustrated in Figure 3A. After excitation (black arrow on the left) to a Franck-Condon state, the solvent molecules will reorient to adapt to the new electronic structure of the solute (gray diagonal arrow), thus lowering the energy. Similarly, after emission has occurred to the Franck-Condon ground state the energy will be lowered again by reorientation. As a consequence, the energy of the transition from the lowest vibrational level of the S_0 to the lowest vibrational level of the S_1 (referred to as 0,0 transition) will be lower in emission than in excitation. This difference is usually denoted as the Stokes' shift and corresponds with the reorientation energy in the excited state plus that in the ground state. This

shift will be large when the reorientation energy is large (compare Figure 3A and B), as will be the case for polar molecules in polar solvents.

The degree of the shift is of course also dependent on the fluorophore. In cases where the excited state has a charge-transfer character, solvent shifts can be dramatic: Stokes' shifts up to 10000 cm^{-1} (150-200 nm) have been reported [15]. Most fluorescent compounds, however, only show minor solvent shifts that are only of the order of 10 nm or less. Therefore, they are of limited use as environment sensitive probes under conventional, low-resolution conditions. In Chapter 3, it will be shown that under low temperature conditions, these minor shifts can be accurately monitored.

1.3 High-resolution fluorescence techniques for probing purposes

The low-resolution spectra typically obtained for solutions at room temperature are composed of broadened vibronic transitions. The origin of this broadening can be homogeneous or inhomogeneous. Homogeneous broadening affects all molecules to the same extent; it comes from vibronic coupling to the rapidly fluctuating surrounding matrix and from the limited lifetime of the states involved. A very short lifetime implies an uncertainty in energy and therefore an increased linewidth. Broadening is called inhomogeneous when it affects all molecules in an ensemble differently, for instance when we are dealing with a distribution of solute molecules with different vibronic transition energies. In the condensed phase, these energy variations are often caused by different interactions with the solvent environment. As noticed above, in a liquid or amorphous solid matrix any fluorophore molecule has its own particular interaction energy with its direct environment at the moment of excitation.

In order to obtain high-resolution molecular fluorescence spectra – i.e., to reduce the inhomogeneous broadening as much as possible - several methods have been described in the literature: molecular beam spectroscopy [19], matrix isolation spectroscopy, Shpol'skii spectroscopy, and fluorescence line-narrowing spectroscopy (FLNS) [7,8]. The latter two approaches have been applied in the experimental work described in this thesis. In both cases

solid solutions are studied at cryogenic temperatures (T = 10 K or lower), but it should be emphasized that freezing alone does not imply that high-resolution will be achieved. Unless special matrices (Shpol'skii) or special excitation conditions (FLNS) are used, a fluorophore solution at 10 K would show little or no improvement in resolution in comparison with the room temperature spectrum.
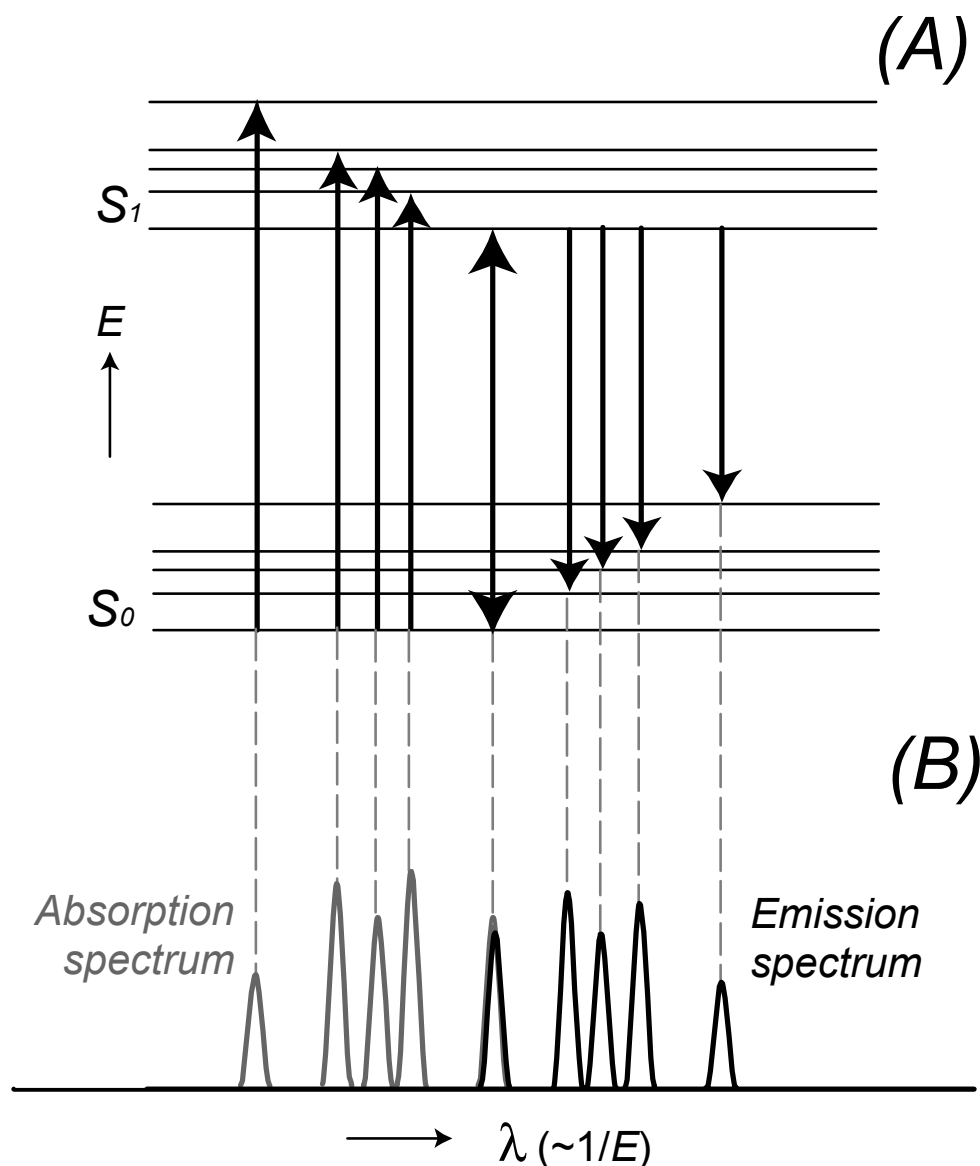

Figure 4: *Jablonski diagram illustrating the concept of Shpol'skii spectroscopy (A) and the resulting spectrum (B). Only five vibrations are shown; in the absence of reorientation, there is no Stokes' shift between the longest-wavelength absorption band and the shortest-wavelength emission band.*

1.3.1 Shpol'skii spectroscopy

For Shpol'skii spectroscopy (see Figure 4) the solvent should form a (poly)crystalline matrix upon cooling. In the ideal situation the analyte molecule displaces a distinct number of solvent molecules in the lattice and fits in a well-defined manner in the available space thus provided. As a result, individual fluorophore molecules will experience exactly the same interaction with the regular matrix, and therefore their S_0-S_1 energy differences will be identical. Almost exclusively *n*-alkane solvents are used as Shpol'skii matrices. In practice, finding the most appropriate matrix for the fluorophore to be studied is not always evident and requires some trial and error. The properties of the fluorophore play an important role here, in particular the three-dimensional shape of the molecule, its rigidity, and the number (and positions) of polar substituents. In general, the difficulty in achieving Shpol'skii spectra increases with the number of polar groups present in the fluorophore since they reduce the solubility in *n*-alkanes and tends to promote the formation of aggregates and clusters during cooling. It should be realized that in Shpol'skii spectroscopy the solidification of the solution should happen as rapidly as possible, so that in practice under cryogenic conditions one deals with a non-equilibrated distribution of "trapped" solute molecules in a matrix.

Often, there is more than one way in which the fluorophore molecules fit in the matrix; in that case the analyte will be present in a (limited) number of distinct sites. A multiplet will appear in the spectrum for every vibronic transition, both in excitation and emission. Within these multiplet clusters, the energy (wavenumber) differences and the intensity ratios are constant; the latter reflect the relative populations of the different sites. By using a narrow-bandwidth light source such as a (tunable) laser, one site can be selectively excited and only this site will appear in the emission spectrum. (A more detailed discussion of Shpol'skii spectroscopy can be found in references [7,9-11])

Spectral linewidths under Shpol'skii conditions

In the ideal situation, all solute molecules experience exactly the same environment so that the only remaining source of broadening of the spectral lines (apart from instrumental contributions) is homogeneous. Significant contributions to the lifetime can be observed if one of the states involved in excitation or emission (usually the final state) has a lifetime shorter than approximately one picosecond. The origin of this so-called lifetime broadening is

the time-energy uncertainty relationship: when the time can be determined accurately, its energy cannot and vice versa. In Shpol'skii spectroscopy this uncertainty is in most cases only observed in excitation when higher electronic states are involved, since subsequent vibrational relaxation and/or internal conversion is fast. As a result, the bands observed in the excitation spectrum tend to be broader at shorter wavelengths.

The lifetime of these homogeneously broadened states can be calculated using:

$$\tau = \frac{1}{2 \cdot \pi \cdot \Delta v \cdot c} \qquad\qquad [2]$$

where τ is the lifetime of the short-living state, Δv the homogeneous broadening (in cm^{-1}) and c the speed of light (in cm/s). This can be particularly useful for studying photochemically active compounds. Consider a molecule that upon excitation undergoes an intramolecular reaction on a femtosecond timescale. This means that the lifetime of the excited state is strongly reduced and consequently homogeneous broadening will be observed in the Shpol'skii absorption/excitation spectrum. Similarly, the ground state reverse reaction can result in homogeneous broadening in the Shpol'skii emission spectrum.

Studying ultrafast proton transfer reactions

Since in Shpol'skii spectroscopy inhomogeneous broadening is minimal and we can readily observe additional broadening effects, it can be used to determine the rates of fast intramolecular reactions. There are, however, some conditions to be fulfilled. First of all, a suitable Shpol'skii matrix must be found for the compound of interest. Secondly, the reaction rate of interest should be faster than 10^{12} s^{-1} in order to observe significant homogeneous broadening. This means that only barrierless reactions or tunneling reactions have to be considered; activated processes would be too slow under cryogenic conditions. Finally, it should be possible to distinguish the broadening due to lifetime effects from inhomogeneous broadening and instrumental contributions to the observed bandwidth.

So far, the application of high-resolution Shpol'skii spectroscopy for studying excited-state intramolecular reactions has not been described in the literature. In Chapter 2, it will be shown that very useful information can be obtained about the excited state intramolecular proton transfer (ESIPT) reaction in 3-hydroxyflavone (3HF), a widely studied compound

[20-39]. Upon excitation, a proton can be transferred from the 3-hydroxy to the 4-carbonyl group, so that tautomer T* is formed (see Figure 5) [20]. Both the normal form N* and the tautomeric form T* of 3HF emit fluorescence; the emission in the blue originates from the N* state, whereas the T* state emits in the green. Of particular interest within the context of fluorescence probing is the fact that the rate of ESIPT in 3HF and in 3HF derivatives is solvent dependent. In nonpolar solvents, only green tautomeric emission is observed, whereas in more polar H-bonding solvents also blue emission originating from the N* form is observed.
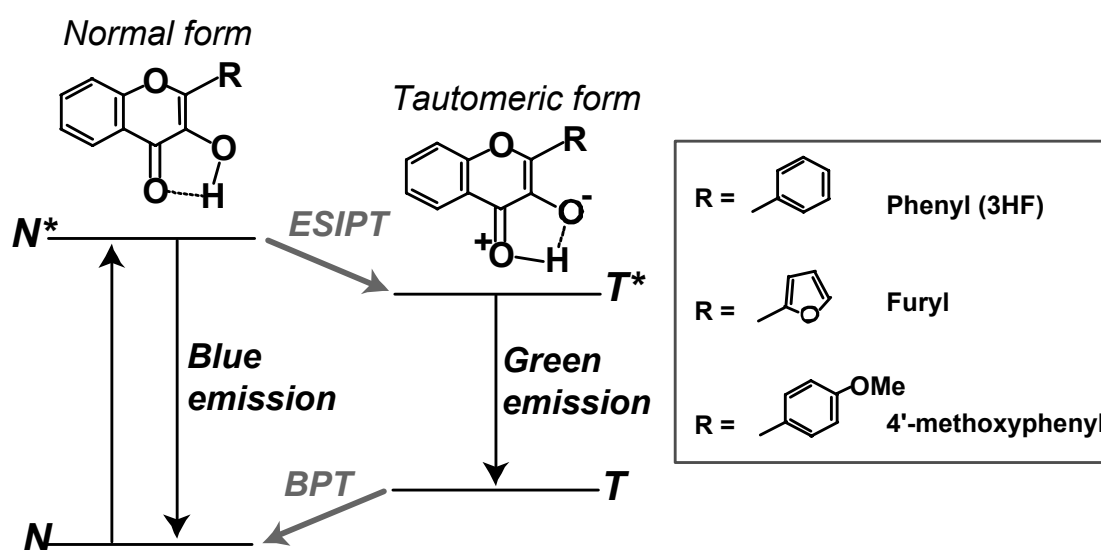
Figure 5: *Schematic explaining the excited state intramolecular proton transfer (ESIPT) and back proton transfer (BPT) for 3-hydroxyflavone (3HF) and derivatives.*

This dual emission has made 3HF one of the most intensively studied molecules undergoing an ESIPT reaction. Most of these studies deal with the dynamics of the ESIPT reaction [21,22]. From Arrhenius plots the barrier of this reaction was determined to be 2.9 kcal/mole [22]. The time constant of the ESIPT reaction is more difficult to determine. In the 1980s, the tautomer fluorescence rise times were reported to be on the picosecond timescale [23-28]. In nonpolar solvents two rise times were observed, the slowest was attributed to torsion of the phenyl ring prior to the ESIPT reaction [25-28]. Improvement in the time-resolution of the available instrumentation resulted in a more accurate estimation of the ESIPT rate in 3HF. In 1992, Schwartz *et al* performed femtosecond transient absorption experiments on 3HF; an ESIPT time constant of 240 fs was found in nonpolar solvents [29]. From transient absorption spectra [30,31] other probe wavelengths were selected, resulting in

an even shorter time constant for ESIPT: for 3HF in methylcyclohexane an instrument-limited value of 35 fs was determined [32].

Alternatively, attempts have been made to determine the time constants from the extent of homogeneous broadening in the spectra. Brucker and Kelley recorded the spectra of 3HF and its deuterated analogue 3-deuteroxyflavone (3DF) in a 10 K Ar matrix [26]. From their poorly resolved emission spectra, they were able to determine the time constants of back proton transfer (BPT; see Figure 5) at 60 and 260 fs for 3HF and 3DF, respectively [26]. However, in such spectra the inhomogeneous broadening is far from being completely removed, so that the contribution from homogeneous broadening may be overestimated (and therefore the actual lifetimes are probably longer). Mühlpfordt *et al* presented the fluorescence excitation spectrum of 3HF and 3DF in a supersonic neon jet [30,33]. The obtained bandwidths were much narrower than predicted on the basis of the time resolved data. This difference was attributed to 2-phenyl and 3-hydroxy torsion that should take place before ESIPT can occur [33].

In Chapter 2, it will be shown that by recording Shpol'skii spectra of 3HF and its derivatives, the rates of ESIPT can be determined in a very elegant way. The major advantage of the Shpol'skii technique is that the inhomogeneous broadening can be reduced to a few wavenumbers [7,9-11]. Furthermore, phenyl torsions are not expected in a Shpol'skii matrix, which allows studying the proton transfer as such. Because deuteron transfer is much slower than proton transfer, the spectra of 3DF can be used to determine the contributions from inhomogeneous (and instrumental) broadening. The additional homogeneous broadening in the spectra of 3HF can then be used to determine the rates of ESIPT and BPT.

Besides the dynamics of the ESIPT reaction, also the solvent dependency of this reaction has been the subject of a large number of studies. In an anhydrous methylcyclohexane (MCH) glass, the fluorescence emission of 3HF is predominantly green (maximum at 523 nm) [34-36]. However, in the presence of minor amounts of H-bonding solvents, two additional emission bands are observed: a blue band with a maximum at 400 nm, and an additional green emission with a maximum at 497 nm [34-38]. These three bands were attributed to tautomeric emission of 3HF (523 nm band), tautomeric emission of 3HF/monohydrate (497 nm band) and normal emission of 3HF/polyhydrate (400 nm band).

In other words, 3HF can form complexes with solvent molecules in which the ESIPT reaction is either affected or completely prohibited. [34-38]. Attempts to elucidate the structure of the 3HF/monosolvate complex have been reported [26,37,38]. Besides H-bonding, electrostatic effects also seem to influence the ESIPT reaction [39]. In solvents such as acetonitrile (polar but without H-bonding properties), the rate of ESIPT can be limited by either the solvent-induced barrier or the rate of solvent reorganization [39].

The matrices used in Shpol'skii spectroscopy are always non-polar. However, in Chapter 2, the effect of adding minor traces of H-bonding impurities will also be discussed. Surprisingly, the complex of 2-octanol and 3HF appears to fit in an n-octane matrix. A high-resolution spectrum is obtained, in which the tautomeric emission is blue shifted over 10 nm. Thus, an isolated 3HF molecule in a 1:1 complex with a hydroxyl group could be studied, and the influence of H-bonding on the rate and mechanism of the ESIPT reaction could be determined.

1.3.2 Fluorescence line-narrowing spectroscopy

In FLNS, the choice of solvent is much less stringent than in Shpol'skii spectroscopy: various solvents or solvent mixtures are used that form an amorphous matrix at cryogenic temperatures. FLNS can also be carried out in crystalline matrices in which the fluorophore molecules will adopt a broad distribution of orientations. This allows one to study biomolecules in aqueous environments [8,40]. In both cases the ensemble of molecules will experience a broad range of different solvent environments (similar to the situation at room temperature), but due to the temperature of 10 K or less this environment will not change during the lifetime of the excited state. In FLNS, excitation is usually carried out with a laser at a wavelength coinciding with the vibronic region of the S_1 state. From the inhomogeneous population of molecules only a sub-selection with matching vibronic transition energies is excited by the laser. This sub-selection or "isochromat" should maintain its matrix interaction energy during vibrational relaxation. Since only the molecules in this sub-selection will emit fluorescence, this will result in narrow emission lines (see Figure 6).
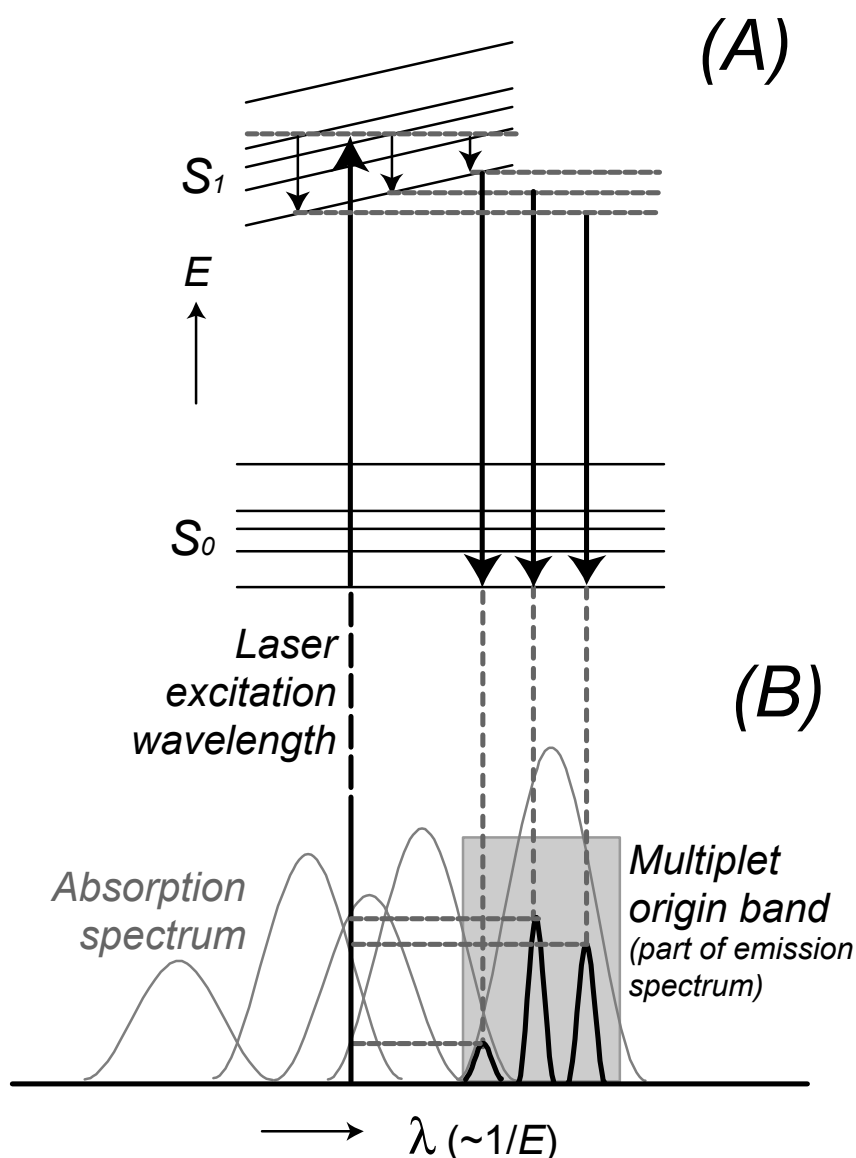
Figure 6: *Jablonski diagram illustrating the range of S_0-S_1 energy differences, the three isochromats selected by the laser in FLN (A), and the resulting spectrum (B). The slanted levels of the S_1 state indicate the inhomogeneous broadening.*

The intensity of the narrow line not only depends on the extinction coefficient of the vibronic transition but also on the position of the laser wavelength in the inhomogeneously broadened absorption band. In a crowded part of the absorption spectrum, the spacing between vibronic bands will be smaller than the inhomogeneous broadening. As a result, more than one vibronic transition will be excited simultaneously. This is illustrated in Figure 6, where three bands overlap with the laser line, each belonging to a different isochromat. As a result, after vibrational relaxation there will be three narrow bands for each transition in the emission spectrum. In the vibronic region in the emission spectrum, this results in a complex

pattern of narrow bands. It is usually more convenient to detect the multiplet origin band, which is composed of the 0,0 transitions. This band often has the highest intensity and is in most cases well separated from vibronic emission. The energy difference between the excitation wavelength and one of the narrow lines in the origin multiplet corresponds to an excited state vibrational energy of the analyte. In other words, this method enables the accurate measurement of both S_0 and S_1 vibrations, and in earlier work this feature of FLNS has proven extremely useful for the fingerprint identification of closely related compounds [8-11].
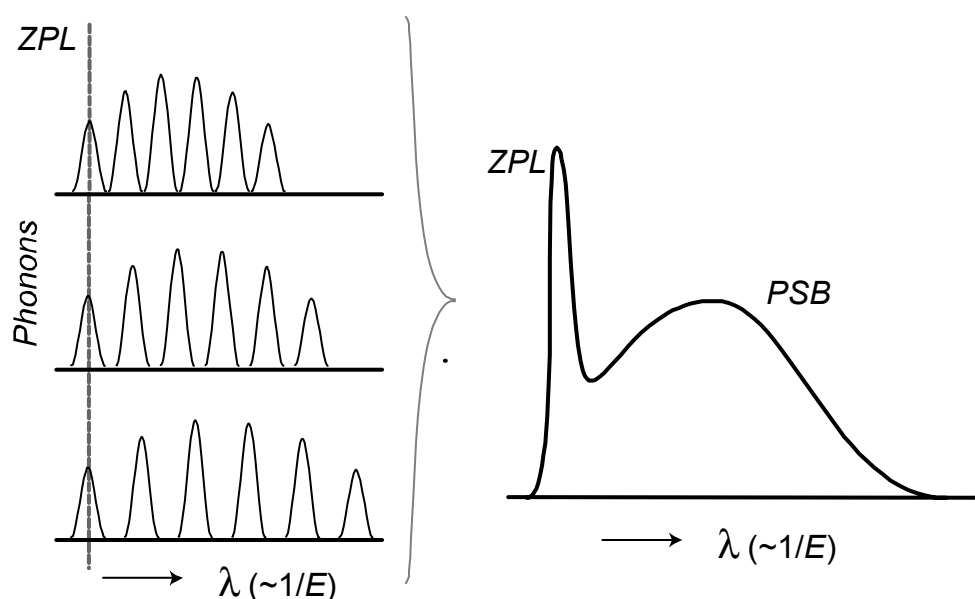
Figure 7: Electron phonon coupling in emission. On the left side three of the many possible phonons are shown, present in a number of overtones. The zero phonon transitions for all phonons coincide, resulting in a sharp zero-phonon line (ZPL). The phonons and their overtones do not overlap exactly and show up as a broad phonon side band (PSB), red-shifted in emission. In practice, excitation into a PSB results in additional broad red shifted emission from an inhomogeneous distribution of ZPLs.

A background-free multiplet origin band as shown in Figure 6 is rarely observed in a real-life FLN spectrum. In many cases a broad, red shifted background is observed. The origin of this background is electron phonon coupling, i.e., coupling of electronic transitions with lattice vibrations of the frozen matrix (referred to as phonons) [8-10]. This solute-solvent interaction results in a broad phonon side band (PSB, see Figure 7), red shifted from the narrow zero phonon line (ZPL, see Figure 7). The temperature and the strength of the solvent-solute interaction determine the intensity of the PSB compared to that of the ZPL. In

order to obtain highly resolved spectra the measurement temperature should be as low as possible, since the ratio of the zero phonon line (ZPL) and the phonon wing intensities is strongly temperature dependent. It should be noticed that for solute-solvent combinations where the coupling is too strong, even at extremely low temperature no FLN spectrum can be obtained.

Figure 8: *Schematic of the solvent dependencies in FLN spectra. Overlap of the laser with four vibronic bands is shown, resulting in four narrow bands in the multiplet origin band (top). More broadening of the vibronic bands in excitation (middle) or a red-shift in S_1-S_0 energy (bottom) results in a change in the relative intensities of the ZPLs in emission.*

Environment sensitivity of FLN spectra

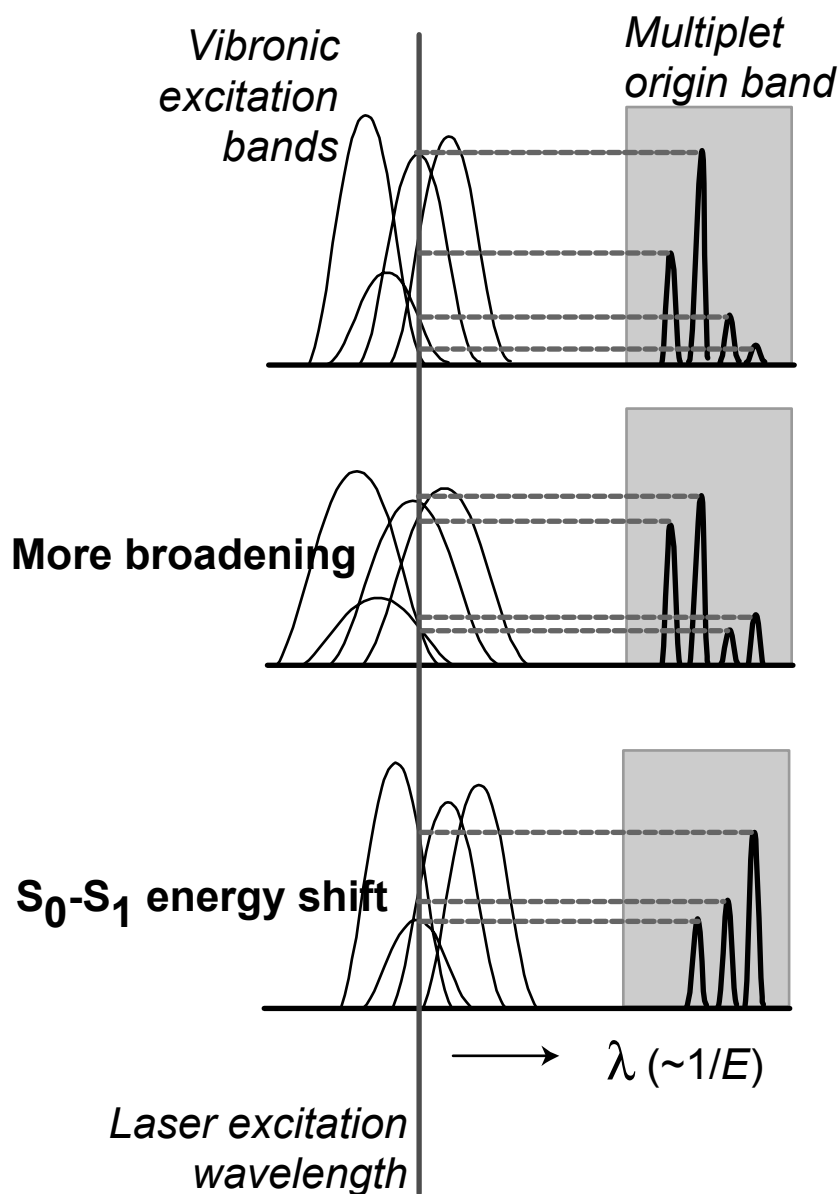Note that unlike conventional fluorescence spectroscopy of liquid solutions under room temperature conditions, there is almost no Stokes' shift for the ZPLs at low temperatures (compare Figures 3 and 6). The reason for this is that solvent reorientation is largely prohibited in a rigid, low-temperature matrix. Only effects due to dipole changes in the solvent molecules (usually minor) can be expected. Thus, the solvent effects in the low temperature emission spectra will be different from the ones observed at room temperature and actually less complex. This brings us to an important conclusion regarding the use of FLNS for probing the local environment: in the absence of reorientation, the blue or red shifts observed in the low temperature emission spectra are expected to be similar to the shifts in (Franck-Condon type) absorption transitions in liquid solutions.

In FLNS, even minor shifts will show up very clearly in the multiplet origin band. This is schematically illustrated in Figure 8 where four vibrations are considered. The top frame corresponds with a "normal" reference solvent. When the solute-solvent interaction (or more precisely the variation in solute-solvent interactions) results in more inhomogeneous broadening, the ZPLs at both edges of the multiplet will increase in intensity (middle frame). A red shift results in an increase of the relative intensities of the ZPLs at the red edge of the multiplet and a decrease at the blue edge (bottom frame). Of course, the opposite will be observed for a blue shift (not shown). Furthermore, the strength of electron-phonon coupling depends on the strength of the interaction between solute and solvent.

Studying ligand-protein interactions

To summarize, the FLN spectrum yields a wealth of information about the solvent/matrix environment the fluorophore experiences. In Chapter 3, a new FLNS approach is presented for studying the local environment of a fluorescent ligand bound inside a protein binding site. A detailed comparison is made of the spectrum of the fluorophore bound to the protein and its spectra in a number of solvents or solvent combinations. These model solvents are selected so as to mimic a specific solvent/solute interaction. The presence or absence of this type of interaction in the protein binding site can now be determined.

A major advantage of using FLNS for probing the local environment is that solvent reorientation is largely prohibited, simplifying the solvent effects observed in the spectra.

Such changes are more easily linked to specific interactions that play a major role in protein/ligand binding. Furthermore, because the multiplet consists of a number of narrow bands, one can easily use intensity ratios as a quantitative measure of solvent effects. Because the overall multiplet's width is in general only 5-8 nm, minor solvent effects can already dramatically change this intensity ratio. As mentioned above, another major advantage of FLNS is its broad range of possible solvents/matrices; one can often study the compound of interest in its "natural" environment. It is assumed that the cooling process from a liquid to an amorphous frozen matrix does not significantly change the structure of the protein [40] and therefore the interaction it has with a ligand. This allows one to use the FLNS spectra to better understand the binding processes occurring at room temperature.

1.4 Scope of this thesis

The objective of the research described in this thesis is to assess the potential of two cryogenic, high-resolution molecular fluorescence techniques to study fluorescent probes and the interactions with their direct environment.

In Chapter 2 high-resolution laser-excited Shpol'skii spectroscopy is used to study the intramolecular proton transfer reactions in 3-hydroxyflavone (3HF) and related compounds. In **Chapter 2.1**, this is demonstrated for 3HF itself, and good estimates of the time constants for the ESIPT and BPT reactions are reported, based on the extent of homogeneous broadening in excitation and emission, respectively. Furthermore, the spectra of the 3HF/monosolvate complexes are shown, using octanol as an additive to the solvent. Significant differences between the spectra of the isolated and monosolvated 3HF are observed and a tentative explanation is presented. Some of the mechanisms suggested earlier for hydroxyl-group interference in the ESIPT reaction can be excluded.

The remaining part of Chapter 2 deals with 3HF derivatives that had been developed earlier as ratiometric environment-sensitive probes, making use of the dual emission phenomenon. The properties of these probes can be tuned by changes in their chemical structure. Incorporating a furyl ring at the 2-position resulted in improved spectroscopic properties, such as an increased quantum yield and a shift of the excitation spectrum to longer

wavelengths [6,41-43]. Systematic investigations of these 3HF derivatives by Demchenko and co-workers have led to a range of 3HF-based solvent environment probes that have been applied to various biological systems [6].

In **Chapter 2.2**, it will be shown that also for various furyl-derivatives of 3HF (see Figure 5), Shpol'skii spectra can be obtained. The amount of homogeneous broadening is negligible, so it can be concluded that the rate of ESIPT is strongly reduced upon substituting the phenyl for a furyl ring. Interestingly, the effect of H-bonding is much stronger in this case; in a monosolvate complex, ESIPT can even be prohibited. Possible mechanisms to rationalize these effects are presented.

In **Chapter 2.3**, the focus is on the role of the electron donating ability of the substituent on the 2-position. In Chapter 2.2, it was shown that the ESIPT reaction was slowed down by substitution of the 2-phenyl by a 2-furyl group. To explain this finding, it is suggested that the ESIPT rate is slowed down when the electron donating ability at the 2-position is increased. To test this hypothesis, the rates of ESIPT and BPT of 3HF and its 2-furyl and 4'-methoxy derivatives (see Figure 5) are compared. The results allowed us to estimate the height and width of the barriers involved in intramolecular proton tunneling. Furthermore, from the shifts in the spectra upon deuteration, the strengths of the OH-bonds could also be calculated.

Chapter 3 deals with the in Chapter 1.3.2 described approach to study the interactions between a fluorophore and its protein binding site by means of fluorescence line-narrowing spectroscopy (FLNS). **Chapter 3.1** focuses on two metabolic products of benzo[*a*]pyrene (BP): the DNA adduct 7-(benzo[*a*]pyren-6-yl)guanine (BP-6-N7Gua) and the metabolite (+)-*trans-anti*-7,8,9,10-benzo[*a*]pyrenetetrol (BP-tetrol). Monoclonal antibodies (MAbs) had been developed for the selective binding of these two compounds and the aim of this study was to determine the binding mode. It is shown that for both antigens information on H-bonding and π-π interaction the binding site can be obtained.

Chapter 3.2 describes more systematic and detailed experiments to test whether the specific binding interactions of ligands in proteins can be derived from the FLN spectra. In this Chapter, the well-known estrogen receptor (ER) is studied. The amino acid side chains that are important for ligand binding in this receptor are known, so solvent combinations that mimic the corresponding interactions could be selected. The ligands used, 3- and 9-

hydroxybenzo[*a*]pyrene (3- and 9-OH-BaP), are known to bind to the ER (although not with high affinity). Possible orientations of these two ligands had been calculated from molecular modelling studies, but so far these could not be experimentally verified. The results of the FLNS experiments show that H-bond donating and accepting interactions can be distinguished and that π–π interaction can be observed. Both FLNS and molecular modelling point to the same orientations of the ligands in the receptor.

1.5 Conclusions and future perspectives

This thesis shows that in favorable cases detailed information on fluorescence probes including the interaction with their local environment can be obtained by the two high-resolution techniques described above, i.e., Shpol'skii spectroscopy and fluorescence line-narrowing spectroscopy (FLNS). Such information is not easily provided by other means, at least not in such detail. In fact also Shpol'skii spectroscopy is more widely applicable than commonly assumed, i.e. it is not limited to polyaromatic hydrocarbons (PAHs) and some of their derivatives. During the experimental work resulting in this thesis, a number of other compounds were successfully measured. For example, for hetero-PAHs like 3-hydroxyflavone (3-HF) and derivatives good Shpol'skii spectra could be recorded (see Chapter 2). Even complexes of these compounds with octanol fitted in an *n*-octane matrix. Furthermore, BODIPY fluorophores yielded both Shpol'skii and FLN spectra (manuscript in preparation, though not included in this thesis). Also large branched [*N*]phenylenes, though formally not aromatic, were found to fit in a Shpol'skii matrix and produced highly resolved spectra [44,45]. In all these cases, *n*-octane seemed suitable to obtain a good Shpol'skii matrix. Also relevant in view of the potential applicability of cryogenic high-resolution techniques is the availability of user-friendly equipment. The closed-cycle helium refrigerator used in Chapters 2 and 3 consumes no helium and can cool four samples to below 5 K in approximately one hour. Within this context also we refer to an interesting new instrumental approach, i.e. the cryogenic fibre optic probe developed by Campiglia and co-workers [46]. Such systems only require a liquid helium storage dewar; no expensive cryostats or closed-cycle refrigerators are involved. Obviously such systems will contribute to the accessibility of low-temperature fluorescence techniques to a broader community of researchers.

Chapter 2 shows that high-resolution laser-excited Shpol'skii spectroscopy can yield very useful background information on dual-wavelength (or ratiometric) probes that undergo excited state intramolecular reactions, the attention being focused on the extremely fast ESIPT and BPT reactions in 3-HF and its derivatives. Homogeneous broadening effects due to proton transfer at a femtosecond timescale could be observed in a very elegant way. The results help us understand how the environment sensitivity is related to chemical modifications in the 3HF derivatives. For Shpol'skii-type measurements it is crucial that a suitable matrix can be found. Addition of an impurity helps to gain further insight as regards the influences of the interaction with the immediate probe environment, as the experiments with adding octanol show.

Earlier work has demonstrated the power of (laser excited) Shpol'skii spectroscopy for fingerprint identification [7,9,11]. It should, however, be noted that Shpol'skii spectroscopy is intrinsically not a very suitable techniques for studying environment sensitivity; only a limited number of nonpolar solvent environment can be studied. Nonetheless, the results in Chapter 2 show that it can be successfully involved to obtain fundamental background information. The potential of the Shpol'skii methodologies lies in studying the photophysics and photochemistry of proton transfer reactions. For such studies the use of Shpol'skii spectroscopy is very promising.

Contrary to Shpol'skii spectroscopy, Fluorescence Line Narrowing Spectroscopy is appropriate to study environmental effects to probes in a variety of solvents, including polar ones. Chapter 3 shows that FLNS can be used to obtain detailed information about the binding interaction of fluorophores and proteins. A distinction can be made between H-bond donating and accepting interactions, as well as π–π stacking or T-shaped conformations. The main requirement is that the ligands that bind the receptor of interest should show native fluorescence and yield high-resolution spectra at low temperatures.

Of course these requirements restrict the number of ligands that can be studied. However, when the starting point is the receptor, one could select a few fluorophores that are known to yield FLN spectra and screen them for affinity. Mono-substituted PAHs are a convenient choice in this case. When a compound binds, a detailed FLNS study may be started. This more systematic approach can become valuable, especially in cases where the crystal structure of the receptor can not be determined.

References

1. Valeur, B., in *Molecular Luminescence Spectroscopy*, Part 3, Schulman, S.G. (ed), John Wiley and Sons, 1993, Chapter 2
2. Lakowicz, J.R. (ed), *Topics in Fluorescence, Volume 4: Probe Design and Chemical Sensing*, Plenum Press, 1994
3. Valeur, B., *Molecular Fluorescence: Principles and Applications*, Wiley VCH, 2001
4. Lakowicz, J.R., *Principles of Fluorescence, 2nd edition*, Kluwer Academic / Plenum Publishers, 1999
5. Kasten,, F.H., in *Fluorescent and Luminescent Probes for Biological Activity*, Mason, W.T. (ed), Academic Press, 1993, 12-33 (1st editon) or 1999, 17-38 (2nd edition)
6. Demchenko, A.P., in *Fluorescence Spectroscopy, Imaging and Probes: New tools in Chemical, Physical and Life Sciences*, Kraaijenhof, R., Visser, A.J.W.G., Gerritsen, H.C. (eds), Springer-Verlag, Heidelberg, 2002, 101-110
7. (a) Renge, I., Wild, U.P. in *Shpol'skii Spectroscopy and Other Site-Selection Methods*, Gooijer, C., Ariese, F., Hofstraat, J.W. (eds), Wiley Interscience, 2000, Chapter 2
   (b) Lamotte, M., in *Shpol'skii Spectroscopy and Other Site-Selection Methods*, Gooijer, C., Ariese, F., Hofstraat, J.W. (eds), Wiley Interscience, 2000, Chapter 3
8. Jankowiak, R., in *Shpol'skii Spectroscopy and Other Site-Selection Methods*, Gooijer, C., Ariese, F., Hofstraat, J.W. (eds), Wiley Interscience, 2000, Chapter 8
9. Hofstraat, J.W., Gooijer, C., Velthorst, N.H., in *Molecular Luminescence Spectroscopy*, Part 3, Schulman, S.G. (ed), John Wiley and Sons, 1993, Chapter 9
10. Hofstraat, J.W., *High-Resolution Molecular Fluorescence Spectroscopy in Low Temperature Matrices*, PhD Thesis, Vrije Universiteit, Amsterdam, 1988
11. Ariese, F., Shpol'skii Spectroscopy and Synchronous Fluorescence Spectroscopy, PhD Thesis, Vrije Universiteit, Amsterdam, 1993
12. Skoog, D.A., Leary, J.L., *Principles of Instrumental Analysis, 4th edition*, Saunders College Publishing, 1992
13. Ingle, J.D., Crouch, S.R., *Spectrochemical Analysis*, Prentice Hall, 1988
14. Haugland, R.P., *Handbook of Fluorescent Probes and Research Chemicals. 9th Edition*, Molecular Probes, 2002
15. Reichardt, C., *Chem. Rev.*, **1994**, *94*, 2319-2358
16. Suppan, P., *J. Photochem. Photobiol. A: Chem.*, **1990**, *50*, 293-330
17. Katritsky, A.R., Fara, D.C., Yang, H., Tamm, K., *Chem. Rev.*, **2004**, *104*, 175-198
18. Kamlet, M.J., Abboud, J.-L.M., Abraham, M.H., Taft, R.W., *J. Org. Chem.*, **1983**, *48*, 2877-2887
19. Scoles, G. (ed), *Atomic and Molecular Beam Methods*, Volume 2, Oxford University Press, 1992
20. Sengupta, P.K.; Kasha, M. *Chem. Phys. Lett.* **1979**, *68*, 382
21. Woolfe, G.J.; Thistlethwaite, P.J.; *J. Am. Chem. Soc.* **1981**, *103*, 6916-6923
22. Itoh, M.; Tokumura, K.; Tanimoto, Y.; Okada. Y.; Takeuchi, H,; Obi, K.; Tanaka, I. *J. Am. Chem. Soc.* **1982**, *104*, 4146-4150
23. Strandjord, A.J.G.; Courtney, S.H.; Friedrich, D.M.; Barbara, P.F. *J. Phys. Chem.* **1983**, *87*, 1125-1133
24. McMorrow, D.; Dzugan, T.P.; Aartsma, T.J. *Chem. Phys. Lett.* **1984**, *103*, 492-496
25. Itoh, M., Fujiwara, Y., Sumitani, M., Yoshihara, K., *J. Phys. Chem.*, **1986**, 90 5672-5678
26. Brucker, G.A.; Kelley, D.F. *J. Phys. Chem.* **1987,** *91*, 2856-2861
27. Dick, B.; Ernsting, N.P. *J. Phys. Chem.* **1987**, *91*, 4261-4265
28. Brucker, G.A.; Kelley, D.F. *J. Phys. Chem.* **1988,** *92*, 3805-3809
29. Schwarz, B.J.; Peteanu, L.A.; Harris, C.B. *J. Phys. Chem. A* **1992**, *96*, 3591-3598
30. Muhlpford, A.; Bultmann, T.; Ernsting, N.P.; Dick, B. in *Femtosecond Reaction Dynamics;* Wiersma, D.A. (ed), Royal Netherlands Academy of Arts and Sciences, Amsterdam, **1993**, 83

31. Ormson, S.M., LeGourrierec, D., Brown, R.G., Foggi, P., *J. Chem. Soc., Chem. Commun.*, **1995**, 2133

32. Ameer-Beg, S.; Ormson, S.M.; Brown, R.G.; Matousek, P.; Towrie, M.; Nibbering, E.T.J.; Foggi, P.; Neuwahl, F.V.R. *J. Phys. Chem. A* **2001**, *105*, 3709- 3718

33. Muhlpford, A.; Bultmann, T.; Ernsting, N.P.; Dick, B., Chem. Phys., **1994**, *181*, 447-460

34. McMorrow, D.; Kasha, M. *J. Am. Chem. Soc.* **1983**, *105*, 5133-5134

35. McMorrow, D.; Kasha, M. *Proc. Natl. Acad. Sci. USA* **1984**, *81*, 3375-3378

36. McMorrow, D.; Kasha, M. *J. Phys. Chem.* **1984**, *88*, 2235-2243

37. Strandjord, A.J.G.; Barbara, P.F. *J. Phys. Chem.* **1985**, *89*, 2355-2361

38. Barbara, P.F.; Walsh, P.K.; Brus, L.E. *J. Phys. Chem.* **1989**, *93*, 29-34

39. Brucker, G.A.; Swinney, T.C.; Kelley, D.F. *J. Phys. Chem.* **1991,** *95*, 3190-3195

40. Vanderkooi, J.M., in *Shpol'skii Spectroscopy and Other Site-Selection Methods*, Gooijer, C., Ariese, F., Hofstraat, J.W. (eds), Wiley Interscience, 2000, Chapter 12

41. Klymchenko, A.S., Ozturk, T., Pivovarenko, V.G. and Demchenko, A.P., *Can. J. Chem.*, **2001**, 79, 358.

42. Ercelen, S., Klymchenko, A.S. and Demchenko, A.P., *Anal. Chim. Acta*, **2002**, 464, 273.

43. Klymchenko, A.S., Ozturk, T., Pivovarenko, V.G. and Demchenko, A.P., *Tetrahedron Lett.*, **2001**, 42, 7967.

44. Dosche, C., Kumke, M.U., Ariese, F., Bader, A.N., Gooijer, C., Dosa, P.I., Han, S., Miljanic, O.S., Vollhardt, K.P.C., Puchta, R., Hommes, N.J.R.V., *Phys. Chem. Chem. Phys.,* **2003**, 5 (20), 4563-4569

45. Dosche, C., Kumke, M.U., Lohmannsroben, H.G., Ariese, F., Bader, A.N., Gooijer, C., Miljanic, O.S., Iwamoto, M., Vollhardt, K.P.C., Puchta, R., Hommes, N.J.R.V., *Phys. Chem. Chem. Phys.,* **2004**,6 (24), 5476-5483,

46. Bystol, A.J., Campiglia, A.D., Gillispie, G.D., *Analytical Chemistry*, **2001**, 73, 5762-5770.

CHAPTER 2

Proton Transfer in 3-Hydroxyflavone and its derivatives
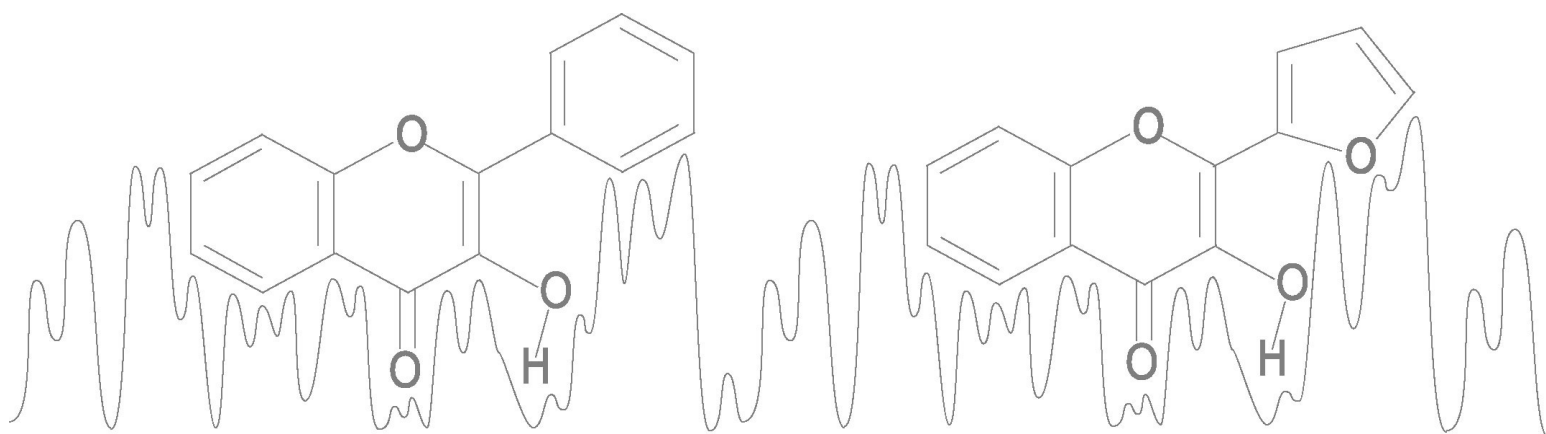
CHAPTER 2.1

Proton transfer in 3-hydroxyflavone studied by high-resolution 10 K laser-excited Shpol'skii spectroscopy

Arjen N. Bader, Freek Ariese, and Cees Gooijer
J. Phys. Chem. A, **2002,** *106 (12),* 2844-2849

Abstract

High-resolution 10 K Shpol'skii spectra of 3-hydroxyflavone (3HF) and its deuterated analogue (3DF) in *n*-octane and *n*-octane/octanol mixtures are presented for the first time. In pure *n*-octane for both 3HF and 3DF, well-resolved excitation and emission spectra were observed, showing fluorescence shifted from 380-460 to 513-550 nm because of excited-state intramolecular proton/deuteron transfer (ESIPT/ESIDT). Compared to those of 3DF, the 3HF excitation and emission bands are much wider because of lifetime-limited homogeneous broadening. Proton transfer is at least a factor of 4 faster than deuteron transfer. From the homogeneous contribution to the total bandwidth of 3HF, the rate constants of ESIPT and ground-state back proton transfer were estimated to be 39 **+/**-10 and 210 +/- 30 fs, respectively. The effect of four octanol additives was investigated. Only for 2-octanol and - though less favorable - 3-octanol, a new site in the emission spectrum was observed, blue-shifted over 7 and 10 nm, respectively, versus the 3HF spectrum in *n*-octane. The new site is attributed to a 1:1 3HF/octanol complex. Its ground-state vibrational pattern differs from that of free 3HF. For 3DF, no Shpol'skii spectrum of a complex could be obtained. It is suggested that in the complex the proton/deuteron transfer mechanisms differ from those of the free molecules; furthermore, a molecular structure for the tautomeric form of the complex is proposed.

Introduction

Compounds that undergo excited-state intramolecular proton transfer (ESIPT) have been intensively studied throughout the last two decades, one of the most striking examples being 3-hydroxyflavone (3HF) [1-17]. This compound is known to have fluorescence bands both in the blue (380-460 nm) and in the green (510-570 nm). As early as 1979, Sengupta and Kasha showed that this dual emission is due to ESIPT and that the two bands can be assigned to the normal and the tautomeric form of excited state 3HF, respectively [1] (see Scheme 1). Since then, a large number of investigations have been carried out to elucidate the mechanism and kinetics of this system [1-17]. Especially the effects of hydrogen-bonding solvents or impurities in nonpolar solvents on the kinetics received wide attention [7,9,11,15,16,17].
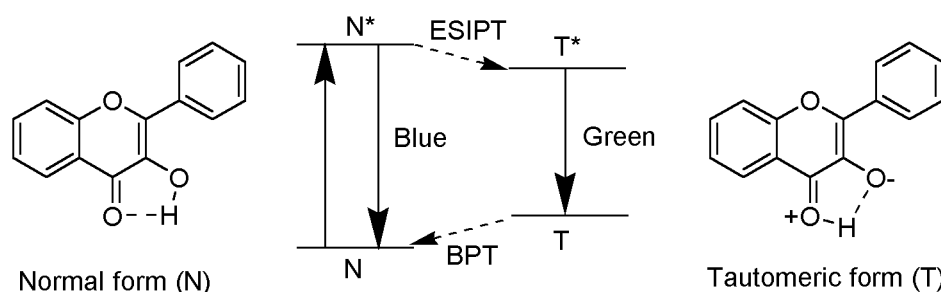
Scheme 1: ESIPT and BPT in 3HF

In highly purified and dried hydrocarbon solvents the ESIPT mechanism is well established; the hydroxy-proton is transferred intramoleculerly to the oxygen of the ketone group on a sub-picosecond timescale [10,11,15,16,17]. Exact lifetimes of N* and T, however, are not easily measured. Recently, ultrafast pump/probe experiments were reported by Ameer-Beg *et al.* [16]; they propose a value of 35 fs for the risetime of T* in methylcyclohexane (MCH) or acetonitrile at room temperature, though their measurements were instrument-limited. For a more accurate determination of the ESIPT rate in 3HF, faster instruments are needed or a different approach should be followed, i.e. the measurement of homogeneous broadening of spectral transitions in excitation and emission.

The latter approach is followed in the present paper, utilising Shpol'skii matrices at 10 K. It is shown that for 3HF – and for its deuterated analogue (3DF) - in n-octane at 10 K highly-resolved fluorescence spectra can be obtained. In the polycrystalline matrix the remaining inhomogeneous broadening is low enough to make homogeneous broadening effects clearly

visible. The homogeneous broadening of the excitation spectrum yields the lifetime of N*, i.e. it reflects the rate of the ESIPT process. Because the lifetime of T* is relatively long (~ns), in emission the homogeneous broadening is a measure for the lifetime of T, i.e., the rate of Back Proton Transfer (BPT).

Earlier attempts to record high-resolution spectra have been reported in the literature [8,10,11,12]. McMorrow and Kasha were the first to report the Shpol'skii spectrum of 3HF in octane at 77K, but unfortunately their spectra were still far from highly resolved [8]. Matrix isolation experiments in argon under cryogenic conditions were mainly carried out to study the isolated 3HF and 3HF/monosolvate complexes [10,11]. Brucker and Kelley used their poorly resolved 30K emission spectra in an argon matrix to estimate the back transfer rates for 3HF and 3DF; they found a substantial difference in lifetimes, i.e. 60 fs and 260 fs, respectively [11].

Apparently, in matrix isolation spectroscopy a significant amount of inhomogeneous broadening remains present, even under cryogenic conditions [18]. In Shpol'skii spectroscopy on the other hand, an impressive increase in resolution can be achieved at temperatures below 30K [19,20], provided that the solidification of the sample is sufficiently fast. For that reason we present here laser-excited Shpol'skii spectra of 3HF and 3DF at 10K; the excitation and emission spectra allow a fairly accurate determination the time constants of the ESIPT and BPT processes.

Interestingly, our approach also enabled us to study proton transfer in the presence of a hydrogen-bonding solvent; in other words, a hydrogen-bonding solvent can be incorporated in the n-octane matrix without destroying the crystalline structure too much. The influence of such solvents received extensive attention in the literature. Already in the first reports about ESIPT in 3HF it was shown that for methylbutane as a solvent there was exclusively green emission, whereas in methanol both the blue and the green emission were observed [1]. In a 77K methylcyclohexane (MCH) glass containing substoichiometric amounts of water, an additional emission around 490 nm was detected, which was attributed to the 3HF/monosolvate complex [4,8]. In matrix-isolated spectra in argon the same effect was observed [11]. Other reports showed that in the presence of a hydrogen-bonding compound the transfer rate decay curve becomes biexponential [6,9,11,15,16,17]. In the recent work of Ameer-Beg *et al.*, dealing with pump/probe experiments, it was shown that the fast component of the

excited state proton transfer rate in ethanol is 60 fs, whereas the slow component is 10 ps [16]. The slow component was attributed to an interaction with a hydrogen-bonding compound. Nonetheless, the detailed mechanism of proton transfer in the presence of a hydrogen-bonding compound remains unknown [16]. In our work, a hydroxy-group was incorporated into the n-alkane matrix by adding various isomers of octanol; the highly resolved spectra obtained for 2-octanol and 3-octanol provide detailed information on the solute-solvent interaction, including vibrations characteristic for the complex.

Experimental

All measurements were done using a 10^{-5} M solution of 3-hydroxyflavone (Extrasynthèse, Genay, France) in *puriss* octane (Fluka). 1-, 2-, 3- and 4-octanol were obtained from Fluka, Sigma, Fluka and Aldrich, respectively. Deuteration of 3HF was achieved by dissolving 3HF in deuterated methanol (Aldrich), followed by evaporation of the solvent. To the 3DF/2-octanol samples D_2O was added to deuterate the octanol; the octane layer was measured. No additional purification steps were applied to any of the samples.

The samples were transferred to a homemade sample holder that contains four sample cells. The sample holder was cooled to 10 K by a Cryodyne Model 21 closed-cycle helium refrigerator (CTI Cryogenics, Waltham, MA, USA). The sample was illuminated at an angle of 30° with a XeCl excimer laser (Lambda Physik LPX 110i, Göttingen, Germany) pumping a dye laser (Lambda Physik, LPD 3002). The excimer laser was operated at 10 Hz, producing 10 ns 50 mJ pulses. Using DMQ as a dye, a tuneable output in the 360-377 nm range was obtained. The fluorescence emission was collected by a 3 cm F/l.2 quartz lens and focused on the entrance slit of a Spex 1877 0.6 m triple monochromator (Edison, NJ, USA) by a 10 cm F/4 quartz lens. The spectral resolution of this monochromator was 0.1 nm. For detection a Princeton Instrument (Trenton, NJ, USA) intensified CCD camera type 576T was used in the gated mode. The gate was opened at the end of the (scattered) laser light pulse.

Results and Discussion

3HF and 3DF in n-octane

High-resolution fluorescence spectra of the tautomeric form of 3HF were obtained using the Shpol'skii approach with n-octane as a solvent. In Figure 1, an excitation-emission plot of

3HF in an n-octane matrix at 10K is shown. In this figure, it can be seen that 3HF is present in two different sites in the matrix, with 0,0 absorption transitions at approximately 365.5 and 367.5nm. The corresponding 0,0 transitions of the tautomeric form are found at 513.1 and 515.0 nm, respectively. Figure 2 shows the same plot for a 3DF sample that also contained some remaining non-deuterated 3HF. The corresponding spectra can be readily distinguished. Obviously, for 3DF there are also two sites in absorption, but compared to 3HF these are blue shifted to 365.1 and 366.7 nm. The 0,0 transitions of the tautomeric form are shifted in the opposite direction, i.e., to 514.1 nm and 515.8 nm, respectively.

Figure 1: *Emission spectra of 3-hydroxyflavone (3HF) in n-octane measured at 10K. The excitation wavelength was varied from 363 to 369 nm with 0.5 nm steps. 3HF is present in two sites, one emitting at λ_{em} = 513.1 nm and one at λ_{em} = 515.0 nm. The emission bandwidth was estimated to be 0.7 nm; the excitation bandwidth was estimated to be 2 nm.*

The selectively excited Shpol'skii emission spectra of 3HF and 3DF are given in Figure 3A-D; the ground state vibration wavenumbers are included in the figure; weak sites are left out of consideration. The spectra shown in Figure 3 have some interesting features. First of all, the bands for 3DF are much sharper than for 3HF – a result that applies to the excitation

spectra as well, see Figures 1 and 2. Secondly, the low frequency vibrations of 3HF and 3DF in the ground state tautomer indicated in the spectra are not significantly different.

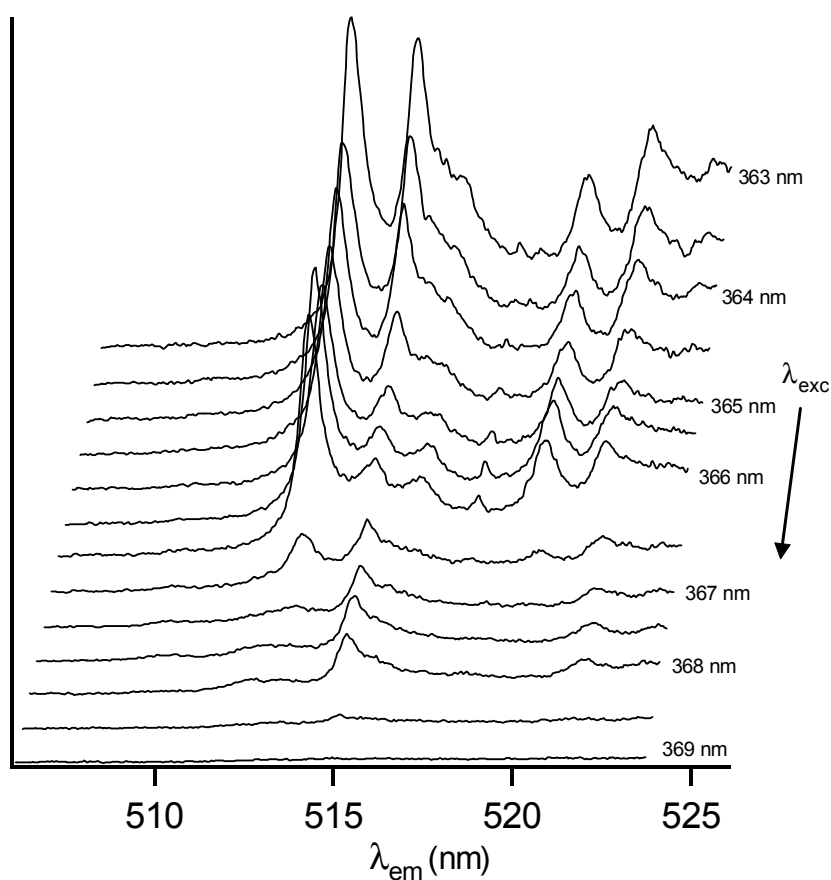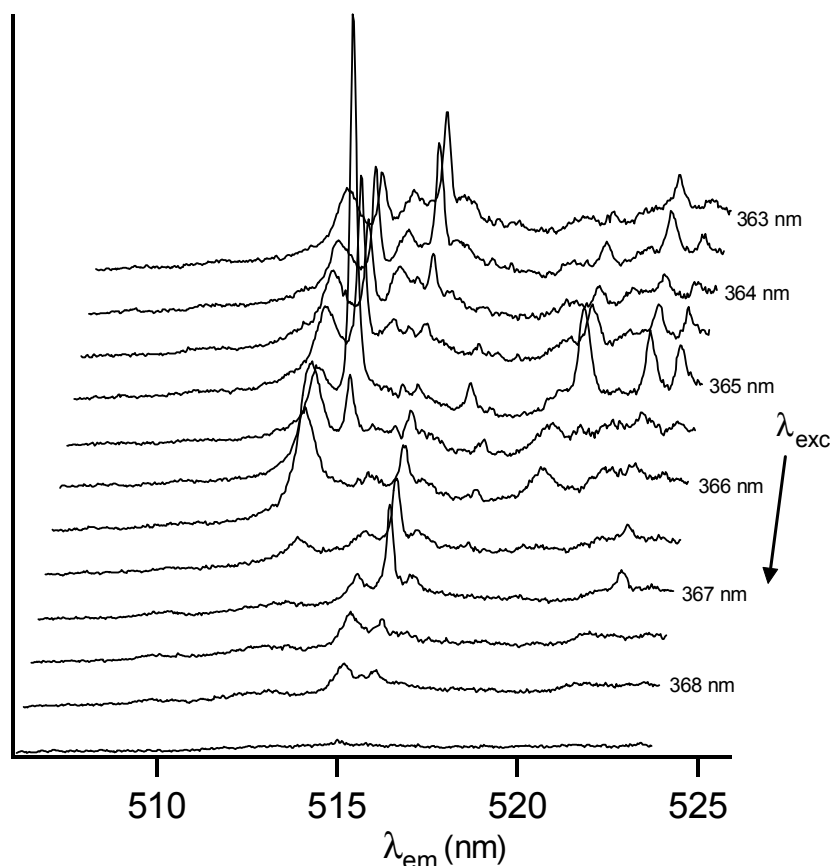***Figure 2:*** *Emission spectra of 3-deuteroxyflavone (3DF) in n-octane measured at 10K. The excitation wavelength was varied from 363 to 368.5 nm with 0.5 nm steps. 3DF is present in two sites, one emitting at λ_{em} = 514.1 nm and one at λ_{em} = 515.8 nm. In the sample there was still 3HF present since the sites at 513.1 and 515.0 nm can still be seen. The emission bandwidth was determined to be 0.20 nm. The excitation bandwidth was estimated to be 0.5 nm.*

There are good reasons to assume that the inhomogeneous broadening in 3HF and 3DF are the same, i.e. that for both molecules the variation in interaction with and the positioning in the crystalline n-octane matrix are equal. So, the linewidth differences observed reflect differences in homogeneous line broadening. In line with the literature, proton transfer reactions are much faster than deuteron transfer reactions [14]. This holds for both ESIPT and BPT. Apparently for 3HF the lifetimes of N* and T are much shorter than for 3DF.

A quantitative analysis of these results can be performed as follows. For convenience, it is assumed that the experimental linewidth is composed of three Gaussian shaped, independent

contributions, i.e., the instrumental resolution (4 cm^{-1}), the inhomogeneous linewidth and the homogeneous linewidth. Furthermore, for 3HF and 3DF the inhomogeneous broadenings are set equal. Though its exact value cannot be inferred form the available data, its maximum value and its minimum value can be readily estimated from the 3DF spectra. Obviously, its minimum is zero. Its maximum is equal to the line width of the 3DF spectra, which applies if homogeneous broadening plays no role at all.
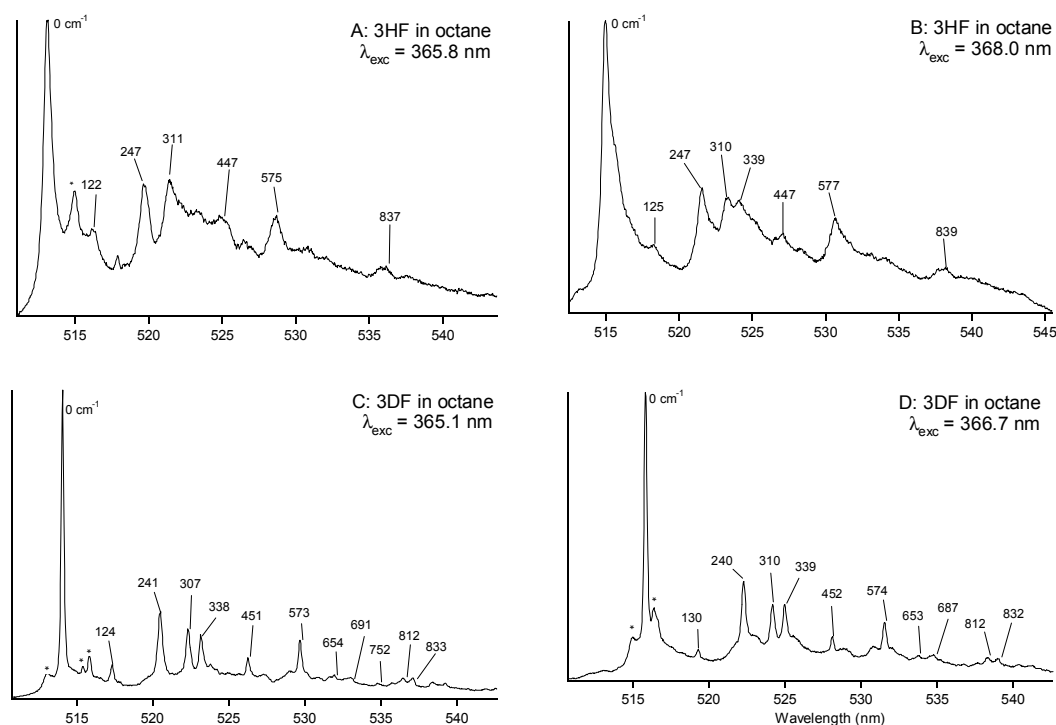
Figure 3: *10K Shpol'skii spectra of 3HF/3DF. In each spectrum one site is selectively excited. [A] and [B], emission spectra of 3HF in n-octane, excited at 365.8 nm and 368 nm, respectively. [C] and [D], emission spectra of 3DF in n-octane, excited at 365.1 nm and 366.7 nm, respectively. Peak labels indicate ground state vibrational frequencies in wavenumbers. The starred peaks are other sites due to non-selective excitation. The 339 cm^{-1} band in spectrum A is not readily visible due an overlap of a vibration band of the 368 nm site.*

The results are collected in Table 1. In excitation the inhomogeneous band broadening ranges from 0 cm^{-1} to 45 cm^{-1}, which implies that the homogeneous broadening in the excitation spectrum of 3HF ranges from 110 cm^{-1} to 180 cm^{-1}. From this homogeneous broadening the lifetime of N* can be calculated using $\tau = 1/(2\pi.\Delta v.c)$ (wherein Δv is the homogeneous broadening); it is found to be 39 ± 10 fs. Analogously, the lifetime of T (determined by the BPT) can be calculated. In this case, the inhomogeneous broadening

ranges from 0 cm^{-1} to 7.3 cm^{-1} so that the homogeneous broadening in the emission lines of 3HF ranges from 22 cm^{-1} to 29 cm^{-1}. As a result, the lifetime of T is found to be 210 ± 30 fs. Thus, the rate constant of ESIPT is five times higher than that of BPT. Considering the lifetimes of 3DF, only the lower limiting values can be estimated. Excited-state intramolecular deuteron transfer is slower than 180 fs while back deuteron transfer is slower than 730 fs.

Table 1: *Rates of excited state intramolecular proton transfer (ESIPT) and back proton transfer (BPT) in 3HF and 3DF. The rate of ESIPT is obtained from the total bandwidth, which was determined to be 2 nm and 0.5 nm for 3HF and 3DF, respectively (an uncertainty of 20 % was included). The rate of BPT was obtained from the total bandwidth of 0.7 nm and 0.2 nm for 3HF and 3DF, respectively (an uncertainty of 10 % was included). The homogeneous broadening (Γ_{hom}) was calculated from the total broadening (Γ_{tot}), the instrumental broadening (Γ_{instr}) and the inhomogeneous broadening (Γ_{inh}) via $\Gamma_{tot}^2 = \Gamma_{instr}^2 + \Gamma_{inh}^2 + \Gamma_{hom}^2$.*

	Γ_{tot} (cm^{-1})		Γ_{instr} (cm^{-1})	Γ_{inh} (cm^{-1})		Γ_{hom} (cm^{-1})		τ_{pt} (fs)
	Min.	*Max.*		*Min.*	*Max.*	*Min.*	*Max.*	
ESIPT								
3DF	30	45	4	0	45	0	45	> 180
3HF	120	180	4	0	45	110	180	39 ± 10
BPT								
3DF	6.8	8.3	4	0	7.3	0	7.3	>730
3HF	24	29	4	0	7.3	22	29	210 ± 30

Of course the three linewidth components considered above do not all have a Gaussian shape. Nevertheless, the results of Table 1 give a good – though rough – estimate of the lifetimes of the N* and T forms of 3HF in a n-octane crystalline matrix at 10K. The reported BPT derived from the bandwidth in the emission spectrum of 3HF in an argon matrix at 30K are three to four times faster (60 fs [11]) than the value shown in Table 1. It should, however, be realised that the spectra reported in that publication were relatively broad, so that the homogeneous component of the bandwidth could only be very roughly estimated. Interestingly the N* lifetimes is in line with the most recent literature data, being obtained by transient absorption measurements in MCH at room temperature [16]. Apparently, there is no strong difference between N* lifetimes at room temperature and under cryogenic conditions.

This points to a tunneling model for ESIPT, a model that is also in correspondence with the fact that for 3DF ESIPT is much slower. In this study we have shown deuteron transfer to be slower by a factor of at least 4.5 and 3.5 for ESIPT and BPT, respectively. These values are in agreement with the isotope effect found by Brucker and Kelley [11] for the same component in frozen argon at 30K. The same group [14] did not find a significant isotope effect in acetonitrile at room temperature, indicating a different mechanism under these conditions.

The observation that the low frequency vibrations of the T form in 3HF and 3DF are not different (see Figure 3) points to a structure of T in which the hydrogen/deuterium atom is indirectly coupled to the π-electronic structure involved in the electronic transition. This might indicate that the mesomeric structure of T, shown in Scheme 2, plays a significant role.
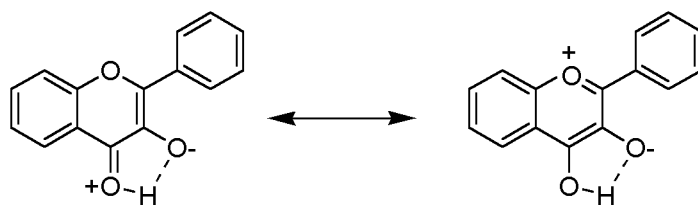
Scheme 2*: Mesomeric structures of 3HF in the T-form*

Addition of octanol

As mentioned in the introduction, the effect of hydrogen bonding caused by impurities has been discussed extensively in the literature. We observed that in a 10K n-octane Shpol'skii matrix, addition of a hydrogen bonding impurity like water, methanol or diethyl ether to the sample does not affect the high-resolution spectra of 3HF. The reason for this is that 3HF fits tightly into the matrix so there is no space available for an additional hydrogen-bonding molecule; upon cooling the added polar solvent is simply frozen out and a phase separation is obtained. If, on the contrary, a hydrogen bonding impurity is added that can replace a particular octane molecule of the crystalline surrounding of a 3HF molecule, an effect can be expected. This was observed for 2-octanol and 3-octanol. Addition of a minor amount of 2-octanol results in the appearance of a new site at 507.2 nm. Addition (of a much larger amount) of 3-octanol results in a new site further shifted to the blue, i.e., at 504.7 nm. On the contrary, addition of 1-octanol or 4-octanol has no effect.

The new site in the emission spectrum at 507.2 nm is already observed at very low concentrations of 2-octanol (see Figure 4), i.e., down to 0.001%. At increasing concentrations of 2-octanol, the intensities of the 513.1 and 515.0 nm sites decrease, while simultaneously the 507.2 nm band is growing in intensity. Therefore, it is likely that in the ground state (N) a 3HF/2-octanol complex is formed, in fact a chemical entity distinguishable from the free 3HF (that is characterised by two emission sites in n-octane). Since the additional site is already present at a low concentration of 2-octanol, it can be concluded that the 3HF/octanol complexes are formed in the liquid phase, in advance to sample solidification. Apparently, the exact position of the hydroxy-group in the octanol molecule determines whether or not the complex fits in the n-octane matrix. Both the 3HF/2-octanol complex and the 3HF/3-octanol complex fit into the matrix in a well-defined way (only weak additional sites are observed), whereas the 3HF/1-octanol and 3HF/4-octanol complexes do not give rise to the Shpol'skii effect.
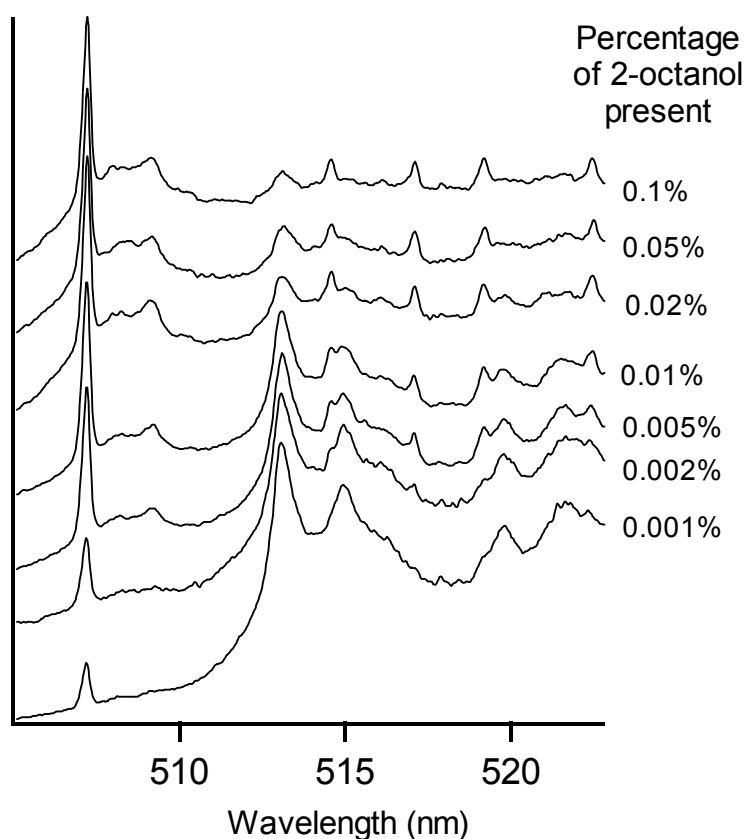

Figure 4: 10K Shpol'skii spectra of 3HF in n-octane with increasing concentration of 2-octanol added. The sample was excited at 365 nm. A 2-octanol concentration of 0.001% corresponds to 70 μM. The concentration of 3HF was 10 μM.

Excitation-emission spectra for 3HF in n-octane containing a minor amount (0.005%) of 2-octanol are depicted in Figure 5. The three sites considered above can be readily observed, i.e., the sites of pure 3HF at 513.1 nm and 515.0 nm (as also observed in Fig. 1), and furthermore the 507.2 nm site showing the 3HF/2-octanol complex. It should be noted that upon excitation at wavelengths higher than 370 nm only the latter site is observed. Figure 6 shows the detailed emission spectra of 3HF/2-octanol and 3HF/3-octanol; the low frequency vibrations – quite similar but not fully identical for the two complexes – are indicated in the spectra.
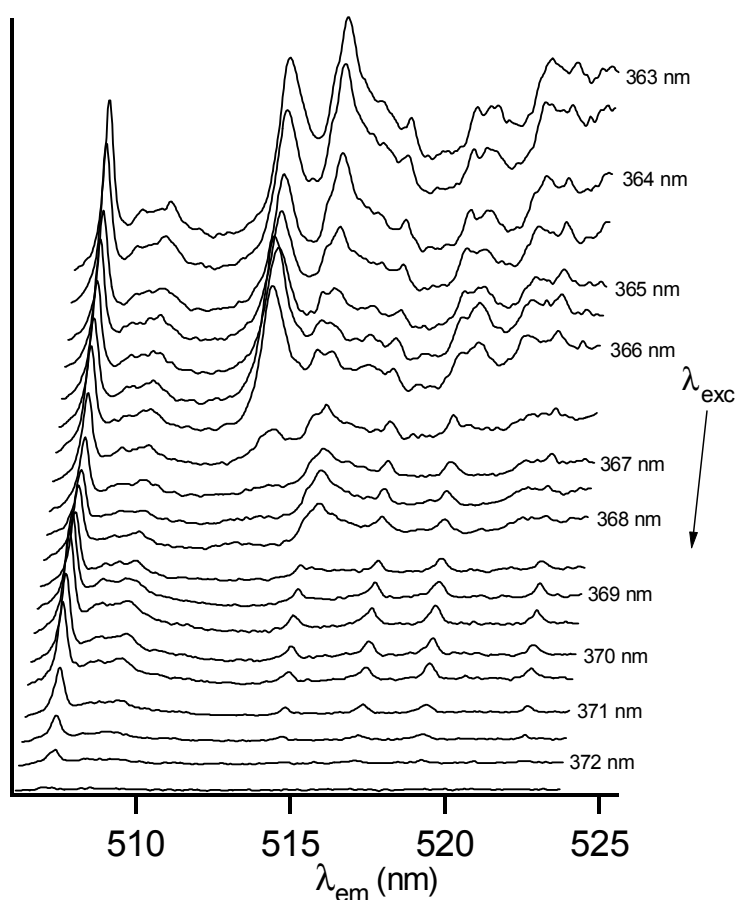
Figure 5: Emission spectra of 3-hydroxyflavone (3HF) in n-octane with 0.005% 2-octanol measured at 10K. The excitation wavelength was varied from 363 to 372.5 nm with 0.5 nm steps. The normal 3HF sites emit at λ_{em} = 513.1 nm and at λ_{em} = 515.0 nm. The site due to the presence of 2-octanol can be found at λ_{em} = 507.2 nm.

Two features emerge from Figures 5 and 6. First of all, a large Stokes' shift is observed for the complexes (507 nm – 372 nm for 3HF/2-octanol). It strongly suggests that, also in the complex, excited-state proton transfer is operative. Secondly, the vibrational pattern in Figure

6 is different from that in Figures 3. In other words, the tautomeric species generated upon excited-state proton transfer in 3HF/2-octanol is structurally different from T in Scheme 1. Some vibrations are equal, for instance 451, 572 and 653 cm⁻¹, while some are distinctly different, for instance 279 and 375 cm⁻¹ in the complex, but 247, 310 and 339 cm⁻¹ in 3HF.
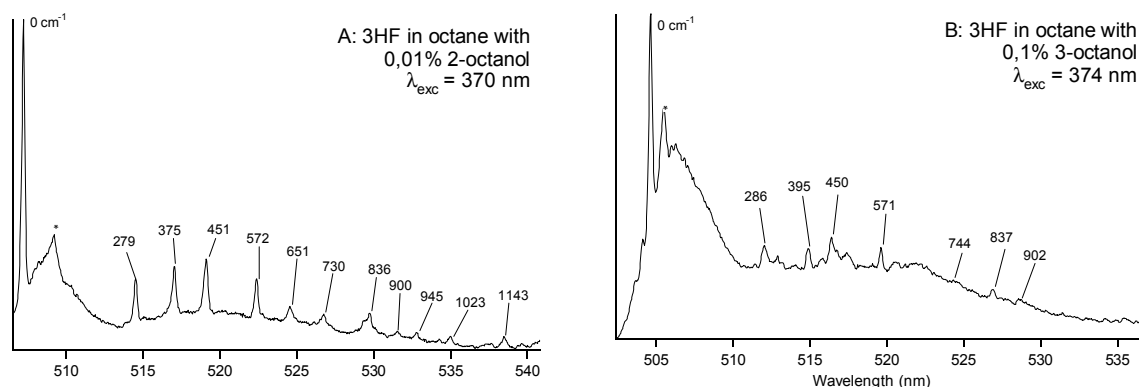
Figure 6: Emission spectra of 3HF in the presence of octanol measured at 10K. [A] 3HF in n-octane with 0.01% 2-octanol present, excited at 370 nm. [B] 3HF in n-octane with 0.1% 3-octanol present, excited at 374 nm. Peak labels indicate ground state vibrational frequencies in wavenumbers. The starred peaks originate from an additional site.

Of course, we also tried to record Shpol'skii spectra of 3DF/2-deuteroxyoctane, the deutero-analogue of the 3HF/2-octanol complex. It could not be observed, i.e. there was no additional site in the emission spectrum of 3DF in octane/2-deuteroxyoctane mixtures when excitation wavelengths in the 365-375 nm range were used. This suggests that in the 3DF/octane complex excited-state deuteron transfer is very slow, i.e., not able to successfully compete with the normal decay of the complex (broad-banded emission in the blue). Apparently, there is an extremely large difference in proton and deuteron transfer rates, a phenomenon that is well-known from the literature [14]. A large rate difference generally indicates a large difference in tunneling distance.

To summarize the above results, the excited-state proton transfer in 3HF/2-octanol is not the same as in 3HF: the tunneling distances or the barrier profiles are different and furthermore the structure of the tautomeric ground-state species generated after emission differs from that of T (see Scheme 1).

It is likely that upon addition of 2-octanol or 3-octanol one octane molecule in the crystalline environment of 3HF is replaced by one octanol molecule. However, the relative orientation of the OH-group of octanol with respect to the 3HF molecule is not easily predicted. Possible structures of the 3HF/2-octanol complex are depicted in Scheme 3 (there are only few possibilities for a 1:1 complex that would fit in the octane matrix). Their appropriateness to explain the above results is discussed successively.
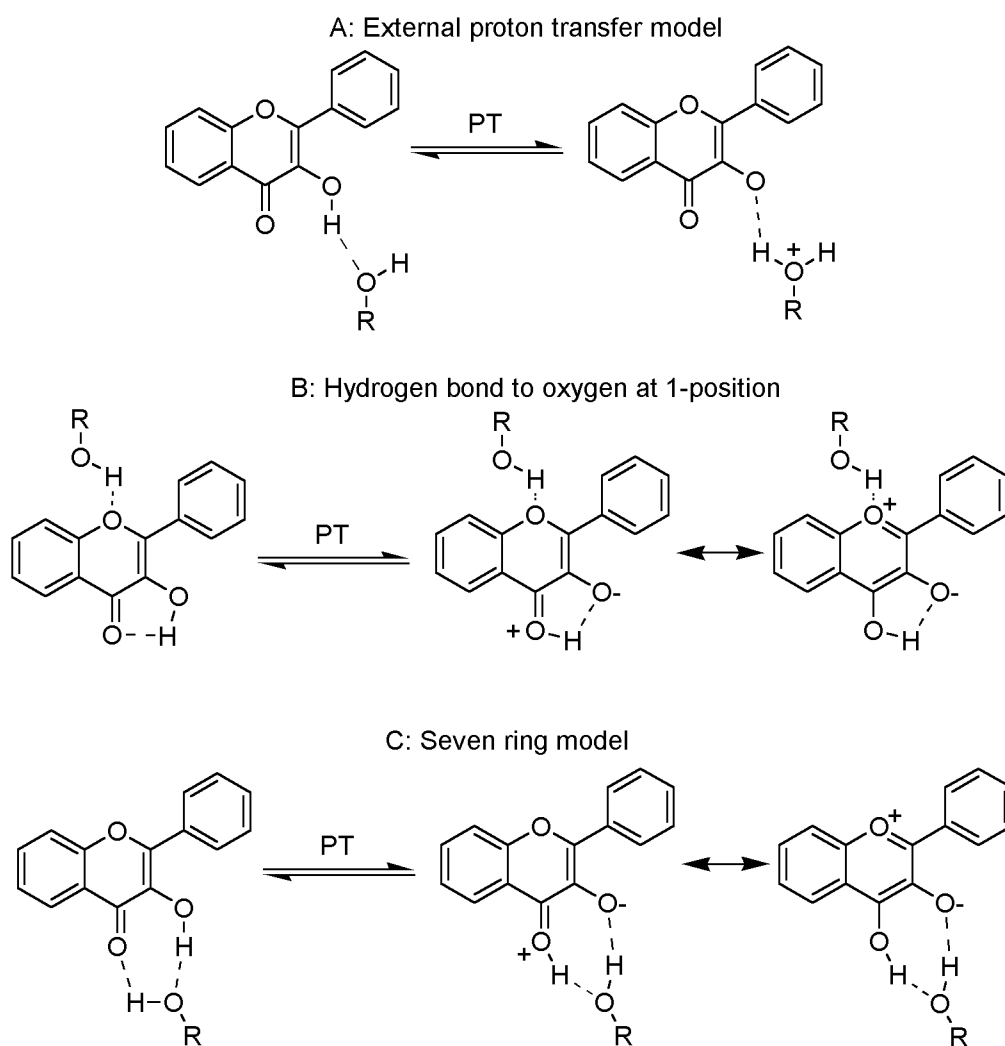
Scheme 3: *Possible structures for external proton transfer*

Scheme 3A shows external proton transfer. After excitation, the 3-OH group in the 3HF molecule becomes acidic and the proton is transferred to the OH-group of octanol. It results in the formation of octyl-OH_2^+ and the anionic form of 3HF. Differences in vibrational frequencies for this species compared to T can be readily conceived. Whereas in T the

positive charge on the proton-accepting group can be delocalised (see Scheme 2), giving 3HF's six-ring an aromatic character, such a delocalisation is impossible for the anion formed upon external proton transfer. Thus, Scheme 3A would account for differences in vibration energies. However, it is not very likely that the tautomeric and the anionic form of 3HF show such similar emission wavelengths, the difference being as small as a few nanometers.

Scheme 3B shows a complex structure with the hydrogen bound to the oxygen at the 1-position of 3HF. For this complex the positive charge can be more efficiently delocalised than in T so that a change in vibrational frequencies might be expected. However, the proton transfer as such will hardly be affected so that the absence of excited state deuteron transfer in the 3DF/octanol complex cannot be rationalised.

Scheme 3C shows a seven-ring model, in which two hydrogen bonds are involved. In such a structure the proton transfer mechanism will differ from that in Scheme 1: two protons are involved and different tunneling distances are dealt with. The first proton is transferred from the OH-group in 3HF to the octanol molecule while the second one goes from octanol to the carbonyl oxygen in 3HF. As such the tautomer in Scheme 3C is structurally rather similar to T in Scheme 2. The major structural difference presumably is that due to the non-flat seven-ring, the hydroxy-group and the carbonyl group in the complex will be located out-of-plane of the six ring of 3HF, thereby changing the low energy, out-of-plane vibrational energies of 3HF.

To conclude this section the following two features should be noted. First, the difference in behaviour observed for the octanol isomers can be conceived as follows: for 1-octanol and 4-octanol the formed 3HF-complexes do not fit adequately in the n-octane matrix, the 3-octanol complex fits to some extent, while the 2-octanol complex fits appropriately. However, the detailed structures of 3HF/2-octanol and 3HF/3-octanol will not be fully identical, especially as regards the hydrogen bond distances.

Secondly, for the 3HF/2-octanol and 3HF/3-octanol complexes it is not possible to derive the rate constants from the linewidths since the inhomogeneous broadening contributions are fully unknown and a comparison with the 3DF complexes cannot be made. Nonetheless, a marked difference in linewidth in excitation and emission is worth to be noted; the linewidth

in excitation is approximately 3 nm but in emission only 0.4 nm, a larger difference than observed for the free 3HF molecule. This supports the abovementioned assumption that the proton transfer mechanisms in 3HF and in the 3HF/octanol complexes are not the same. Furthermore, it indicates that also in the complex the excited state proton transfer rate is much faster than the rate of the proton back transfer.

References

1. Sengupta, P.K.; Kasha, M. *Chem. Phys. Lett*. **1979**, *68*, 382
2. Woolfe, G.J.; Thistlethwaite, P.J.; *J. Am. Chem. Soc.* **1981**, *103*, 6916-6923
3. Itoh, M.; Tokumura, K.; Tanimoto, Y.; Okada. Y.; Takeuchi, H,; Obi, K.; Tanaka, I. *J. Am. Chem. Soc.* **1982**, *104*, 4146-4150
4. McMorrow, D.; Kasha, M. *J. Am. Chem. Soc.* **1983**, *105*, 5133-5134
5. Strandjord, A.J.G.; Barbara, P.F. *Chem. Phys. Lett.* **1983**, *98*, 21-26
6. Strandjord, A.J.G.; Courtney, S.H.; Friedrich, D.M.; Barbara, P.F. *J. Phys. Chem.* **1983**, *87*, 1125-1133
7. McMorrow, D.; Dzugan, T.P.; Aartsma, T.J. *Chem. Phys. Lett*. **1984**, *103*, 492-496
8. [A] McMorrow, D.; Kasha, M. *Proc. Natl. Acad. Sci. USA* **1984**, *81*, 3375-3378 [B] McMorrow, D.; Kasha, M. *J. Phys. Chem.* **1984**, *88*, 2235-2243
9. Strandjord, A.J.G.; Barbara, P.F. *J. Phys. Chem.* **1985**, *89*, 2355-2361
10. Dick, B.; Ernsting, N.P. *J. Phys. Chem.* **1987**, *91*, 4261-4265
11. Brucker, G.A.; Kelley, D.F. *J. Phys. Chem.* **1987,** *91*, 2856-2861
12. Brewer, W.E.; Studer, S.L.; Chou, P-T. *Chem. Phys. Lett.* **1989**, *158*, 345-350
13. Barbara, P.F.; Walsh, P.K.; Brus, L.E. *J. Phys. Chem.* **1989**, *93*, 29-34
14. Brucker, G.A.; Swinney, T.C.; Kelley, D.F. *J. Phys. Chem.* **1991**, *95*, 3190-3195
15. Schwarz, B.J.; Peteanu, L.A.; Harris, C.B. *J. Phys. Chem. A* **1992**, *96*, 3591-3598
16. Ameer-Beg, S.; Ormson, S.M.; Brown, R.G.; Matousek, P.; Towrie, M.; Nibbering, E.T.J.; Foggi, P.; Neuwahl, F.V.R. *J. Phys. Chem. A* **2001**, *105*, 3709- 3718
17. Muhlpford, A.; Bultmann, T.; Ernsting, N.P.; Dick, B. in *Femtosecond Reaction Dynamics;* Wiersma, D.A. (ed), Royal Netherlands Academy of Arts and Sciences, Amsterdam, **1993**, 83
18. Renge, I.; Wild, U.P. in *Shpol'skii Spectroscopy and Other Site Selection Methods*, Gooijer, C.; Ariese, F.; Hofstraat, J.W. (eds), John Wiley & Sons, New York, **2000**, 19-71
19. Hofstraat, J.W.; Schenkeveld, A.J.; Engelsma, M.; Gooijer, C.; Velthorst, N.H. *Spectrochim. Acta Part A* **1988**, *44*, 1019-1025
20. Hofstraat, J.W.; Gooijer, C.; Velthorst, N.H. in *Molecular Luminescence Spectroscopy: Methods and Applications, Part 2*, Schulman, S.G. (ed), John Wiley & Sons, New York, **1988**, 383-459

CHAPTER 2.2

Solvent influence on excited-state intramolecular proton transfer in 3-hydroxychromone derivatives studied by cryogenic high-resolution fluorescence spectroscopy

Arjen N. Bader, Vasyl Pivovarenko, Alexander P. Demchenko, Freek Ariese, Cees Gooijer , *Spectrochim. Acta A*, **2003**, *59 (7)*, 1593-1603

Abstract

High-resolution Shpol'skii spectra (recorded at 10 K in *n*-octane) of 3-hydroxychromone (3HC) substituted at the 2-position with a furan (3HC-F), a benzofuran (3HC-BF) or a naphthofuran group (3HC-NF) are presented. Being close analogues of 3-hydroxyflavone (3HF), these compounds can undergo Excited-State Intramolecular Proton Transfer (ESIPT). Luminescence can occur from the normal N* state (blue) or from the tautomeric T* state (green). Whether blue or green emission is observed is strongly dependent on hydrogen bonding interactions with the environment. For all three chromones studied, high-resolution emission spectra in the green region (T* →T) were obtained in pure n-octane, showing four sites with distinct emission bands and detailed vibrational structures, whereas no blue emission was detected. Contrary to the spectra published for 3HF, the emission lines were very narrow (line-broadening effects beyond detection) which implies that the ESIPT rate constants are slower than 10^{12} s^{-1}, at least 25 times lower than for 3HF. In order to study the effects of hydrogen bonding solvents, four isomers of octanol (1-, 2-, 3- and 4-octanol) were added, forming 1:1 complexes with the 3HC derivatives. For all the combinations considered both blue and additional green emission was observed and in some cases narrow-banded spectra were obtained, mostly in the green. Only for the 3HC-NF/2-octanol complex narrow-banded emission was found both in the blue and in the green region. It is demonstrated that these emissions come from different configurations of the complex. Possible structures for the two complex species are proposed, supported by semi-empirical calculations on complex formation enthalpies.

Introduction

For more than 20 years it has been known that 3-hydroxyflavone (3HF, see Scheme 1) undergoes Excited State Intramolecular Proton Transfer (ESIPT) [1]. The interesting feature of this molecule is that fluorescence can be observed originating from two different excited states, its normal form (N*) and its tautomeric form (T*). Numerous experiments have demonstrated that, in solution, the occurrence of these emissive forms depends on both non-specific interactions with the solvent (polarity effects) and on competition from hydrogen-bonding solvent molecules for the intramolecular hydrogen bond between the 3-hydroxy group and the 4-carbonyl, which is the site of the ESIPT reaction [2-7]. In the presence of a hydrogen bonding solvent mainly blue emission (380-460 nm) originating from N* is observed. In a non-polar solvent, however, ESIPT takes place and the tautomer T* is formed that emits in the green (510-570 nm). Various methods, including fluorescence lifetime measurements [2-7], matrix isolation in argon [8,9] and ultrafast pump/probe experiments [10-12] have been used to determine the rate of the transfer process and to study the transfer mechanism both in the presence and absence of a hydrogen bonding solvent.
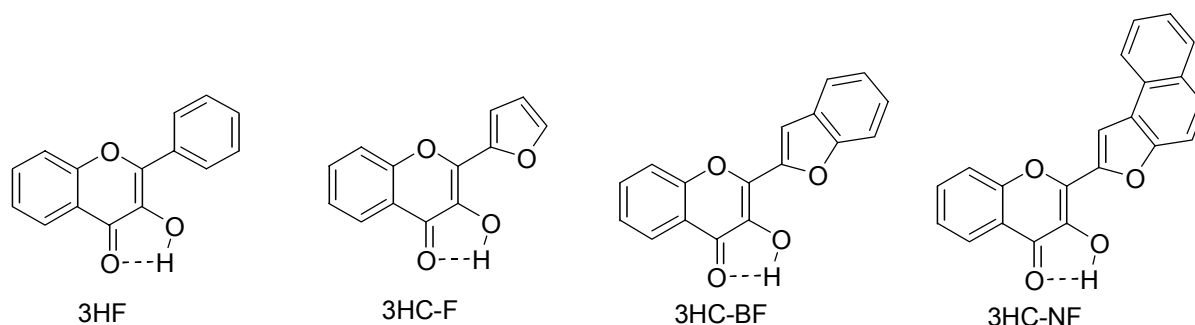
Scheme 1: *Chemical structures of 3-hydroxyflavone, 2-furyl-3-hydroxychromone, 2-benzofuryl-3-hydroxychromone, and 2-naphthofuryl-3-hydroxychromone.*

The application in these studies of high-resolution spectroscopy in cryogenic Shpol'skii matrices is very attractive, since it allows one to exclude the universal solute-solvent interactions that generate the inhomogeneous broadening of spectra and produce solvent polarity effects that may influence the ESIPT kinetics. In a recent paper [13], we showed that detailed kinetic and mechanistic information about the proton transfer in 3HF can be obtained using steady-state Shpol'skii spectroscopy in *n*-octane at 10 K. When comparing the Shpol'skii excitation and emission spectra of 3HF to those of its deuterated analogue 3-deuterioxyflavone (3DF), the bandwidths observed for the latter were much narrower. The

reason for this is that deuteron transfer is much slower than proton transfer; apparently for 3HF the additional (homogeneous) broadening is due to lifetime effects, whereas for 3DF such effects are rather small. Since the lifetime of N* is limited by ESIPT, the additional broadening in the excitation spectrum is a measure for the rate of that process. In a similar way, the rate of Back Proton Transfer (BPT) from the tautomeric ground state T to the normal ground state N can be obtained from the additional broadening in the T* → T emission spectrum. Thus, it was estimated that ESIPT takes place in 39 ± 10 fs, whereas BPT is five times slower: 210 ± 30 fs. These results are in good agreement with the data obtained in recent ultrafast pump/probe experiments, where an instrument-limited 35 fs was reported for the rise time of T* [10]. Furthermore, it should be noted that the results point to a tunnelling mechanism of proton/deuteron transfer that may be coupled with vibrations along the intramolecular hydrogen bond.

In addition, it was shown that the Shpol'skii approach can be used to study the effect of a hydrogen bonding impurity in detail [13]. It was found that only a few hydrogen bonding impurities are able to form a complex with 3HF that fits in the *n*-octane matrix and that their geometrical structure is a key factor; only two of the four octanol isomers yielded high-resolution Shpol'skii spectra. It was observed that when a minor amount of 2-octanol was added, an additional site appeared in emission that was about 7 nm blue shifted. Addition of a much larger amount of 3-octanol had a similar effect, whereas addition of 1-octanol or 4-octanol did not change the spectrum at all. Apparently, the position of the hydroxy group in octanol determines whether or not the 3HF/octanol complex fits in the matrix and gives rise to the narrow banded structure of the spectrum. The vibrational energies of the additional sites observed in the presence of 2-octanol or 3-octanol were different from the ones of uncomplexed 3HF. It was concluded that the additional sites originate from 3HF/2-octanol (or 3HF/3-octanol) complexes. Both ESIPT and BPT are influenced by the presence of the OH-group of octanol and a model for the changed proton transfer mechanism in these complexes was suggested.

As mentioned earlier, 3HF and its derivatives show very intense fluorescence spectra with a large separation between the N* and T* emission bands. They are highly sensitive to the polarity and the hydrogen bonding properties of the environment. Because of these unique features, they are often used as fluorescent probes for micelles, proteins and biological

membranes [14-20]. Most important in this respect is their application as two-wavelength ratiometric probes for spectroscopy and microscopy of living cells [14]. Attempts to improve these properties have been made during recent years [14,21-23]. Most successful in this respect was the substitution of the 2-phenyl group by furyl derivatives, which led to an increase in fluorescence quantum yield and lifetime and a shift in both absorption and fluorescence spectra to longer wavelengths. These molecules show increased sensitivity to solvent perturbations. In this paper, we focus on three 2-furyl derivatives, i.e. on 2-furyl-3-hydroxychromone (3HC-F), 2-benzofuryl-3-hydroxychromone (3HC-BF) and 2-naphthofuryl-3-hydroxychromone (3HC-NF) (see Scheme 1). The spectroscopic properties of 3HC-BF and 3HC-NF have already been described in previous papers [14,21]. In order to understand their increased sensitivity to solvent perturbations, detailed information about the structures of the complexes between the 3HC derivatives and the hydrogen-bonding molecule is needed. In this paper, steady-state Shpol'skii spectroscopy is used for this purpose. It will be shown that two different types of monosolvate complexes can be formed, one in which the proton transfer is fully prohibited and one in which the proton transfer is influenced to a minor extent. Furthermore, the most likely structures of these complexes are presented.

Experimental

The synthesis of 2-benzofuryl-3-hydroxychromone (3HC-BF) and 2-naphthofuryl-3-hydroxychromone (3HC-NF) has been described in earlier work [21]. A.S. Klymchenko (TUBITAK RIGEB, Turkey) kindly provided these samples. 2-Furyl-3-hydroxychromone, (3HC-F) was prepared by alkaline condensation of 2-furaldehyde with 2-hydroxyacetophenone (both obtained from Aldrich) and subsequent oxidative heterocyclization of the resulting chalcone with hydrogen peroxide [24]. Light green-yellow crystals of 3HC-F were recrystallized twice from ethanol to give a pure product according to TLC and ^1H-NMR with m.p. 171-172 °C. In the mass spectrum the chromone 3HC-F showed the peak of the molecular ion M$^+$ at 228 c.u. (the calculated molecular mass for $C_{13}H_8O_4$ is 228.2). The ^1H-NMR spectrum of 3HC-F was measured on a Varian *Mercury-400* apparatus in DMSO-d_6. Below are the chemical shifts, multiplicities (*s* – singlet, *d* – doublet, *t* – triplet, *m* – multiplet), and signal intensities (in brackets): 9.80*s*(1H); 8.12*d*(1H); 7.90*s*(1H); 7.74*t*(1H); 7.63*d*(1H); 7.43*t*(1H); 7.31*d*(1H); 6.70*m*(1H). The ^{13}C-NMR spectrum of 3HC-F

was measured in acetone-d_6: 147.7; 136.5; 128.5; 127.6; 121.2; 118.8; 115.7 (all - tertiary carbons); 175.4; 157.9; 147.3 141.9 139.4 124.2 (quaternary carbons).

Semi-empirical theoretical calculations were performed to determine the possible geometrical structures in the electronic ground state and the formation energies of a number of 3HC-F/octanol complexes. Energy minimization *in vacuo* was done with the semi-empirical AM1 method using the MOPAC 6.0 program.

10 μM solutions of 3HC-F, 3HC-BF or 3HC-NF in *puriss n*-octane (Fluka) were studied. The solvents 1-, 2-, 3- and 4-octanol (all > 97% purity) were obtained from Fluka, Sigma, Fluka and Aldrich, respectively. The samples were transferred to a homemade sample holder containing four sample cells. The sample holder was cooled to 10 K by a Cryodyne Model 21 closed-cycle helium refrigerator (CTI Cryogenics, Waltham, MA, USA). The sample was illuminated at an angle of 30° with a XeCl excimer laser (Lambda Physik LPX 110i, Göttingen, Germany) pumping a dye laser (Lambda Physik, LPD 3002). The excimer laser was operated at 10 Hz, producing 10 ns 50 mJ pulses. Using QUI as a dye, a tuneable output in the 370 to 400 nm range was obtained, while Exalite 411 was used to excite in the range from 403 nm to 420 nm; excitation spectra were recorded with 0.05 nm steps. The fluorescence emission was collected by a 3 cm F/l.2 quartz lens and focused on the entrance slit of a Spex 1877 0.6 m triple monochromator (Edison, NJ, USA) by a 10 cm F/4 quartz lens. The spectral resolution of this monochromator was 0.1 nm. For detection an Andor Technologies (Belfast, Northern Ireland) intensified CCD camera type iStar DH720-25U-03 was used in the gated mode. The gate was opened at the end of the (scattered) laser light pulse.

Results and Discussion

Site structures

High-resolution Shpol'skii spectra of the tautomeric form of 3HC-F were obtained using *n*-octane as a solvent, the same solvent used for 3HF. In Figure 1, an excitation-emission plot of 3HC-F in an *n*-octane matrix at 10 K is shown. It can be seen that 3HC-F is present in four sites in the matrix, with T* →T (0,0) emission transitions at 520.3 nm, 522.3 nm (probably two overlapping sites), 523.5 nm and 525.9 nm, respectively. Three of these sites are

simultaneously excited at about 373 nm. Only the λ_{em} = 525.9 nm site has a distinctly red shifted N → N* (0,0) excitation transition, i.e., at 381 nm. Despite the relatively large energy difference between the four sites dealt with, their vibrational energies in emission are the same, i.e. unaffected by the differences in surrounding. Also for 3HC-BF, four sites are present in the high-resolution Shpol'skii spectra obtained in *n*-octane (see Figure 2). The T*→T (0,0) emission transitions can be found at 534.2 nm, 537.4 nm, 538.9 nm and 539.7 nm; their vibrational energies are practically identical. For the third compound studied here, i.e. 3HC-NF, high-resolution fluorescence spectra in a 10 K *n*-octane matrix were recorded as well with analogous results. The excitation-emission plot in Figure 3 shows that 3HC-NF fits in the matrix in four different ways with (0,0) emission transitions at 550.1 nm, 552.9 nm, 555.2 nm and 558.6 nm, all having similar vibrational energies.
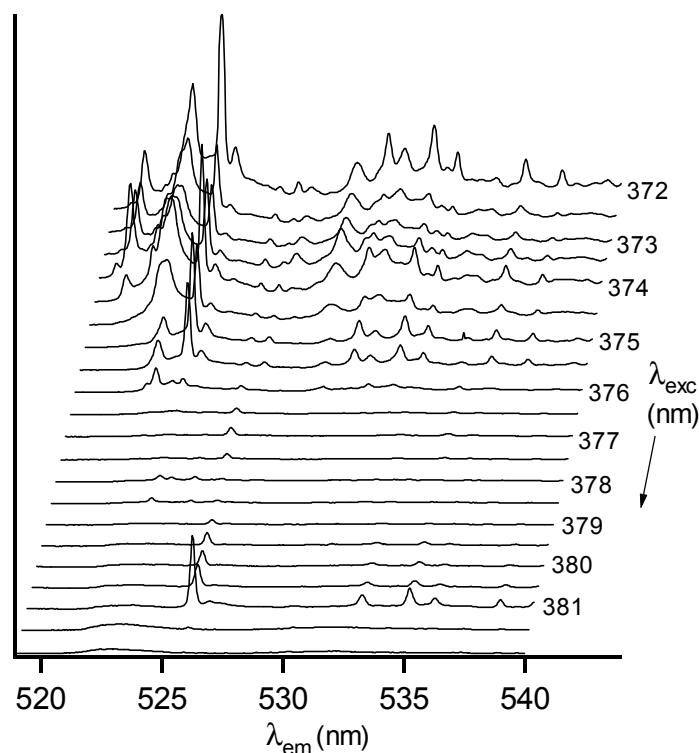
Figure 1: *Emission spectra of 3HC-F in n-octane, step-scanning the excitation wavelength from 372 to 382 nm. 3HC-F is present in four sites, emitting at 520.3 nm, 522.3 nm (probably two overlapping sites), 523.5 nm and 525.9 nm.*
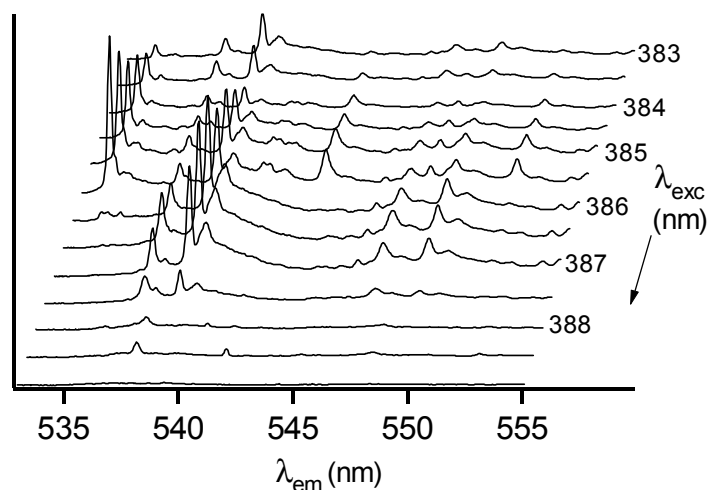
Figure 2: *Emission spectra of 3HC-BF in n-octane, step-scanning the excitation wavelength from 383 to 389 nm. 3HC-BF is present in four sites, emitting at 534.2 nm, 537.4 nm, 538.9 nm and 539.7 nm*
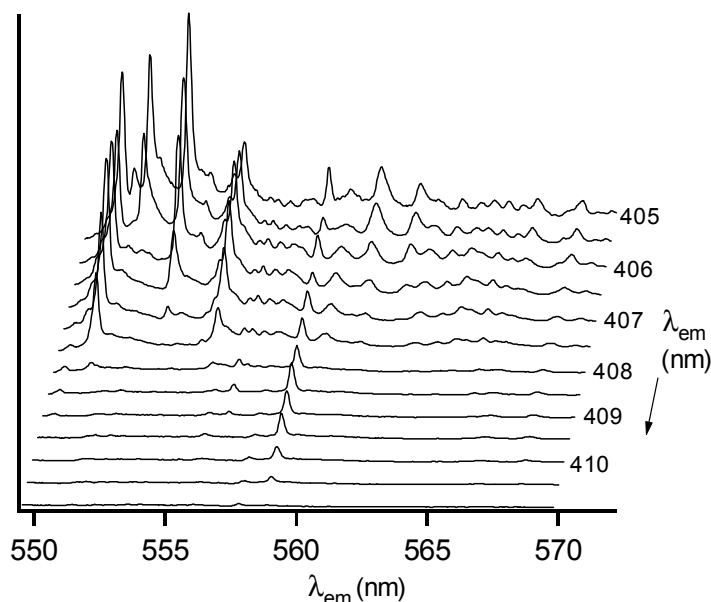
Figure 3: *Emission spectra of 3HC-NF in n-octane, step-scanning the excitation wavelength from 405 to 411 nm. 3HC-NF is present in four sites, emitting at 550.1 nm, 552.9 nm, 555.2 nm and 558.6 nm*

The three compounds studied here have in common that they all fit in an *n*-octane matrix in four different ways, whereas 3HF shows only two sites. This difference in site structure can be understood as follows. Probably, the molecule 3HF embedded in the polycrystalline *n*-octane matrix prefers to adopt a planar configuration, although semi-empirical AM1 calculations for this molecule *in vacuo* indicate that a twisted configuration ($\phi=30°$) is somewhat more favourable (0.6 kcal/mole) [25]. In the Shpol'skii emission spectrum, two

substitutional sites are observed [13] since for the planar 3HF molecule two different orientations are possible in the *n*-octane matrix, a phenomenon quite frequently observed for planar hydrocarbons [26]. Contrary to 3HF, for the three 3HC derivatives concerned the molecule is present in two inequivalent planar conformations, one in which the oxygen of the furan ring is directed towards the oxygen at the 1-position of the chromone ring ($\phi=0°$ conformer) and the other in which the oxygen of the furan ring is pointing towards the 3-hydroxy-group of the chromone ring ($\phi=180°$ conformer). Because these two conformers will have different (0,0) transitions, the total number of sites for 3HC-F increases to four. Semi-empirical AM1 calculations for the isolated 3HC-F molecule support this interpretation. Contrary to 3HF, for which the $\phi=0°$ and the $\phi=180°$ conformers are identical; there are indeed two planar conformations, which differ 2.5 kcal/mole in energy. Obviously, these energies may be different in a crystalline *n*-octane matrix and cannot straightforwardly be used to calculate the intensity distribution over the sites.

Bandwidths

Compared to 3HF, the bandwidths of 3HC-F, 3HC-BF and 3HC-NF in both emission and excitation are very narrow, for the (0,0) line as well as for the vibronic transitions. The bandwidths, obtained from the excitation and emission spectra, are approximately 0.2 nm in all cases. In comparison, for 3HF in excitation the bandwidth is ten times larger (2 nm; 150 cm^{-1}) and in emission three to four times larger (0.7 nm; 26 cm^{-1}) [13]. The bandwidths as observed for the 3HC derivatives are amongst the narrowest that can be obtained with our approach. Line-broadening effects in excitation – reflecting the rate of excited state proton transfer N* $\rightarrow$ T* – are therefore beyond detection. The same holds for the bandwidth in emission that reflects the back proton transfer from T to N in the electronic ground state. Also here, the proton transfer rates in 3HC-F, 3HC-BF and 3HC-NF appear to be too low to affect the bandwidths. Nonetheless, from the observed widths the maximum values of the ESIPT and BPT rates of furyl derivatives of 3-hydroxychromone can be inferred; they are both lower than 10^{12} s^{-1}. This is much slower than ESIPT (25×10^{12} s^{-1}) and BPT (5×10^{12} s^{-1}) in 3HF [13]. Apparently, the energy barrier heights and the energy differences between N* and T* for ESIPT and between N and T for BPT are significantly different for both molecules, leading to very different tunnelling rates. Theoretical calculations to support and quantify this interpretation are beyond the scope of the work presented here.

Effects of hydrogen bonding impurities

As mentioned in the introduction, liquid state experiments have shown that in comparison to 3HF the 3HC derivatives have an increased sensitivity to solvent effects, but in hydrogen bonding solvents one cannot distinguish the effects of polarity and of hydrogen bonding proper. Since in Shpol'skii matrices the inhomogeneous broadening is largely eliminated, these spectra provide more detailed information and one can study the effects of the furyl moiety on hydrogen bonding under conditions that are not influenced by solvent polarity. This approach was successfully applied in the studies of 3HF [13]. In the present study we have systematically investigated the complexes formed between the 3HC derivatives and a hydrogen bonding impurity by Shpol'skii spectroscopy. Since the 3HC derivatives considered fit in an *n*-octane matrix, four octanol isomers were used to model the hydrogen bonding impurity; these solvent molecules have the highest probability of forming a complex that fits in the matrix as well.

Figure 4: Shpol'skii emission spectra of 3HC-F in n-octane at 10K. The upper spectrum shows one of the sites in absence of octanol, the lower spectrum shows the additional site upon addition of 0.5% 2-octanol. For ease of comparison the spectra are plotted as a function of the energy difference in wavenumbers with respect to the (0,0) transition, giving the ground state vibrational energies. The wavelengths of the (0,0) transitions are also given.
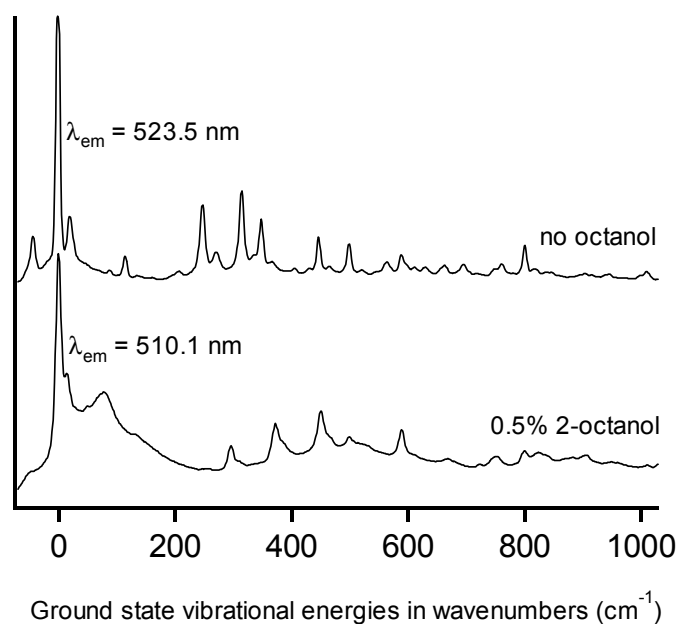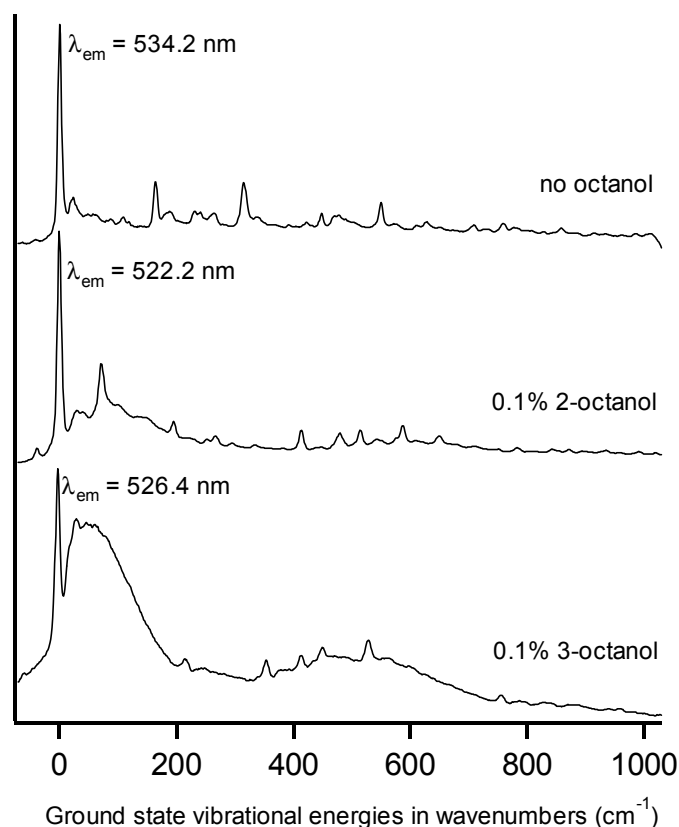
Figure 5: *Shpol'skii emission spectra of 3HC-BF in n-octane at 10K. The upper spectrum shows one of the sites in absence of octanol, the middle spectrum shows the additional site when 0.1% 2-octanol was added and the lower spectrum shows the additional site in the presence of 0.1% 3-octanol. For ease of comparison the spectra are plotted as a function of the energy difference in wavenumbers with respect to the (0,0) transition, giving the ground state vibrational energies. The wavelengths of the (0,0) transitions are also given.*

We observed that when any of the octanol isomers was added to 3HC-F, 3HC-BF or 3HC-NF, in the low temperature emission spectra both blue emission of the N* form and additional green emission of the T* form could be seen. Interestingly, not all the emission observed was narrow-banded. In the case of 3HC-F, only in the presence of 2-octanol did we obtain narrow banded green emission, coming from an additional site with the (0,0) emission transition at 510.1 nm (see Figure 4); in the blue emission no sharp lines could be observed. For 3HC-BF, only addition of 2-octanol or (although less favourable) 3-octanol gave rise to narrow banded additional emission in the green (see Figure 5) and also here not in the blue. The (0,0) emission transitions of the 3HC-BF/2-octanol and 3HC-BF/3-octanol complexes were found at 522.2 nm and 526.4 nm, respectively. It should be emphasized that narrow bands in the blue region were observed for 3HC-NF with 1-octanol or 2-octanol added. The

same molecule showed narrow banded green emission as well, i.e., upon addition of 2-octanol or 3-octanol (see Figure 6). The associated sites have (0,0) emission transitions at 424.7 nm (1-octanol added), 416.5 nm, 535.0 nm (2-octanol added) and 544.3 nm (3-octanol added).
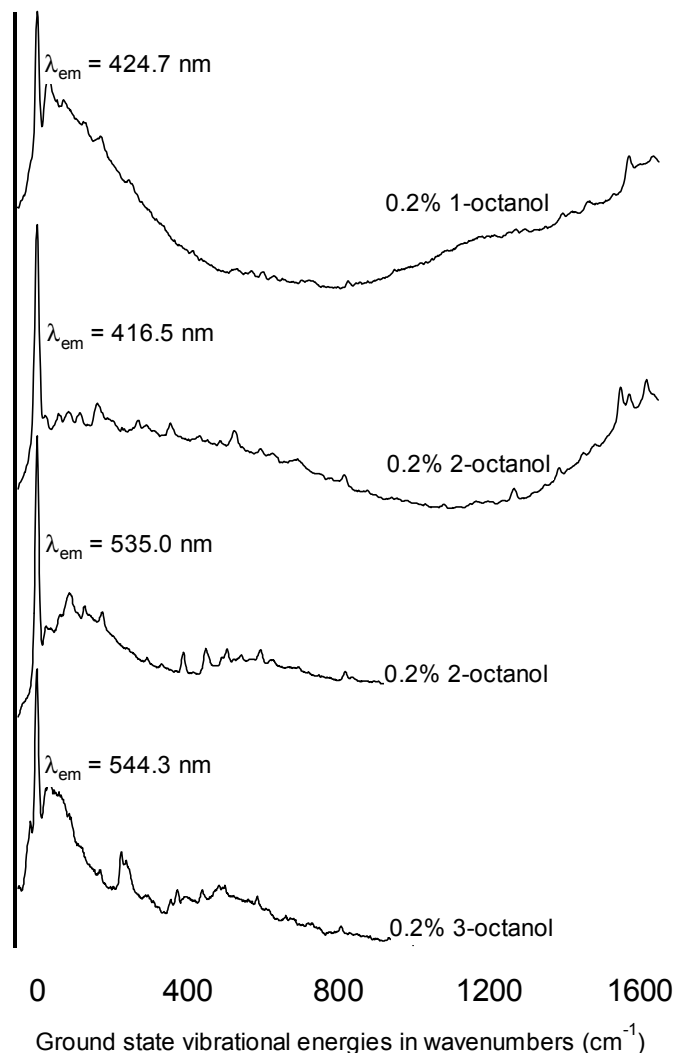
Figure 6: *Shpol'skii emission spectra of 3HC-NF in n-octane at 10K. The upper spectrum shows the blue emission when 0.2% of 1-octanol is added, the second spectrum shows the blue emission upon addition of 0.2% of 2-octanol, the third spectrum shows the additional green site when 0.2% 2-octanol is added and the lower spectrum shows the additional green site in the presence of 0.2% 3-octanol. For ease of comparison the spectra are plotted as a function of the energy difference in wavenumbers with respect to the (0,0) transition, giving the ground state vibrational energies. The wavelengths of the (0,0) transitions are also given.*

From the results shown here, the following can be concluded. Considering the vibrational patterns of the additional green sites, it should be noted that these are different from the ones

of the uncomplexed compounds. This indicates that for the complexed and the uncomplexed molecules the tautomeric species formed are different. Of course, for 3HC-NF, the high-resolution emission spectrum in the blue reflects the ground state vibrations of the N-form of 3HC-NF in a complex with 1-octanol or 2-octanol. Unfortunately, the vibrational bands in the presence of 1-octanol are very low in intensity; nonetheless they appear to be rather similar to those for the 2-octanol complex. We only obtained more than marginal differences in vibrational energies for the bands at 815/825 cm^{-1}, 1460/1486 cm^{-1}, 1550/1570 cm^{-1} and 1619/1637 cm^{-1} for the N-form of 3HC-NF complexed to 1-octanol and 2-octanol (see figure 6).

The most striking feature of the results obtained here is the simultaneous presence of both additional green and blue emission upon addition of a hydrogen bonding impurity, which indicates the emission of both N* and T* forms. In principle, this could be explained in two ways. Either the rate of ESIPT is slowed down so heavily that it becomes of the same order of magnitude as the fluorescence decay rate of N*, i.e. with a factor as large as 10^3 to 10^4, or, alternatively, two different complex species are observed that behave quite differently as far as ESIPT is concerned. In one of these complexes the proton transfer is influenced, but nonetheless it must be much faster than about 10^{10} s^{-1} so that blue emission is obstructed and green emission is observed exclusively. In the other complex the proton transfer is fully prohibited, i.e. slower than 10^9 s^{-1} so that blue emission of N* is observed and T* is not formed at all.

If the former explanation were correct, both the blue and the green emission would originate from the same conformation of the 3HC-NF/octanol complex, i.e. from a single species. If such a complex fits in the matrix, then narrow bands are expected both in the blue and in the green. However, from the results shown above it is clear that the presence of narrow bands in the green region does not necessarily mean that the blue emission is narrow banded as well. Therefore the latter explanation is more likely: the complexes that give emission in the blue are different from the ones that give green emission. Special attention should be given to the case of 3HF-NF in the presence of 2-octanol that showed both narrow-banded blue and green emission (see figure 6). In Figure 7, the Shpol'skii excitation spectra recorded at λ_{em} = 445.3 nm and at λ_{em} = 535.0 nm are compared. Because both the band

positions and the shapes of these spectra are different, we can conclude that the blue and the additional green fluorescence are emitted from two different complexes indeed.
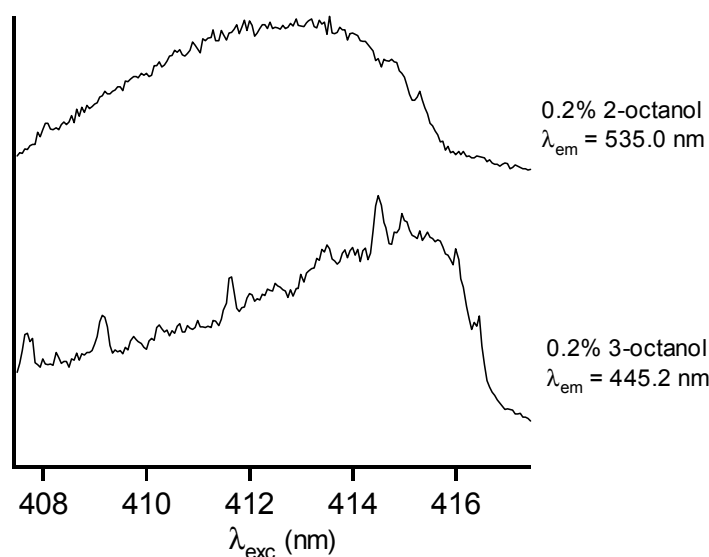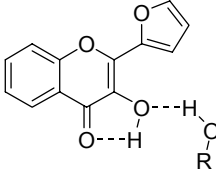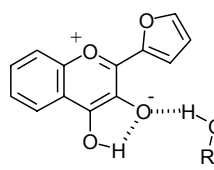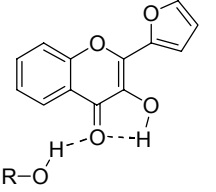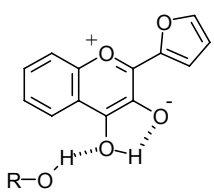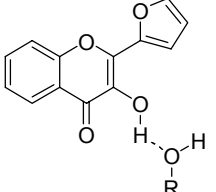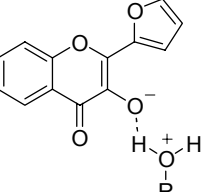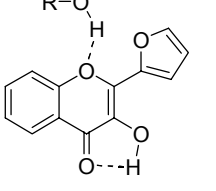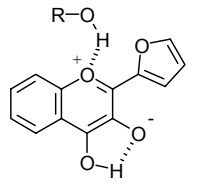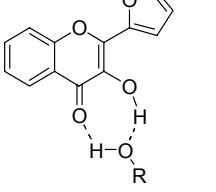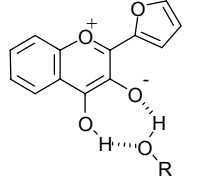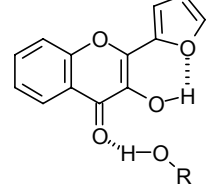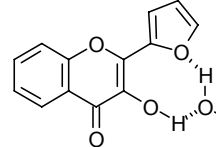
Figure 7: Shpol'skii excitation spectra of 3HC-NF in n-octane upon addition of 0.2% of 2-octanol. The spectrum was obtained by scanning the dye laser and recording a spectrum every 0.05 nm. The upper spectrum shows the excitation spectrum of the additional green site at λ_{em} = 535.0 nm. The lower spectrum shows the excitation spectrum of the blue emission at λ_{em} = 445.2 (the vibrational band at 1570 cm^{-1} was chosen as emission wavelength to be able to excite in the (0,0) region as well).

When considering the possible structures of the "blue" and the "green" complexes, the following has to be taken into account. The complexes are observed at a similar concentration of octanol and show a similar intensity of emission. Furthermore, since a complex composed of more than one solvent molecule is not likely to fit in the matrix in a regular way, only 1:1 complexes composed of one 3HC derivative and one octanol molecule need to be considered. For the "green" 1:1 complexes, ESIPT takes place while the interaction with the octanol induces a change of the T ground state vibrational pattern. For the "blue" 1:1 complexes, the internal hydrogen bond between the carbonyl and the hydroxy-group is probably weakened or even broken, so that ESIPT is inhibited. Finally, the complexes considered should be stable in the N-form of the electronic ground state, otherwise they would not have been formed in the *n*-octane matrix at all. Of course, they should also fit in the matrix in order to show Shpol'skii spectra; unfortunately this property cannot be easily related to the detailed molecular structure of the complex.

Possible structures for the "green" complexes are given in Table 1, configurations 1 to 5. Enthalpies of formation based on minimization in vacuum for the suggested complexes are included in the table. 3HC-F/methanol complexes were used as model systems, because their enthalpies of formation have the same dependence on the structure as 3HC-F/octanol complexes, whereas the calculations for 3HC-F/octanol are less precise than for 3HC-F/methanol because the latter has fewer degrees of freedom. According to the calculations, the binding of a methanol molecule causes a red shift (1–4 nm) of the absorption maximum in all cases. This is in line with the experimental results.

In the first possible structure, configuration 1 in Table 1, there is a hydrogen bond between the hydrogen of octanol and the oxygen of the chromone's 3-hydroxy group, while in configuration 2 the oxygen of the carbonyl group of the chromone is involved. It is very unlikely that one of these two structures gives the extra green spectra observed because the vibrational pattern of configurations 1 and 2 are not expected to be different from that of uncomplexed 3HC-F. A structure in which – instead of ESIPT – the proton is transferred externally to the hydroxy group of octanol (configuration 3 in Table 1) is unlikely as well: the anion thus created will certainly not emit fluorescence in the narrow green region concerned. The hydrogen bond between the octanol's hydrogen and the oxygen at the 1-position in the chromone ring (configuration 4) is presumably weak so that this structure should also be left out of consideration. This holds even more for the S_1 state where the lone pair electrons of the chromone's oxygen are involved in the π-electronic system that makes it less basic, contrary to the oxygen of the chromone's carbonyl group. The hydrogen bond to the latter group is therefore expected to be much stronger, especially in the S_1 state, where charge transfer from the furan to the chromone ring takes place. The most likely structure is therefore configuration 5 in Table 1. It is characterised by two hydrogen bonds in which the octanol's hydrogen as well as the octanol's oxygen atom are involved. For this seven-ring complex, the vibrational energies are expected to be different from those of free 3HC-F. Interestingly, configuration 5 has the most favourable enthalpy of formation within the series of structures considered this far. Although one has to be careful in using such quantitative gas phase data, they may serve to support the above conclusion. Last but not least, it should be recalled that a similar complex has been proposed in the case of 3HF/octanol [13].

Table 1: *Possible configurations of complexes formed between the 3HC derivatives and a hydrogen bonding impurity. For simplicity 3HC-F is shown. The drawn structures correspond to the 0° conformer, unless otherwise indicated.*

Configuration	H_f (kcal/mole) [a]	Normal form	Tautomeric form
1	-110.9 ($\phi=0°$) -110.0 ($\phi=180°$)		
2	-112.5 ($\phi=0°$) -110.1 ($\phi=180°$)		
3	(No accurate calculation of H_f possible)		
4	-112.3 ($\phi=0°$) -109.1 ($\phi=180°$)		
5	-113.1 ($\phi=0°$) -110.5 ($\phi=180°$)		
6	-109.3 ($\phi=180°$)		
7	-109.5 ($\phi=166°$)		

[a] Formation enthalpy values were calculated for the 3HC-F/methanol 1:1 complexes.

Possible structures of the "blue" complex in which ESIPT is weakened or even blocked are configurations 6 and 7 in Table 1. In these structures, the orientation of the 3-hydroxy group of the chromone is no longer towards the carbonyl group. Furthermore, since the furyl chromones are much stronger influenced by the presence of a hydrogen bonding impurity than 3HF, it is feasible that the oxygen of the furan group plays an important role in the complex formation, so the furan chromone is probably present in the $\phi=180°$ conformation. If the octanol molecule forms a hydrogen bond with the carbonyl group of the chromone, the 3-hydroxy group of the chromone can form a hydrogen bond with the oxygen of the furan ring (configuration 6). Another possibility is the formation of a hydrogen bond between the octanol and the 3-hydroxy group of the chromone on the one hand and the furan oxygen on the other (see configuration 7). The latter structure is less likely than complex 6 because the seven-ring might cause a non-planarity that will not fit very well in the matrix. Gas phase AM1 calculations indicate that configuration 7 has the energetically most favourable structure at $\phi=166°$.

Conclusions

Rather unexpected, for the three uncomplexed furyl derivatives considered the excitation and emission spectra in Shpol'skii matrices at 10 K are much narrower than in the case of 3HF. This means that both ESIPT and BPT are much slower than for 3HF; the associated rate constants cannot be inferred from the bandwidth effects on the spectra. Detailed theoretical studies have to be performed to explain these differences. Furthermore, Shpol'skii spectroscopy provides detailed insight into the influence of hydrogen bonding on the emission of the compounds. The spectra recorded for the 1:1 complexes formed with octanol isomers show both blue (of the N* form) and green (of the T* form) emissions that cannot be attributed to a single species but point to different types of the complex. These two complexes are observed simultaneously, one undergoing fast ESIPT and thus producing green emission whereas in the other complex ESIPT is fully inhibited. Obviously, in the liquid state where inhomogeneous broadened bands are observed in emission and excitation, such a distinction cannot be made. The ability to form different types of hydrogen-bonding complexes with different abilities to exhibit ESIPT is probably a unique property of 3HC – 3HF systems. These molecules are specifically susceptible to external hydrogen-bonding

perturbations, since in the ground state there is only a weak intramolecular hydrogen bond, which is part of a five-membered ring [27].

References

1. P.K. Sengupta and M. Kasha, *Chem. Phys. Lett.*, **1979**, 68, 382.
2. G.J. Woolfe and P.J. Thistlethwaite, *J. Am. Chem. Soc.*, **1981**, 103, 6919.
3. M. Itoh, K. Tokumura, Y. Tanimoto, Y. Okada, H. Takeuchi, K. Obi and I. Tanaka, *J. Am. Chem. Soc.*, **1981**, 103, 4146.
4. A.J.G. Strandjord and P.F. Barbara, *Chem. Phys. Lett.*, **1983**, 98, 21.
5. A.J.G. Strandjord, S.H. Courtney, D.M. Friedrich and P.F. Barbara, *J. Phys. Chem.*, **1983**, 87, 1125.
6. D. McMorrow, T.P. Dzugan and T.J. Aartsma, *Chem. Phys. Lett.*, **1984**, 103, 492.
7. A.J.G. Strandjord and P.F. Barbara, *J. Phys. Chem.*, **1985**, 89, 2355.
8. B. Dick and N.P. Ernsting, *J. Phys. Chem.*, **1987**, 91, 4261.
9. G.A. Brucker and D.F. Kelley, *J. Phys. Chem.*, **1987**, 91, 2856.
10. S. Ameer-Beg, S.M. Ormson, R.G. Brown, P. Matousek, M. Towrie, E.T.J. Nibbering, P. Foggi and F.V.R. Neuwahl, *J. Phys. Chem. A*, **2001**, 105, 3709.
11. B.J. Schwarz, L.A. Peteanu and C.B.J. Harris, *J. Phys. Chem.*, **1992**, 96, 3591.
12. A. Muhlpford, T. Bultmann, N.P. Ernsting and B. Dick, Femtosecond Reaction Dynamics, Royal Netherlands Academy of Arts and Sciences, Amsterdam, **1993**; p. 83.
13. A.N. Bader, F. Ariese and C Gooijer, *J. Phys. Chem. A*, **2002**, 106, 2844.
14. A.P. Demchenko, A.S. Klymchenko, V.G. Pivovarenko and S. Ercelen, in R. Kraayenhof, A.J.W.G. Visser and H.C. Gerritsen (Eds.) Fluorescence Spectroscopy, Imaging and Probes - New Tools in Chemical, Physical and Life Sciences (Springer Series on Fluorescence Methods and Applications, Vol. 2, Springer-Verlag, Heidelberg, **2002**.
15. O.P. Bondar, V.G. Pivovarenko and E.S. Rowe, *Biochim. Biophys. Acta*, **1998**, 1369, 119.
16. A. Sytnik, D. Gormin and M. Kasha, *Proc. Natl. Acad. Sci. USA*, **1994**, 91, 11968.
17. J. Guharay and P.K. Sengupta, *Spectrochim. Acta A*, **1997**, 53, 905.
18. S.M. Dennison, J. Guharay and P.K. Sengupta, *Spectrochim. Acta A*, **1999**, 55, 1127.
19. J. Guharay, B. Sengupta and P.K. Sengupta, *Proteins*, **2001**, 43, 71.
20. G. Duportail, A.S. Klymchenko, Y. Mely and A.P. Demchenko, *FEBS Lett.*, **2001**, 508, 196.
21. A.S. Klymchenko, T. Ozturk, V.G. Pivovarenko and A.P. Demchenko, *Can. J. Chem.*, **2001**, 79, 358.
22. S. Ercelen, A.S. Klymchenko and A.P. Demchenko, *Anal. Chim. Acta*, **2002**, 464, 273.
23. A.S. Klymchenko, T. Ozturk, V.G. Pivovarenko and A.P. Demchenko, *Tetrahedron Lett.*, **2001**, 42, 7967.
24. M.A. Smith, R.M. Neumann and R.A.Webb, *J. Heterocyclic Chem.*, **1968**, 5, 425.
25. A.S. Klymchenko, V.G. Pivovarenko and A.P. Demchenko, *Spectrochim. Acta, A*, submitted.
26. I. Renge and U.P. Wild, Principles in matrix-induced high-resolution optical spectroscopy and electron-proton coupling in doped organic glasses, in C. Gooijer, F. Ariese and J.W. Hofstraat (Eds.) Shpol'skii spectroscopy and other site selection methods, Wiley and Sons, New York, **2000**.
27. D. McMorrow and M. Kasha, *J. Phys. Chem.*, 1984, 88, 2235.

CHAPTER 2.3

Excited state and ground state proton transfer rates of 3-hydroxyflavone and its derivatives studied by Shpol'skii spectroscopy; the influence of redistribution of electron density

Arjen N. Bader, Vasyl Pivovarenko, Alexander P. Demchenko, Freek Ariese, Cees Gooijer, *J. Phys. Chem. B*, **2004,** *108 (29),* 10589-10595

Abstract

We studied the mechanisms of excited-state intramolecular proton transfer (ESIPT) and ground-state back proton transfer (BPT) in 3-hydroxyflavone (3HF) at cryogenic temperatures. The focus was on substituents that change the distribution of electronic density on the chromophore and their influence on these reaction rates. Shpol'skii spectroscopy was applied for comparative studies of three compounds – 3HF, 3-hydroxy-4'-methoxyflavone (3HF-4'OMe) and 2-furyl-3-hydroxychromone (3HC-F). By comparing the spectral bandwidths with those of deuterated analogues we could distinguish the lifetime broadening components in the high-resolution excitation and emission spectra, from which the time constants of the ESIPT and BPT reactions were calculated. The time constants for the ESIPT reaction were 0.093 ps for 3HF, 0.21 ps for 3HF-4'OMe and slower than 0.6 ps for 3HC-F. For the same compounds the BPT rate were 0.21 ps, 0.47 ps and >2 ps, respectively. No change in bandwidth was observed over the temperature range 4 – 20 K, in agreement with a tunnelling mechanism. Estimates for the barrier heights and proton transfer distances are given. In addition, a systematic change in O-H bond strengths between ground and excited states was calculated from the isotope effect, observed as the shifts of the 0-0 bands in the excitation and emission spectra upon deuteration. The substantial effect of electron donating substituents on the rates of ESIPT and BPT reactions is in agreement with these changes.

Introduction

3-Hydroxyflavone (3HF; see Scheme 1) is one of the most intensively studied compounds that undergo excited-state intramolecular proton transfer (ESIPT). The unique feature of this molecule is that dual fluorescence emission can be observed: the normal form of the excited state (N*) emits in the blue and the excited-state tautomeric form (T*) in the green [1-7]. Since the rate of ESIPT (and therefore whether blue, green or dual emission is observed) depends on the interaction with the surrounding solvent molecules [2-7], it can be used as a ratiometric probe [8-10]. Newly synthesized 3HF derivatives exhibit a more significant electronic charge separation in the N* state [11-13]. This allowed us to observe dual emission in low polarity environments, and thus to extend dramatically the range of two-band ratiometric responses [14-18]. These ratiometric probes based on the 3HF chromophore become more and more functional; they allow efficient sensing at the molecular level of solvent polarity and electronic polarizability [19], hydrogen bond donor ability [20] and electrostatic field effects [21]. Their applications range from micelles [22] to proteins [23] and biomembranes and their phospholipid models [24-28]. Meanwhile, one of the fundamental questions remains unanswered: how do these changes in molecular structure influence the basic ESIPT rates? Since in the design of new probes the substitutions are commonly made at sites remote from the groups participating in ESIPT, we hypothesize that the proton transfer barrier heights could be strongly dependent on changes in electronic density in the groups involved. This study on ESIPT and BPT rates as a function of molecular (and primarily, electronic) structure will help us understand the underlying mechanisms and will be useful for the development of new advanced probes based on 3HF.

One of the most recent approaches for studying the ESIPT reaction in 3HF is using Shpol'skii spectroscopy [29,30]. Moreover, the rates of fast T→N ground-state back proton transfer (BPT) reaction can also be obtained, which is not possible using common time-resolved techniques [31,32]. When embedded in a cryogenic crystalline n-octane matrix, no solvent reorganisation can take place and to a good approximation all guest molecules experience the same solvent/solute interaction. As a result, for many compounds that fit in the Shpol'skii matrix in terms of polarity and geometry, the inhomogeneous broadening can be reduced to ca. 4 cm^{-1}. The idea behind using this approach for measuring proton transfer rates is that in cases where the rate of ESIPT is extremely fast - and therefore the lifetime of the N*

state extremely short - additional broadening in the excitation spectrum will be observable. Similarly, additional broadening observed in the emission spectrum will indicate a very short lifetime of the T state caused by the fast BPT reaction. A distinction between the effects of homogeneous (lifetime-dependent) broadening and inhomogeneous broadening (dependent on solvent environment effects) can be made by comparing the Shpol'skii excitation and emission spectra of 3HF and its deuterated analogue 3-deuteroxyflavone (3DF). Excited state intermolecular deuteron transfer (ESIDT) and back deuteron transfer (BDT) are much slower than ESIPT and BPT, respectively. The longer lifetime of the N* and T states and the insignificant homogeneous broadening contribution to the spectral lines allow us to determine the extent of inhomogeneous broadening in 3DF. Using these values for 3HF (the inhomogeneous broadening for protonated and deuterated compounds will be equal), the contribution from homogeneous broadening can be derived from the total broadening observed in the spectra, and the lifetimes of the N* and T states can be obtained [29].

Following this approach, it was estimated that ESIPT in 3HF in cryogenic Shpol'skii matrices takes place in approximately 40 fs [29]. Unfortunately, due to limited data handling possibilities of the CCD camera used in those experiments, the resolution in the excitation dimension was still relatively poor, i.e. no better than 0.5 nm. With our recently improved set-up, a kinetic series of a large number of emission spectra can be recorded, while the excitation wavelength of the dye laser is slowly scanned at a constant rate. This has resulted in a much better resolution in the excitation spectrum: in the present set-up the resolution is comparable to the one in emission (0.05 nm), which allows us to achieve a much higher precision in the determination of ESIPT rates in the femtosecond time range.

In a previous paper we studied derivatives of 3HF that contained at the 2-position a π-donor heterocycle with higher electron donor ability than phenyl: furyl, benzofuryl and naphthofuryl groups [30]. Interestingly, for these derivatives no broadening due to lifetime effects was observed and we concluded that ESIPT and BPT must take place at the picosecond timescale. Possible reasons for this slower proton transfer in both excited state and ground state are steric effects of the substituents with different geometry or electronic effects caused by different redistribution of electron density in the molecule. The oxygen in the furyl group might form a hydrogen bond with the 3-hydroxy group, resulting in a geometric effect, i.e., in a longer proton transfer distance to the carbonyl at the 4-position. As

will be shown below, these long proton transfer distances do not agree with the rates of proton transfer dealt with. The focus in this paper will therefore be on the electron donating ability of the 2-position of the chromone. An electron donating group at this position may affect the acidity of the 3-hydroxy group and the bond order of the 4-carbonyl group and therefore the basicity of its oxygen atom; both effects will influence the proton transfer rates.

In this paper we investigate the dynamics of the ESIPT and BPT processes in 3HF and in two of its derivatives (see scheme 1) in more detail using Shpol'skii spectroscopy, i.e., besides 3HF and 2-furyl-3-hydroxychromone (3HC-F), also 3-hydroxy-4'-methoxyflavone (3HF-4'OMe). The *p*-methoxy group in the latter compound is known for its electron donating properties, which makes it similar to the furyl-group. However, the *p*-methoxy group is expected to be somewhat less efficient in redistributing the electron density over the chromone moiety than a furyl group is.

3-hydroxyflavone (3HF)   **4'methoxy-3-hydroxyflavone (3HF-4'OMe)**   **2-furyl-3-hydroxychromone (3HC-F)**
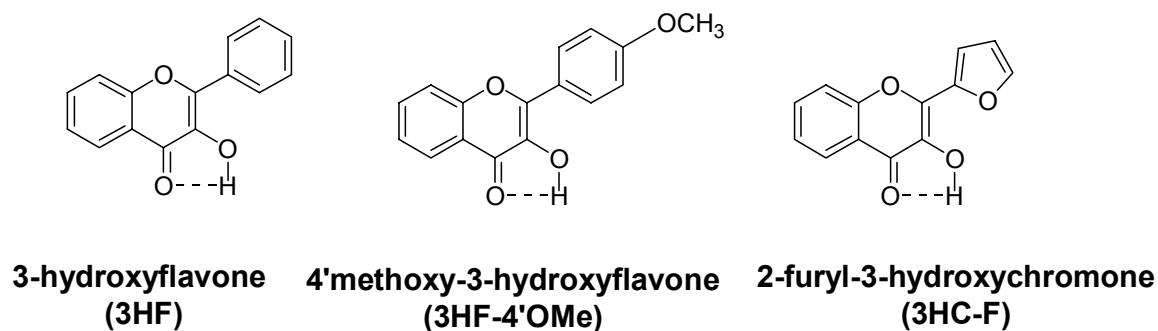
***Scheme 1:** Structures of the studied 3-hydroxyflavone derivatives*

The Shpol'skii spectroscopy approach to determine the rates of ESIPT and BPT allows us to study another effect as well. In the Shpol'skii excitation spectra of 3HF and 3DF, an energy difference between their N-N* transitions can be seen [29]. This isotope effect is not expected to be due to changes in the purely electronic $S_0 \rightarrow S_1$ energy difference, since substitution of a proton by a deuteron will not result in significant changes in the electronic structure of the molecule. However, if the strength of the O-H bond changes upon excitation, then the distance between the zero point energy (ZPE) levels in the ground and excited states will be different for 3-OH and 3-OD derivatives. The observation of such a difference in ZPE for these two isotope species gives direct information about the change in the 3-OH vibrational energy upon excitation and can therefore be used to verify the changes in the acidity or basicity of this group. Similar observations in emission deal with the tautomeric

forms of 3HF and 3DF and therefore indicate the changes in vibrational energy of the 4-OH group (formed as a result of ESIPT reaction). We will examine such shifts for 3HF-4'OMe and 3HC-F in order to study the effects of electron donating substituents on the proton transfer process.

Experimental

All measurements were done using 10^{-5} M solutions of 3-hydroxyflavone (Extrasynthèse, Genay, France), 2-furyl-3-hydroxychromone (synthesis described in earlier work [30]) and 3-hydroxy-4'-methoxyflavone (synthesis described below) dissolved in *puriss. n*-octane (Fluka). Deuteration of the flavones was achieved by adding the same volume of D_2O (Aldrich) to a solution of the flavone in octane. After shaking this two-phase system, deuteration of the 3-OH group of the flavone was achieved in 30 minutes. The upper layer formed is a solution of the deuterated flavone in *n*-octane. Any traces of incomplete deuteration could be clearly distinguished in the Shpol'skii spectra. No additional purification steps were applied to any of the samples. 30 μL of the sample solution was transferred to a 2 mm i.d. quartz tube that was closed with a septum.

3-Hydroxy-4'-methoxyflavone, (3HF-4'OMe) was prepared by alkaline condensation of 4-methoxybenzaldehyde with 2'-hydroxyacetophenone (both purchased from Aldrich) and subsequent oxidative heterocyclization of the obtained chalcone with hydrogen peroxide [33]. Light green-yellow crystals of 3HF-4'OMe were recrystallized twice from a 1% solution of acetic acid in ethanol and dried in vacuum at 110°C. The obtained crystals with m.p. 233-234°C (231-232°C [33]) presented a homogeneous product according to ^1H-NMR and TLC criteria. TLC was run on 50×150 mm plates of "Silufol" using 98:2, 95:5 and 9:1 (v/v) chloroform-methanol eluents. Checking for impurities was done under UV illumination at 254 and 356 nm. The ^1H-NMR spectrum of 3HF-4'OMe was measured on a Varian *Mercury-400* apparatus in DMSO-d_6. The chemical shifts, multiplicities (*s* – singlet, *d* – doublet, *t* – triplet, *m* – multiplet), and signal intensities (in brackets) were: 9.18*s*(1H); 8.21*d*(2H); 8.10*d*(1H); 7.75*t*(1H); 7.66*d*(1H); 7.41*t*(1H); 7.04*d*(2H); 3.86*s*(3H). The ^{13}C-NMR spectrum of 3HF-4'OMe was measured in DMSO-d_6 and showed the following chemical shifts: 173.2; 161.0; 155.0; 146.1; 138.7; 134.0; 130.0; 125.3; 125.0; 124.1; 121.9; 118.9; 114.6; 55.9.

Four quartz tubes at a time were placed in a row in a home made sample holder that was mounted to the top of the cold head of a closed cycle 4K liquid helium refrigerator (SRDK-205 Cryocooler, Janis Research Company, Wilmington, MA, USA). The excitation source was a XeCl excimer laser (Lambda Physik LPX 110i, Göttingen, Germany) pumping a dye laser (Lambda Physik, LPD 3002) at a repetition rate of 10 Hz. The excimer laser was operated at 10 Hz, producing 10 ns 50 mJ pulses. Using DMQ as a dye, a tuneable output in the 340 nm to 375 nm range was obtained, while QUI was used to enable excitation in the range from 370 to 400 nm. The four samples could be measured separately by moving the cold head at an angle of 45° with respect to both the excitation and emission beam. Fluorescence emission was collected with a 3 cm F/l.2 quartz lens at a 90° angle to the excitation beam, focused by a 10 cm F/4 quartz lens on the entrance slit of a Spex 1877 0.6 m triple monochromator (Edison, NJ, USA) and detected with an intensified CCD camera (iStar DH720-25U-03, Andor instruments, Belfast, Northern Ireland) operated in the gated mode to reject stray and scattered light. The spectral resolution of the emission spectrum was 0.1 nm.

The excitation spectra were obtained by measuring a kinetic series of emission spectra while the dye laser was scanned at a constant rate. In this study, this rate was 0.05 nm/spectrum. Every 5 seconds (or 50 pulses of the dye laser) a spectrum was recorded. The excitation spectra were obtained by plotting the intensity of a T←T* emission band (three pixels were summed) versus the excitation wavelength. In order to reduce the noise due to pulse-to-pulse intensity fluctuations, three kinetic series of emission spectra were recorded and averaged. No correction was applied for the wavelength dependency of the intensity of the dye laser nor for the intensity loss due to photodecomposition.

Results and discussion

The Shpol'skii emission spectra of 3-hydroxy-4'-methoxyflavone (3HF-4'OMe) in *n*-octane matrix recorded at different excitation wavelengths, are shown in Figure 1. The spectrum displays many sites, which overlap due to broadening effects (for the deuterated analogue much better resolution was observed, as shown below). As can be seen in this figure, there is one separate site at 519 nm and a cluster of approximately four sites between 520 – 524 nm. We will focus on the separate site to study line broadening effects. The excitation spectra of 3-hydroxyflavone and 2-furyl-3-hydroxychromone (3HC-2F) have been

published in earlier work [29,30]. Here, we report the improved spectra recorded under better instrumental resolution conditions.
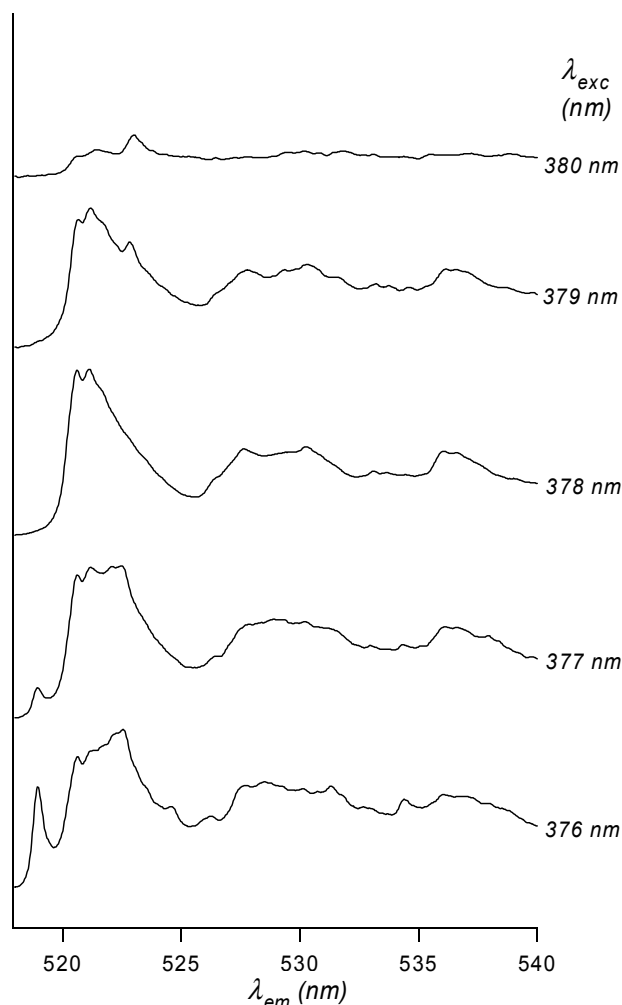
Figure 1: 4K Shpol'skii emission spectra of 3HF-4'OMe in n-octane, recorded at different excitation wavelengths.

The laser excited Shpol'skii excitation and emission spectra of all compounds (recorded using the same set-up) are shown in Figures 2 and 3, respectively. Because the focus is on bandwidths, only the (0,0) region of the major site is shown for each compound. As regards the line positions, for the deuterated compounds the major sites are found at excitation and emission wavelengths that differ from those of the non-deuterated compounds. In excitation the bands of the deuterated compounds are blue shifted whereas in emission they are red-shifted; this will be discussed in more detail below. Nonetheless, apart from the bandwidth, the site structures observed for the deuterated and the non-deuterated compounds are equal,
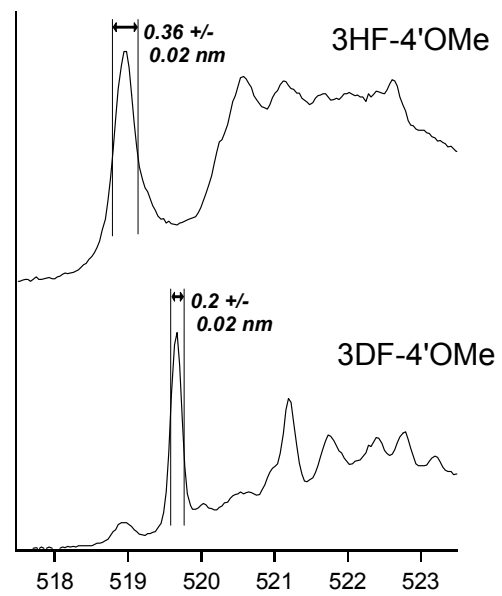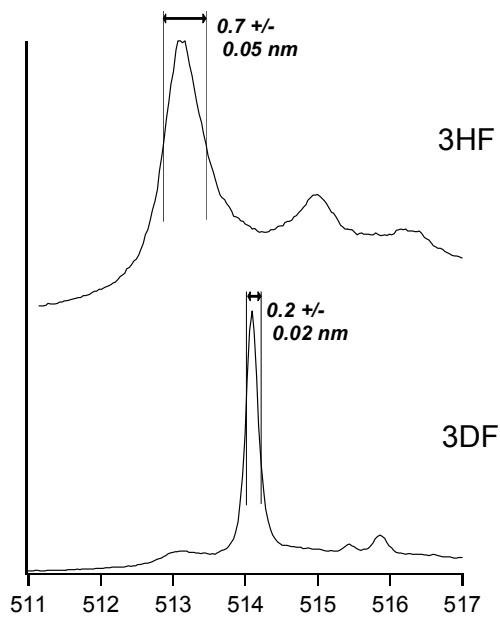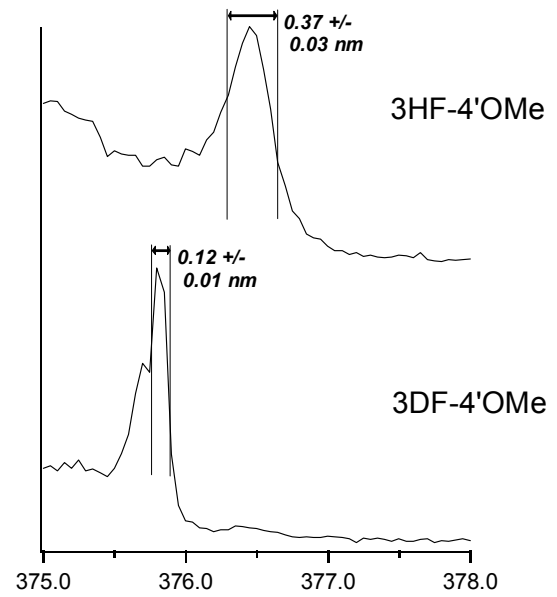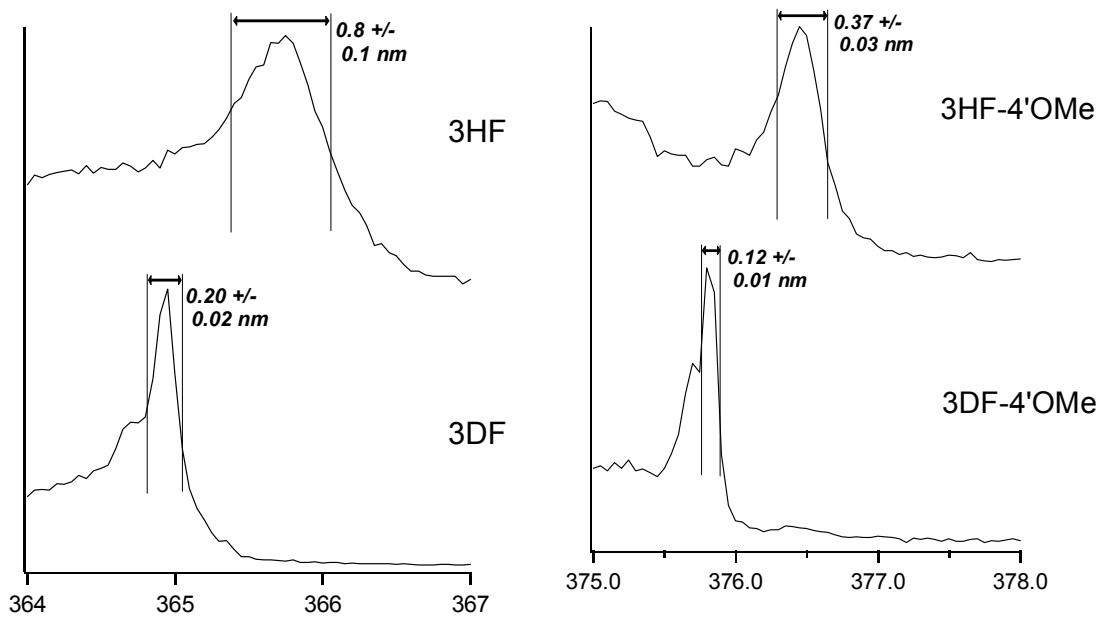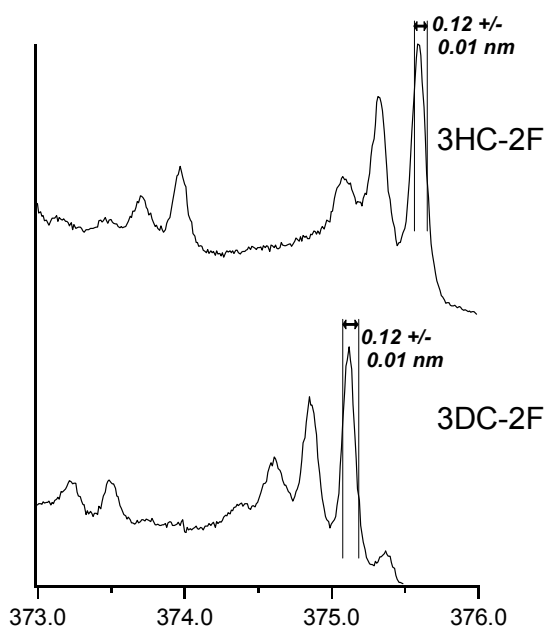
Figure 2: *4K Shpol'skii excitation spectra (0,0 regions) of 3HF, 3HF-4'OMe and 3HC-F and their deuterated analogues. The wavelengths of emission are given in Table 3. From the indicated values of the bandwidth, the rates of ESIPT are calculated (listed in Table 1).*
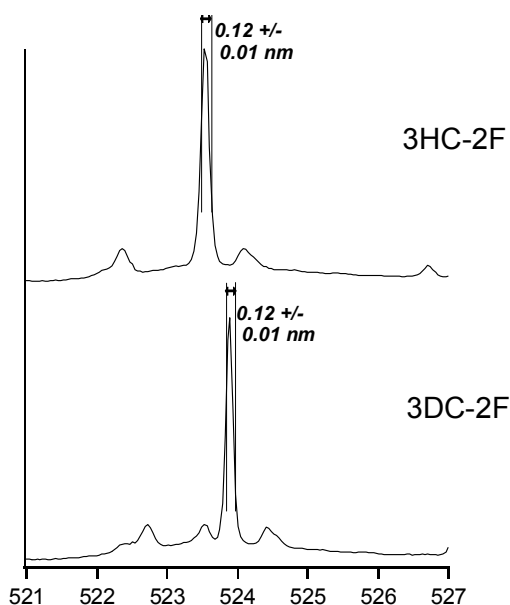
Figure 3: *4K Shpol'skii emission spectra (0,0 regions) of 3HF, 3HF-4'OMe and 3HC-F and their deuterated analogues. The wavelengths of excitation are given in Table 3. From the indicated values of the bandwidth, the rates of BPT are calculated (listed in Table 1)*

confirming that the fit of the studied compounds in the *n*-octane matrix is not changed by deuteration. The estimation of the excitation bandwidth Γ_{exc} from Figure 2 is much more accurate than that presented in earlier work [29,30], because of the smaller 0.05 nm scan steps applied. It should be emphasized that this improvement is not due to the lower sample temperature applied in the new set-up; when the new cryostat was set at 11K instead of 4K identical excitation spectra were observed.

Considering the three compounds in Figures 2 and 3, the bandwidths both in the excitation and in the emission spectra decrease in the order: $\Gamma_{3HF} > \Gamma_{3HF-4'OMe} > \Gamma_{3HC-2F}$. From these bandwidths, the lifetimes of the N* and T states can be calculated following the procedure outlined before [29]. Crucial is the assumption that for the deuterated compounds the (deuteron) transfer rates are too low to cause observable homogeneous broadening. The results are presented in Table 1. The calculated lifetimes of the N* and T state correspond to the rates of fast ESIPT and BPT, respectively.

Table 1 reveals that the differences between the ESIPT and BPT rates of 3HF and 3HF-4'OMe are similar and relatively small, they differ by only a factor of 2.2. For 3HC-2F, this regularity cannot be verified because the ESIPT and BPT rates are too slow to induce measurable line width changes. More interesting are the differences in ESIPT rates between the studied compounds. In 3HF-4'OMe compared to 3HF, the ESIPT is slower by only a factor of 2. ESIPT in 3HC-2F is much slower, i.e., more than 6 times compared to 3HF. These slower time constants observed for 3HF-4'OMe and 3HC-F, are expected to be due to the increase of electronic density located on the γ-pyrone ring of the molecule: stronger electron donating groups at the 2-position will result in a slower ESIPT reaction.

The observed spectral bandwidths, and therefore the proton transfer rates, were found to be temperature independent over a 4 – 20 K temperature range (not shown). This observation rules out thermal activation as the mechanism of proton transfer at low temperatures. Combined with the observed large differences between ESIPT and ESIDT (and similarly between BPT and BDT) rates, the conclusion can be drawn that tunnelling is the most likely mechanism of proton (and deuteron) transfer. Of course at higher temperatures, thermally activated processes will become more significant.

Table 1: *Rates of excited state intramolecular proton transfer (ESIPT) and back proton transfer (BPT) determined for 3HF and its derivatives. The rate of ESIPT is obtained from the total bandwidths of the site-selected band in the excitation spectra (see Figure 2). The rate of BPT was obtained from the total bandwidth of the site-selected band in the emission spectra (see Figure 3). The homogeneous broadening (Γ_{hom}) was calculated from the total broadening (Γ_{tot}), the instrumental broadening (Γ_{instr}) and the inhomogeneous broadening (Γ_{inh}) via $\Gamma_{tot}^2 = \Gamma_{instr}^2 + \Gamma_{inh}^2 + \Gamma_{hom}^2$.*

	Γ_{tot} (cm^{-1})		Γ_{instr} (cm^{-1})	Γ_{inh} (cm^{-1})		Γ_{hom} (cm^{-1})		τ_{pt} (ps)
	Min.	*Max.*		*Min.*	*Max.*	*Min.*	*Max.*	
3HF								
ESIPT	52	67	4	0	16	50	67	**0.093 ± 0.01**
ESIDT	14	17	4	0	16	0	16	> 0.3
BPT	24	28	4	0	7.3	23	28	**0.21 ± 0.02**
BDT	6.7	8.2	4	0	7.3	0	7.3	> 0.7
3HF-4'OMe								
ESIPT	24	29	4	0	8.3	22	29	**0.21 ± 0.03**
ESIDT	7.8	9.2	4	0	8.3	0	8.3	> 0.6
BPT	12	14	4	0	7.2	10	14	**0.47 ± 0.08**
BDT	6.7	8.2	4	0	7.2	0	7.2	> 0.7
3HC-2F								
ESIPT	7.8	9.2	4	0	8.3	0	8.3	**> 0.6**
ESIDT	7.8	9.2	4	0	8.3	0	8.3	> 0.6
BPT	4.0	4.7	4	0	2.5	0	2.5	**> 2**
BDT	4.0	4.7	4	0	2.5	0	2.5	> 2

In an oversimplified way, tunnelling in a proton transfer reaction can be described using a one-dimensional semi-classical model [34-36]. In this model, a parabolic barrier is used with width R (proton transfer distance) and height ΔE (maximum barrier height above the zero point energy) as parameters. Under these constraints, the rate of proton tunnelling (k_H) obeys the following equation:

$$k_H = \nu_H \exp \left[- (\pi^2 / h) \, R \, (2 \, m_H \, \Delta E)^{1/2} \right] \qquad (1)$$

wherein h is Planck's constant, m_H the proton mass and ν_H the vibrational frequency along the proton transfer reaction coordinate.

For the 3HF derivatives dealt with in the present study, an estimation of ν_H can not be easily made. This is due to the fact that the proton will presumably not be transferred exactly in the same direction as the OH-group's vibrational motions. The proton transfer coordinate will predominantly be determined by the OH stretching component, but the OH bending component and some (skeleton) vibrations may also be involved. In order to estimate the corresponding barrier heights according to the simple model of Equation (1), $\nu_H = 3500$ cm^{-1} was used. The resulting values of $R(\Delta E)^{1/2}$ and the values of ΔE (for a distance R = 0.2 Å and R = 0.4 Å) are given in Table 2.

Table 2: *Calculated values for the barrier in the ESIPT reaction using equation (1). For the vibrational frequency ν_H a value of 3500 cm^{-1} was chosen for all compounds.*

	ν_H	τ_{ESIPT}	$R(\Delta E)^{1/2}$	ΔE (R=0.2 Å)	ΔE (R=0.4 Å)	$\Delta E/\Delta E_{3HF}$
	(cm^{-1})	(ps)	(Å.(J/mol)$^{1/2}$)	(kJ/mol)	(kJ/mol)	
3HF	3500	0.093	20.6	10.5	2.6	1
3HF-4'OMe	3500	0.21	27.9	19.9	5.0	1.9
3HC-F	3500	> 0.58	>38	>36	>9.0	>3.4

For further analysis it is assumed that the proton transfer distances (i.e. the barrier widths) for 3HF and 3HF-4'OMe are equal, an assumption that seems quite reasonable in terms of molecular structures of these compounds. It should be noted that, although the calculated barrier heights are very low (especially when R = 0.4 Å), because of the low temperatures dealt with they are still higher than the activation energies. It was observed that 3HF-4'OMe shows a two times lower ESIPT rate (and BPT rate) than 3HF. Assuming that the barrier widths are equal for the three compounds, this implies that upon methoxy substitution at the 4'-position the barrier height increases with a factor of 1.9; it should be noticed that this outcome is independent of the proton transfer distance. Similarly, for 3HC-F a reduction in proton transfer rates – at least 6 times slower in comparison to 3HF - was observed. Therefore, the barrier height is thought to be enhanced at least 3.4 times upon substitution of the phenyl group in 3HF by a furyl group.

Equation (1) can also be used for a crude approximation of the rate of ESIDT (k_D); incorporation of deuteron mass m_D, vibrational frequency ν_D (= $2^{-1/2}\,\nu_H$) and ΔE_D (= ΔE_H − $ZPE_H + ZPE_D$) results in a one order decrease in the transfer rate when R = 0.2 Å and almost two order decrease in the transfer rate when R = 0.4 Å. This agrees with the results presented here: ESIDT should be slower than 0.5 ps (no additional homogeneous broadening in the excitation spectrum was observed), but significantly faster than the blue emission from the N* state ($\approx$ 1 ns), since such an emission is not observed. For 3HC-F, this means that the time constant for ESIPT is in the low picosecond range, since also its deuterated analogue is emitting in the green (again no blue emission was observed) and therefore has a sub nanosecond ESIDT time constant. Furthermore, as mentioned in the Introduction, H-bond formation between the 3-OH/3-OD group and the oxygen of the furyl group seems highly unlikely. In that case the barrier width would increase to more than 1.5 Å, resulting in an isotope effect of more than 5 orders of magnitude. This is in disagreement with the experiment.

Interestingly, the N→N* transitions for all the three compounds are blue shifted upon deuteration. As mentioned in the Introduction, this can be explained by a difference in ZPE. When the strength of the O-H vibration changes upon excitation, the ZPE of the electronic ground state is not equal to the ZPE in the excited state and a shift in the (0,0) transition energy upon deuteration can be expected, as illustrated in Figure 4. When comparing the ZPEs of the normal forms of 3HF and 3DF, only the contribution of the 3-OH vibrations to the total ZPE needs to be considered since to a good approximation the other molecular vibrations will not be affected. Upon deuteration the difference in reduced mass is approximately a factor of 2, so that the ZPE in 3HF has to be multiplied by $2^{-1/2}$ to obtain the value of the ZPE of 3DF. Therefore, from the (0,0) energy difference in excitation between 3HF and 3DF, the difference in ZPE between the ground ($ZPE_{H,N}$) and first excited ($ZPE_{H,N*}$) state can be calculated using:

$$ZPE_{H,N} - ZPE_{H,N*} = (1-2^{-1/2})^{-1}\,(\,\Delta E_H - \Delta E_D\,) \qquad = 3.414\,(\,\Delta E_H - \Delta E_D\,) \qquad (2)$$

as illustrated in Figure 4. In Equation (2), ΔE_H and ΔE_D are the observed (0,0) transition energies for the protonated and deuterated compound, respectively. Since only the 3-OH group is deuterated, the change in ZPE between ground and first excited state will be the net

result of the changes in the three OH-group vibrations (one stretching and two bending modes). Similarly, the change in ZPE can be calculated for the T*→T transition from the (0,0) bands in the emission spectra.

$$N^*$$

$$ZPE_{H,N^*}$$
$$ZPE_{D,N^*} = 2^{-1/2}\,ZPE_{H,N^*}$$

$$\Delta E_H = \Delta E_{N,N^*} + ZPE_{H,N^*} - ZPE_{H,N}$$

$$\Delta E_{N,N^*}$$

$$\Delta E_D = \Delta E_{N,N^*} + 2^{-1/2}\,(ZPE_{H,N^*} - ZPE_{H,N})$$

$$N$$

$$ZPE_{H,N}$$
$$ZPE_{D,N} = 2^{-1/2}\,ZPE_{H,N}$$
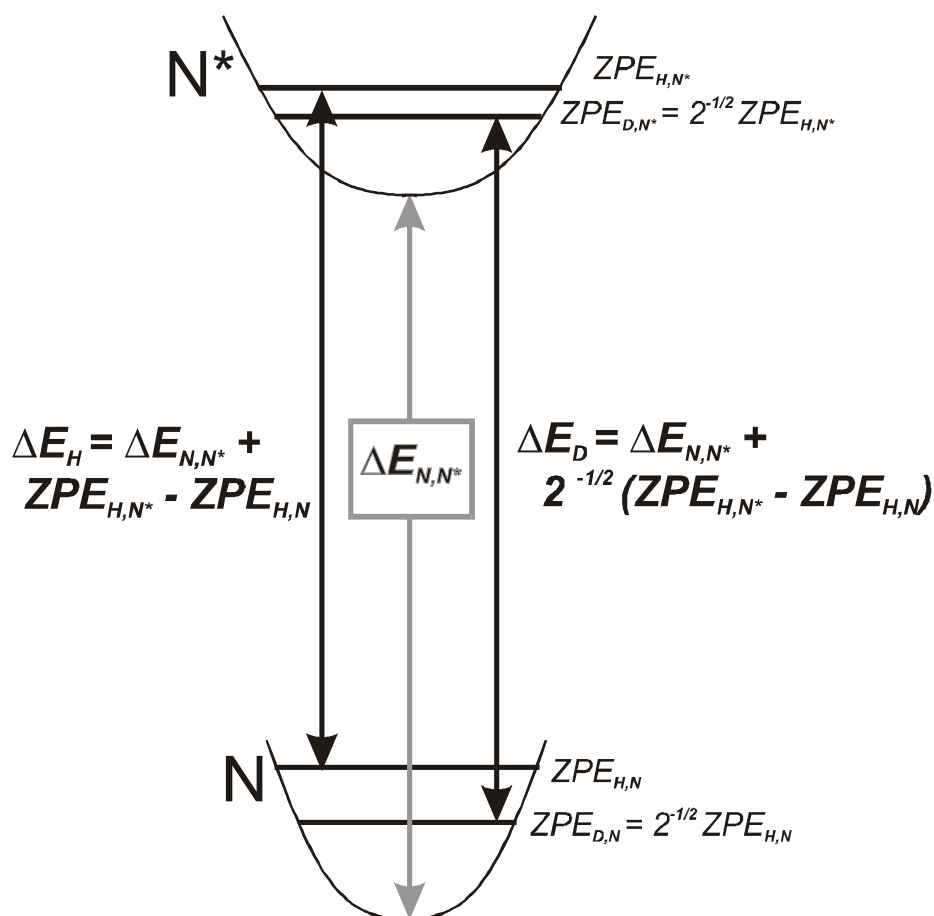
Figure 4: Zero point energy (ZPE) levels of the protonated compound (subscript index "H") and deuterated compound (subscript index "D") in ground state N and excited state N*. Energy differences ΔE_H and ΔE_D are the measured values obtained from the (0,0) bands in the Shpol'skii excitation spectrum. Combining the equation for ΔE_H and ΔE_D results in equation (2).

In Table 3, the values of ($ZPE_{H,N}$ - ZPE_{H,N^*}) and ($ZPE_{H,T}$ - ZPE_{H,T^*}) are given for the three compounds studied here. In excitation, the blue shift indicates that the difference in ZPE - and therefore the energies of the three O-H vibrations - decrease upon going from the N state to the N* state. This indicates a weakening of the O-H bond. Similarly, the red-shift of the (0,0) transition observed in the emission spectra upon deuteration implies a decrease of the difference in ZPE between protonated and deuterated derivatives after the T←T* transition. This indicates that the 4-OH group formed as the result of ESIPT is weakened if T←T* takes place. Both effects can be readily conceived: the OH bond becomes less strong before proton

transfer is taking place. This explains the observed fast ESIPT (N* → T*) in the excited state and the fast BPT (T → N) in the ground state.

Table 3:*Wavelengths of the main sites in the Shpol'skii excitation and emission spectra. For every compound, the difference between λ_H and λ_D is used to calculate the difference in zero-point energy (ZPE), both for the normal form and the tautomeric form.*

	λ_{exc}	$\Delta E_H - \Delta E_D$	$ZPE_{H,N} - ZPE_{H,N*}$	λ_{em}	$\Delta E_H - \Delta E_D$	$ZPE_{H,T} - ZPE_{H,T*}$
	(nm)	*(cm^{-1})*	*(cm^{-1})*	*(nm)*	*(cm^{-1})*	*(cm^{-1})*
3HF	365.75	60	205	513.14	-36	-123
3DF	364.95			514.09		
3HF-4'OMe	376.45	44	150	518.95	-27	-91
3DF-4'OMe	375.82			519.67		
3HC-F	375.60	34	116	523.55	-13	-44
3DC-F	375.12			523.90		

Interestingly, by comparing the magnitude of the changes in ZPE found for the three compounds, the largest O-H weakening is observed for 3HF, the compound with the highest proton transfer rates, and the smallest effect is observed for the compound with the lowest proton transfer rates, 3HC-F. The weakening of the OH-bond in the N* state means an increase in the acidity of this group, which may explain the fast ESIPT. In presence of an electron donating group at the chromone's 2-position, there is a smaller increase in the acidity of the 3-OH group, resulting in a lower ESIPT rate. Similarly for the BPT reaction, the weakening of the O-H bond at the 4-position in the T state compared to the T* state implies that the acidity of this group becomes higher in the ground state. Consequently, the weakening of the O-H bond will increase the C-O bond order at the 4-position. This explains the high rate of BPT in 3HF. Electron donating substituents in 3HF-4'OMe and 3HC-F, however, will reduce both effects and therefore cause a reduced BPT rate.

It can be concluded that the electron donating substituents have a strong influence on the proton tunnelling rates of 3HF and its derivatives. They can significantly reduce the rate of both ESIPT and BPT. These results will help us understand the photophysical behaviour of this important class of compounds.

Acknowledgements

References

1. Sengupta, P.K.; Kasha, M. *Chem. Phys. Lett*. **1979**, *68*, 382-385
2. Woolfe, G.J.; Thistlethwaite, P.J.; *J. Am. Chem. Soc.* **1981**, *103*, 6916-6923
3. Itoh, M.; Tokumura, K.; Tanimoto, Y.; Okada. Y.; Takeuchi, H,; Obi, K.; Tanaka, I. *J. Am. Chem. Soc.* **1982**, *104*, 4146-4150
4. Strandjord, A.J.G.; Courtney, S.H.; Friedrich, D.M.; Barbara, P.F. *J. Phys. Chem.* **1983**, *87*, 1125-1133
5. McMorrow, D.; Kasha, M. *J. Phys. Chem.* **1984**, *88*, 2235-2243
6. Strandjord, A.J.G.; Barbara, P.F. *J. Phys. Chem.* **1985**, *89*, 2355-2361
7. Brucker, G.A.; Kelley, D.F. *J. Phys. Chem.* **1987,** *91*, 2856-2861
8. Sytnik, A., Gormin, D. and Kasha, M., *Proc. Natl. Acad. Sci. USA*, **1994**, *91,* 11968-11972.
9. Sarkar, M., Ray, J.G. and Sengupta, P.K. *Spectrochim. Acta A* **1996**, *52*, 275-278.
10. Guharay, J., Sengupta, B. and Sengupta, P.K., *Proteins*, **2001**, *43,* 75-81.
11. Swiney, T. C.; Kelley, F. D. *J. Chem. Phys.* **1993**, *99*, 211-221.
12. Chou, P. T.; Martinez, M. L.; Clements, J. H. *J. Phys. Chem.* **1993**, *97*, 2618-2622.
13. Ormson, M. S.; Brown, R. G.; Vollmer, F.; Rettig, W. *J. Photochem. Photobiol.* **1994**, *81*, 65-72.
14. A.P. Demchenko, A.S. Klymchenko, V.G. Pivovarenko and S. Ercelen, in R. Kraayenhof, A.J.W.G. Visser and H.C. Gerritsen (Eds.), *Fluorescence Spectroscopy, Imaging and Probes - New Tools in Chemical, Physical and Life Sciences* (Springer Series on Fluorescence Methods and Applications, Vol. 2, Springer-Verlag, Heidelberg, 2002). pp. 101-110.
15. Klymchenko, A.S., Ozturk, T., Pivovarenko, V.G. and Demchenko, A.P., *Can. J. Chem.*, **2001**, *79,* 358-363.
16. Klymchenko, A.S., Ozturk, T., Pivovarenko, V.G. and Demchenko, A.P., *Tetrahedron Lett.*, **2001**, *42*, 7967-7970.
17. Ercelen, S., Klymchenko, A.S. and Demchenko, A.P., *Anal. Chim. Acta*, **2002**, *464*, 273-287.
18. Klymchenko, A.S., Pivovarenko, V.G., Ozturk, T., Demchenko, A.P. *New J. Chem.* **2003**, *27*, 1336-1343.
19. Klymchenko, A.S., Demchenko, A.P., *Phys. Chem. Chem. Phys.* **2003,** *5*, 461-468.
20. Klymchenko, A.S., Pivovarenko, V.G., Demchenko, A.P., *J. Phys. Chem. A.* **2003,** *107*, 4211-4216.
21. Klymchenko, A. S., Demchenko, A. P. *J. Am. Chem. Soc.* **2002**, *124*, 12372-12379.
22. Klymchenko, A. S., Demchenko, A. P. *Langmuir* **2002**, *18*, 5637-5639.
23. Ercelen, A.S., Klymchenko, A. S., Demchenko, A. P. *FEBS Lett.* **2003**, *538*, 25-28.
24. Bondar, O.P., Pivovarenko, V.G., and Rowe, E.S., *Biochim. Biophys. Acta,* **1998**, *1369,* 119-130.
25. Dennison, S.M., Guharay, J. and Sengupta, P.K., *Spectrochim. Acta A*, **1999,** *55,* 1127-1132.
26. Duportail, G., Klymchenko, A.S., Mely, Y. and Demchenko, A.P., *FEBS Lett.,* **2001**, *508,* 196-200.
27. Klymchenko, A. S.; Duportail, G.; Ozturk, T.; Pivovarenko, V. G.; Mély, Y.; Demchenko, A. P. *Chem. Biol.* **2002**, *9*, 1199-1208.
28. Klymchenko, A.S., Duportail,G., Mely, Y., Demchenko, A.P. *Proc. Natl. Acad. Sci. USA* , **2003**, *100*, 11219-11224.
29. Bader, A.N., Ariese, F. and Gooijer, C., *J. Phys. Chem. A*, **2002**, *106*, 2844-2849.

30. Bader, A.N., Pivovarenko, V.G., Demchenko, A.P., Ariese, F. and Gooijer, C., *Spectrochim. Acta A*, **2003**, *59,* 1593-1603.
31. Schwarz, B.J.; Peteanu, L.A.; Harris, C.B. *J. Phys. Chem. A* **1992**, *96*, 3591-3598
32. Ameer-Beg, S.; Ormson, S.M.; Brown, R.G.; Matousek, P.; Towrie, M.; Nibbering, E.T.J.; Foggi, P.; Neuwahl, F.V.R. *J. Phys. Chem. A* **2001**, *105*, 3709- 3718
33. Smith, M.A., Neumann, R.M., Webb, R.A., *J. heterocyclic Chem.* **1968**, *5*, 425-426
34. Yu, W.-S., Cheng, C.-C., Chang, C.-P., Wu, G.-R., Hsu, C.-H., Chou, P.-T., *J. Phys. Chem. A*, **2002,** 106, 806-8012
35. Douhal, A., Lahmani, F., Zewail, A.H., Chem. Phys. **1996**, *207*, 477-498
36. Bell, R.P., The tunnel effect in chemistry (Chapmann and Hall, New York, 1980), chapter 2

CHAPTER 3

Protein-ligand interaction
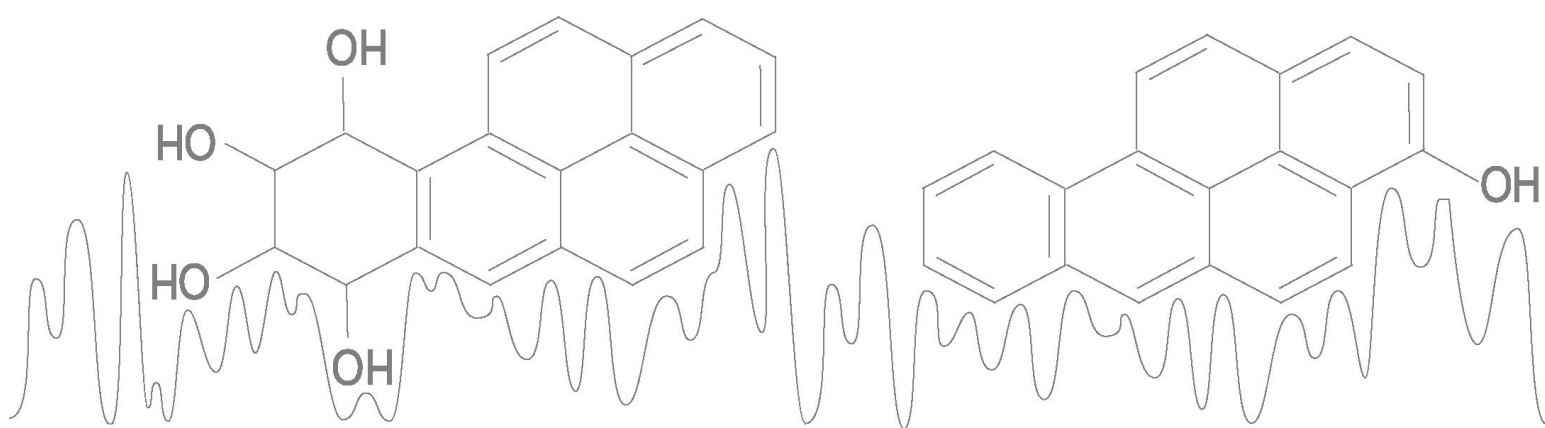
Probing the interaction of benzo[*a*]pyrene adducts and metabolites with monoclonal antibodies using fluorescence line-narrowing spectroscopy

Arjen N. Bader, Nenad M. Grubor, Freek Ariese, Cees Gooijer,
Ryszard Jankowiak, and Gerald J. Small, *Anal. Chem.*, **2004**, *76 (3)*, 761-767

Abstract

A new approach for studying antibody/antigen interactions of DNA adducts and metabolites of polycyclic-aromatic hydrocarbons (PAHs) is demonstrated in which fluorescence line-narrowing spectroscopy (FLNS) is used. It is based on the fact that in an FLN spectrum the relative intensities of the line-narrowed bands that correspond to the excited state vibrations in an FLN spectrum (that correspond to the excited state vibrations) are, in general, strongly dependent on the local environment of the fluorophore. Information on the nature of the interactions can be obtained by comparing the FLN spectra of the antigen/antibody complexes to the spectra of the antigen in different types of solvents (H-bonding, aprotic, π-electron containing solvent molecules) recorded under the same conditions. The antigens used were the DNA adduct 7-(benzo[*a*]pyren-6-yl)guanine (BP-6-N7Gua) and the metabolite (+)-*trans-anti*-7,8,9,10-benzo[*a*]pyrenetetrol (BP-tetrol) of benzo[*a*]pyrene; two monoclonal antibodies (MAb) have been developed to selectively bind these compounds. It is shown that for BP-tetrol, H-bonding solvents have a pronounced effect on the FLN spectra. The presence of π-electrons in the solvent molecules results in relatively small but still significant changes in the spectra. When BP-tetrol is bound to its MAb, however, neither of these effects is observed; its spectrum is very similar to the one obtained with an aprotic solvent, methylcyclohexane. Therefore, we can conclude that this MAb has an internal binding site in which the interaction with BP-tetrol is of a hydrophobic character. For BP-6-N7Gua, however, there is a strong effect of the presence of π-electrons in the solvent molecules. The FLN spectrum of this antigen bound to its MAb is very similar to its spectrum in acetone, indicating that π–π interactions play an important role in the binding.

Introduction

In recent years monoclonal antibodies (MAbs) have become increasingly popular in bioanalytical chemistry [1]. When immobilized on a chip or optical fiber, they can be used as biosensors [2,3]. Because MAbs can be developed that selectively bind the compound(s) of interest, sample pre-treatment and separation requirements can be less stringent in the total analytical scheme. Even for the analysis in complex biological matrices like blood, urine and plasma they can often be used directly [1]. Several papers have addressed the mechanisms of ligand-MAb binding [4-7]. Nonetheless, not in all cases are MAbs specific enough; they show cross-reactivity [8]. Thus, there is a need for simple methodologies that provide insight on the nature of antibody-antigen interactions.

One application of MAbs is the monitoring of DNA adducts and metabolites of polycyclic aromatic hydrocarbons (PAHs) in urine [9]. PAHs are formed after incomplete combustion of organic material and many PAHs are potent carcinogens. Benzo[*a*]pyrene (B[*a*]P), known as one of the most carcinogenic PAHs, is present in relatively high concentrations in traffic exhaust, cigarette smoke, and grilled or smoked food products [10,11]. In vertebrates, PAHs are oxidized in order to form more polar and, therefore, more easily excretable metabolites. However, some metabolic processes lead to reactive, electrophilic intermediates that can initiate cancer. B[*a*]P can be metabolically activated via three main pathways [12-14]: one-electron oxidation to yield radical cations, monooxygenation to produce bay-region diol epoxides and, thirdly, the formation of reactive and redox active o-quinones by dihydrodiol dehydrogenases. The active intermediates can bind to DNA to form stable and/or depurinating adducts [12-14]. The depurinating adducts are released from DNA by destabilization of the N-glycosidic bond and excreted in urine. Determination of depurinating adducts or metabolites in urine can be used for cancer risk assessment studies. For that purpose antibodies have been developed that selectively bind such compounds [15].

Since most PAHs are highly fluorescent, fluorescence spectroscopy can be used for the detection of PAH adducts bound to MAbs. However, most MAbs lack the specificity required to bind only one adduct or metabolite, so that conventional fluorescence is not always adequate for distinguishing between different antigens possessing the same parent fluorophore. Under such conditions a more specific, high-resolution technique like

fluorescence line-narrowing spectroscopy (FLNS) can be used for additional selectivity [8,15]. FLNS has proven to be useful for the detection of PAH adducts and metabolites, since it can distinguish between (stereo-)isomers and between metabolites bound to different nucleophilic sites [16]. FLN spectra of PAH-derived metabolites and/or PAH-DNA adducts bound to a MAb have also been reported [17].

The principles of FLN spectroscopy have been discussed in earlier work [20,21]. Briefly, in FLNS solute molecules are imbedded in an amorphous host matrix held at a temperature in the vicinity of 4 K. At such temperatures, thermal broadening of the origin and vibronic fluorescence bands is minimized. However, the structural disorder of the host results in severe static inhomogeneous broadening (typically $\sim$ 100-300 cm^{-1}) of the origin and vibronic absorption and emission bands. The basic idea of FLNS is that with narrow-line laser excitation, only those solute molecules whose absorption transition frequency overlaps the laser profile are excited, and only this subselection ("isochromat") will fluoresce. Typically, such line-narrowing leads to a two order of magnitude improvement in resolution. The sharpest bands in a FLN spectrum are referred to as zero-phonon lines (ZPLs) because low frequency lattice vibrations (phonons) of the solute/host system are not involved. However, electron-phonon coupling associated with the $S_0 \rightarrow S_1$ transition may lead to a broad phonon sideband (PSB) that builds on the red side of the sharp ZPLs in the emission spectrum. Upon tuning the laser wavelength λ_{exc} to a vibronic region of the S_1 state, typically several different vibrations are simultaneously excited. Subsequently, these excited molecules rapidly relax to the zero point vibrational level of the S_1 state after which fluorescence occurs. This results in the so-called multiplet origin structure in the FLN spectrum. The differences in energy between the ZPLs of the multiplet origin structure and λ_{exc} yield the excited state vibrational frequencies of the $S_0 \rightarrow S_1$ transition [20]. The relative intensities of the ZPLs in the multiplet depend strongly on their position in the inhomogeneously broadened vibronic absorption band. These absorption bands can shift in energy and vary in width, depending on the solvent. Therefore, the relative intensities of the ZPLs in the multiplet origin bands are extremely sensitive to the interaction with the solvent and can thus be used to probe the local environment of the fluorophore [22]. Furthermore, the intensity ratio between the ZPLs and the broad background is a measure for the strength of the coupling of the fluorophore with the matrix (electron-phonon coupling) [23].

So far, few applications of FLNS for probing purposes have been reported. Kumke *et al* used FLNS to probe pyrene - humic acid interactions [22], and Suh *et al* [23] showed that FLN spectra of intercalated B[*a*]P-DNA adducts are strongly influenced by π−π interactions with neighbouring DNA bases. Here, it will be shown for the first time that the binding interaction between antibodies and antigens can be studied using FLNS. The approach followed here is to compare the FLN spectrum of an antibody/antigen complex with the FLN spectra of the antigen in various solvents of different chemical nature. Whereas other methodologies like surface plasmon resonance [5] and ELISA [6] give information about the affinity of antibody-antigen binding as such, our approach provides information on the nature of the intermolecular interactions that lead to binding. Furthermore, the crystal structure of the MAb is not needed, as in molecular modeling studies [4,7].

In this paper we will focus on one particular B[*a*]P adduct and one particular B[*a*]P metabolite for which MAbs have been developed. The adduct, 7-(benzo[*a*]pyren-6-yl)guanine (BP-6-N7Gua), is formed upon one-electron oxidation, whereas the metabolite (+)-*trans-anti*-7,8,9,10-benzo[*a*]pyrenetetrol (BP-tetrol), is formed upon monooxygenation and hydrolysis (see Scheme 1). Both the metabolite and adduct are biomarkers and can be found in urine; BP-tetrol is a biomarker of exposure and metabolism and BP-6-N7Gua is a biomarker of actual DNA damage [18,19].
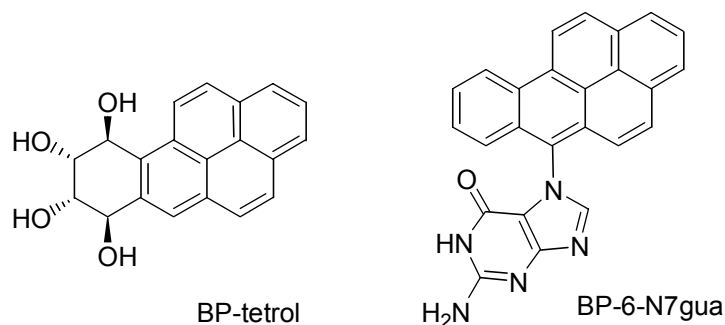
Scheme 1: Structures of BP-tetrol and BP-6-N7Gua.

Experimental

Caution: PAHs are hazardous chemicals and should be handled carefully in accordance with NIH guidelines.

The solvents used were dimethylsulfoxide, acetone, methylcyclohexane (Aldrich, Milwaukee, WI), ethanol (Fisher, Fair Lawn, NJ), glycerol (Spectrum Chemical Mfg. Corp.,

Gardena, CA) and an aqueous PBS buffer (0.1M sodium phosphate, 0.15 M sodium chloride). 10 μM solutions of BP-tetrol and BP-6-N7Gua were used to record FLN spectra with a sufficiently high intensity to make a peak assignment with a S/N ratio > 3 and a wavenumber reproducibility better than 5 cm^{-1}. Increasing the concentration will not result in better spectra, because at higher concentrations energy transfer will result in additional broadening [24]. The MAbs used in this study were monoclonal antibody CB53 (raised against BP-6-N7Gua, provided by Dr. G. Casale, University of Nebraska Medical Center, Omaha, NE) and *anti*-BPDE antibody 8E11 obtained from Trevigen (Gaithersburg, MD). The latter also has an affinity for BP-tetrol [25]. The antigen bound to the MAb was measured in solution: 2 mL of an aqueous solution containing 1 μM of antigen and 5 μg/ml MAb was incubated for 2 hours. The excess of antigen was removed using an ultrafree–4 centrifugal filter with Biomax-5 membrane (Millipore Corporation, Bedford, MA). Two additional washing steps were performed and the samples were concentrated by reducing the volume to 100 μL. These samples were diluted (1+1) with glycerol to obtain a glassy matrix under cryogenic conditions. 30 μL samples were transferred to quartz tubes (2 mm i.d.) for FLN analysis, the irradiated volume was about 1 μL.

The quartz tubes were immersed in liquid helium contained in a cryostat with quartz optical windows (H. S. Martin Inc., Vineland, NJ). The excitation source was a Lambda Physik Scanmate 2 pulsed dye laser, pumped by a Lambda Physik Lextra 100 XeCl excimer laser (Lambda Physik, Ft. Lauderdale, FL) at a repetition rate of 10-30 Hz. Fluorescence emission was collected with a 2-inch lens at a 90° angle to the excitation beam, focused onto the entrance slit of a 1-m monochromator (McPherson model 2061), and detected with an intensified linear photodiode array (model IRY-1024/GRB, Princeton instruments, Trenton, NJ) operated in the gated mode to reject scattered light. With the 2400 G/mm grating the spectral resolution was 0.05 nm (high-resolution conditions: FLN measurements of the ZPL origin multiplet structure). A 150 G/mm grating and a resolution of 0.8 nm was used for recording full fluorescence emission spectra at 77K (low-resolution conditions). Background subtraction was performed with Origin 5.0 (Microcal Software Inc, Northampton, MA) by creating a 50-point baseline using the software's "create baseline" option and manual modification.

Results and Discussion

In this study the FLN spectra of MAb-bound BP-tetrol and BP-6-N7Gua are compared to their spectra in various solvents of different chemical nature. For BP-tetrol, the stereochemistry of its four hydroxyl groups attached to the saturated ring has a large effect on the FLN spectrum [18] and, thus, an effect of H-bonding solvents can be expected. In the case of BP-6-N7Gua, the only H-bonding atoms are located on the guanine moiety and any effect on the fluorophore from H-bonding is expected to be less pronounced. However, it has been shown that $\pi-\pi$ interactions have a strong effect on the FLN spectra of B[a]P-DNA adducts. This is the result of interactions of the intercalated fluorophore with the DNA bases which results in the fluorophore's S_1 state possessing charge-transfer character [23].

Apart from their chemical characteristics, the solvents were chosen such that under cryogenic conditions the solute molecules would be in an amorphous matrix. For this purpose, 50% glycerol is often added to aqueous solutions, and also in this study the antigen/antibody complexes were dissolved in 50/50 glycerol/buffer solution. In order to study the effect of H-bonding two protic solvents were selected: ethanol (EtOH) and 50/50 glycerol/buffer. The latter was also used to dissolve the antibody/antigen complex, so a difference in the FLN spectrum would indicate that the antigen is not free in solution and therefore must be bound to the antibody. As an aprotic aliphatic solvent, methylcyclohexane (MCH) was chosen. For the study of the effect of π-electron containing solvent molecules, acetone and dimethylsulfoxide (DMSO) were chosen. The two hydrogen bonding solvents and the two π-electron containing solvents all have different dielectric constants, so a possible dependency on this parameter should also be visible in the spectra.

BP-tetrol

The 77K fluorescence spectrum of BP-tetrol bound to MAb was recorded and compared to its spectra in the five abovementioned solvents, recorded under the same conditions (see Figure 1). In the low-resolution spectra of Figure 1 no major differences in the positions and the relative intensities of the bands can be observed, only some minor shifts and changes in bandwidth. Although reproducible, these effects were relatively small compared to the spectral bandwidth observed under these conditions. Therefore we concluded that high-

resolution spectra would be needed to obtain more detailed information about antibody/antigen binding.
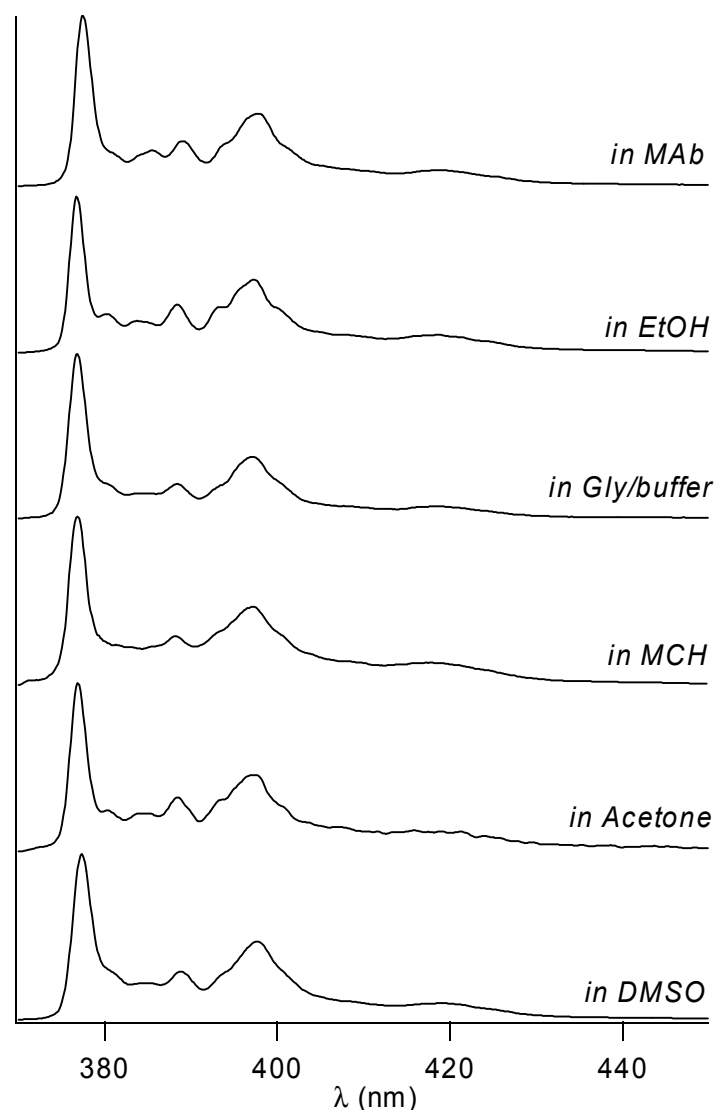
Figure 1: *77K low-resolution fluorescence spectra of BP-tetrol in various solvents. Excitation wavelength is 350 nm into the $S_0 \rightarrow S_2$ transition.*

Under high resolution FLN conditions the solvent effects for BP-tetrol in the (0,0) band region (375 to 380 nm, see Figure 2) are much more pronounced. The FLN spectra show pronounced ZPLs superimposed on a relatively weak broad fluorescence background (dotted lines). This background is a genuine part of the spectrum and is due to phonon sidebands and spectral congestion, *i.e.,* it is not related to impurities or solvent blank. The positions of the multiplet origin ZPLs are virtually identical in the different solvents (experimental

uncertainty $\pm$ 3 cm^{-1}), indicating that the intramolecular vibrational energies of the S$_1$ state are not significantly affected by the environment. In Figure 3 for each spectrum a background (the dotted lines in Figure 2) is subtracted in order to better compare the relative intensities of the ZPLs (this background was determined manually using the system's software). Apparently, the FLN spectrum of BP-tetrol is hardly influenced by the dielectric constant (ε_r) of the solvent: in aprotic polar solvents like acetone ($\varepsilon_r = 20$) and DMSO ($\varepsilon_r = 47$) and in the non-polar solvent MCH ($\varepsilon_r = 2$) similar spectra were obtained. The same was observed for other excitation wavelengths probing different S$_1$ vibronic regions (not shown).
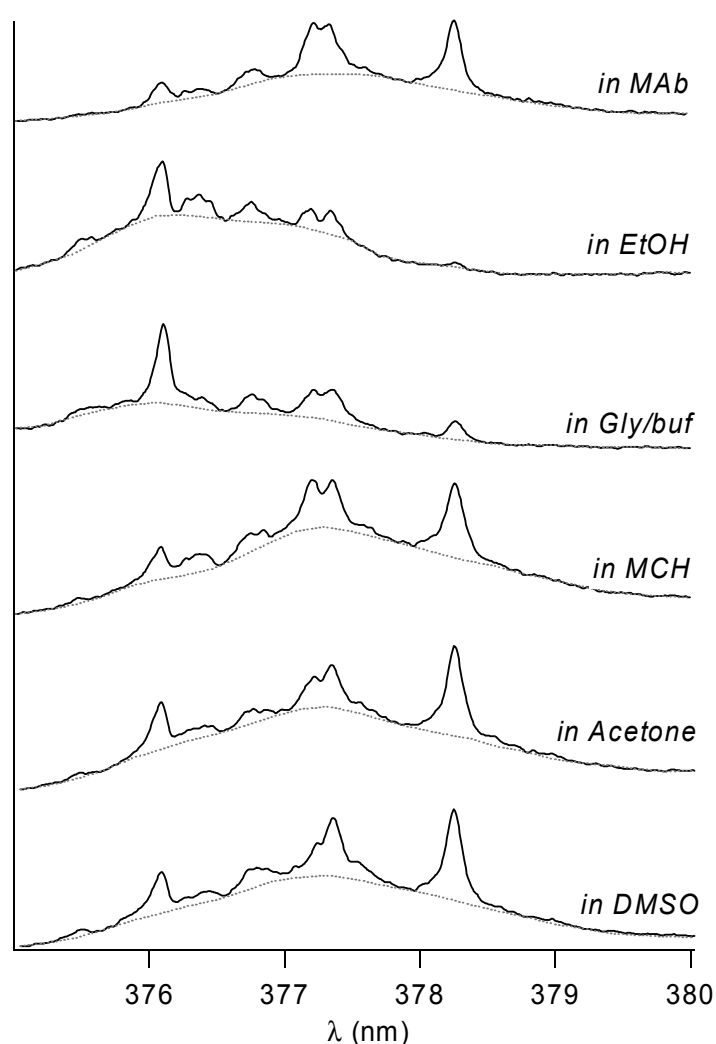
Figure 2: *FLN spectra of the multiplet origin band of BP-tetrol bound to MAb and in various solvents, excited at 363.0 nm. The dotted lines are the background spectra that are subtracted to yield figure 3.*
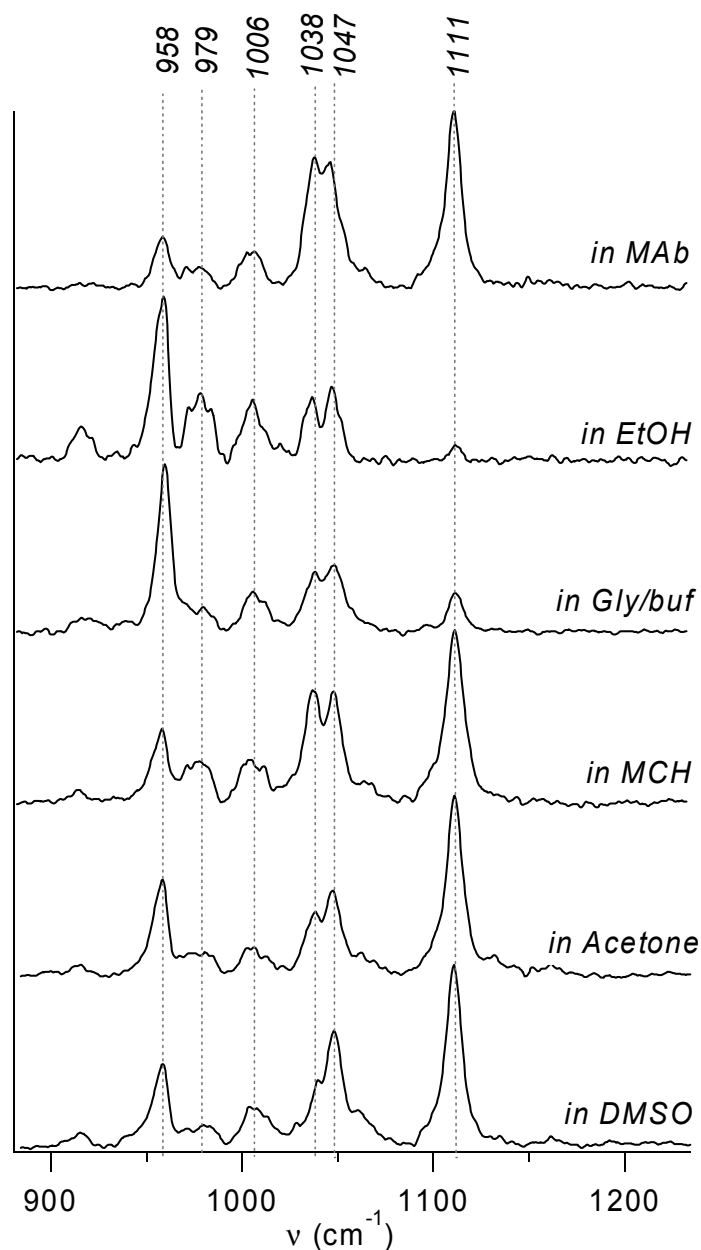
Figure 3: *Background subtracted FLN spectra of the multiplet ZPL origin region of BP-tetrol in various solvents, excited at 363.0 nm (background: see figure 2). The numbers labeling the ZPLs are the S_1 state vibrational energies in cm^{-1}.*

On the contrary, the ZPL intensity distributions for the aprotic solvents differ significantly from the distributions for the H-bonding solvents EtOH and 50/50 glycerol/buffer. This is most evident by comparing the intensities of the ZPLs at 958 and 1111 cm^{-1} in the various spectra. For BP-tetrol in EtOH and 50/50 glycerol/buffer, the excited state mode at 958 cm^{-1} is much more intense than the mode at 1111 cm^{-1}. Conversely, in the aprotic solvents MCH, acetone and DMSO, the opposite is observed. This indicates that the spectrum is strongly

influenced by H-bonding that leads to a blue-shift of the $S_0{\rightarrow}S_1$ transition. (That π-π^* states are blue-shifted in H-bonding solvents has been observed before [26]). Under close examination this shift is already noticeable in the 77K emission spectra of Figure 1, but under FLN conditions this blue shift is much more apparent, since it is accompanied by a significant increase in the intensity of the ZPLs at the blue flank of the origin band and a corresponding decrease at the red flank. For the two ZPLs at 1038 and 1047 cm^{-1} there is a solvent effect as well, which is not related to H-bonding or blue shifting. In EtOH, 50/50 glycerol/buffer and MCH the two bands are of approximately equal intensity, whereas in acetone and in DMSO the intensity of the 1038 cm^{-1} band is considerably lower than that of the 1047 cm^{-1} band. These differences are presumably due to π–π interactions between the pyrene moiety and acetone or DMSO; such interactions are absent for the other solvents.

The solvent dependencies discussed above can be used to describe the binding of BP-tetrol to the MAb. If H-bonding were important, the spectrum would resemble those recorded in EtOH or 50/50 glycerol/buffer. The intensity ratio between the 958 and the 1111 cm^{-1} band observed for MAb indicates that this is not the case. Since the antibody is in 50/50 glycerol/buffer glass, the conclusion can be drawn that BP-tetrol is not located at the surface but well embedded inside the antibody. This also confirms the affinity of the *anti*-BPDE MAb for BP-tetrol [25]. Comparing the spectrum of BP-tetrol bound to MAb to its spectra in aprotic solvents, we note that the two peaks at 1038 and 1047 cm^{-1} are of approximately equal intensity, similar to the spectrum in MCH. Furthermore, the relative intensity of the 958 cm^{-1} and 1111 cm^{-1} bands in the spectrum of BP-tetrol bound to MAb is more similar to that in MCH than to those in acetone and DMSO. These observations indicate that the binding site in the MAb is of a nonpolar character, and that H-bonding and π–π interactions play no major role. Thus, it is most likely that the antigen/antibody binding is mainly due to hydrophobic interactions.

BP-6-N7Gua

Similar experiments were performed with BP-6-N7Gua. The 77K fluorescence spectra are shown in Figure 4. The origin bands are located near 405 nm and a major vibronic transition can be seen near 430 nm. Again, only small differences in the position of the origin band and in bandwidth could be observed under these conditions. Much more detailed information can

be obtained from the 4K FLN spectra of the BP-6-N7Gua samples; these spectra differ considerably (see Figure 5). For BP-6-N7Gua bound to MAb and dissolved in acetone or DMSO, the ZPLs have a low intensity and are superpositioned on a broad background with a maximum around 408.5 nm. This red shifted background is due to increased electron-phonon coupling. In the spectra of BP-6-N7Gua dissolved in EtOH, 50/50 glycerol/buffer or MCH this broad background is much weaker. Therefore, the increased electron-phonon coupling is probably due to $\pi-\pi$ interactions, similar to intercalated B[a]P-DNA adducts [23]. Unlike the case of BP-tetrol, only a minor influence of H-bonding solvents was observed: the spectra in 50/50 glycerol/buffer and MCH are largely similar.
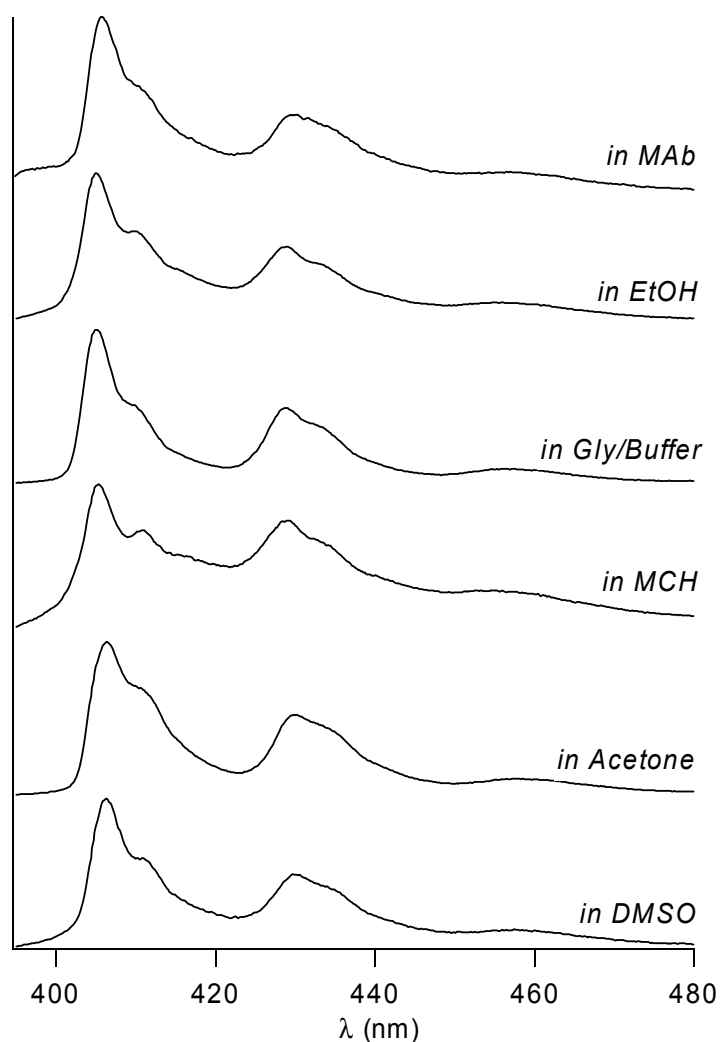
Figure 4: 77K low-resolution fluorescence spectra of BP-6-N7Gua, excited at λ_{ex} = 360 nm.
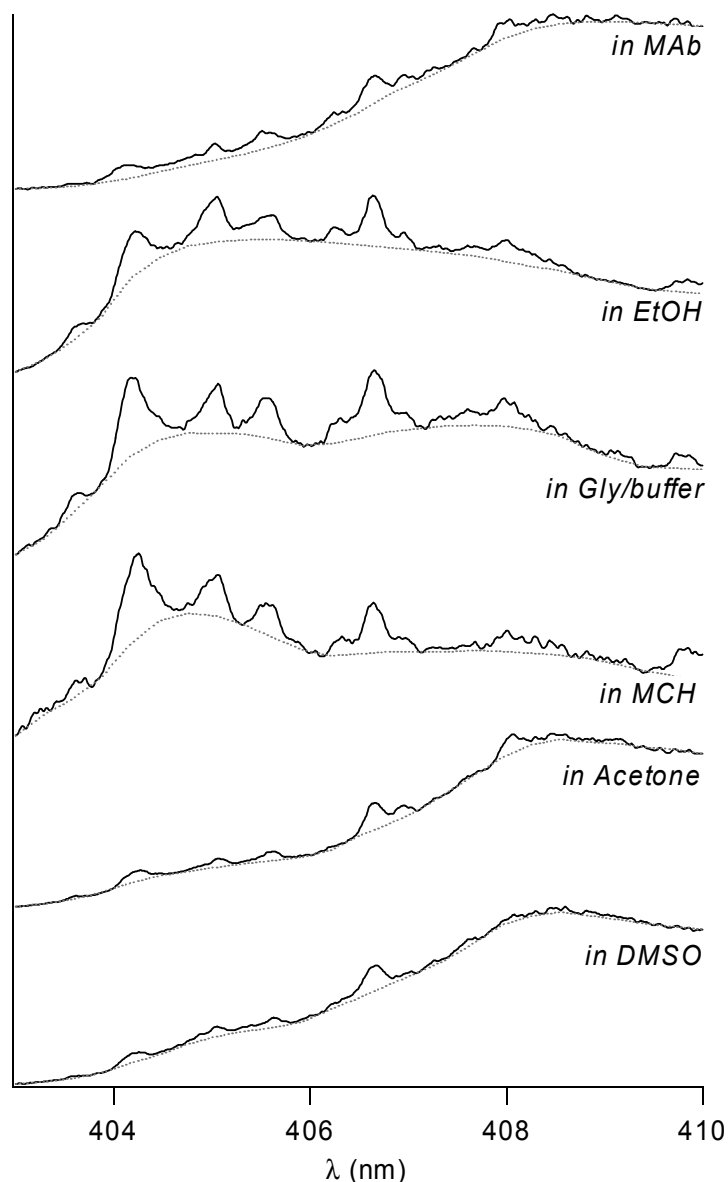
Figure 5: *FLN spectra of the multiplet origin band of BP-6-N7Gua bound to MAb and in various solvents, excited at 386.0 nm. The dotted lines are the background spectra that are subtracted into yield figure 6.*

After background subtraction (the backgrounds used are shown in Figure 5 as the dotted lines) the relative intensities of the ZPLs can be more easily compared (see Figure 6). Although there is some noise at the red end of the spectra, the multiplet origin bands can be readily distinguished. It should be noted that their positions in the various solvents are virtually identical, indicating that the S_1 vibrational energies are not affected by the solvent. Some clear differences can be observed when comparing the relative intensities of the 1168 cm^{-1} and 1315 cm^{-1} bands. For EtOH and 50/50 glycerol/buffer these two bands have similar intensities. In MCH, however, the intensity of the 1168 cm^{-1} band is approximately two times

higher. For BP-6-N7Gua bound to MAb and BP-6-N7Gua in acetone or DMSO, the opposite is observed: the 1315 cm^{-1} band is twice as intense as the 1168 cm^{-1} band. Another difference is the presence of the 1397 cm^{-1} band: in acetone and in the spectrum of BP-6-N7Gua bound to MAb it can be clearly observed, whereas in DMSO it is beyond detection.
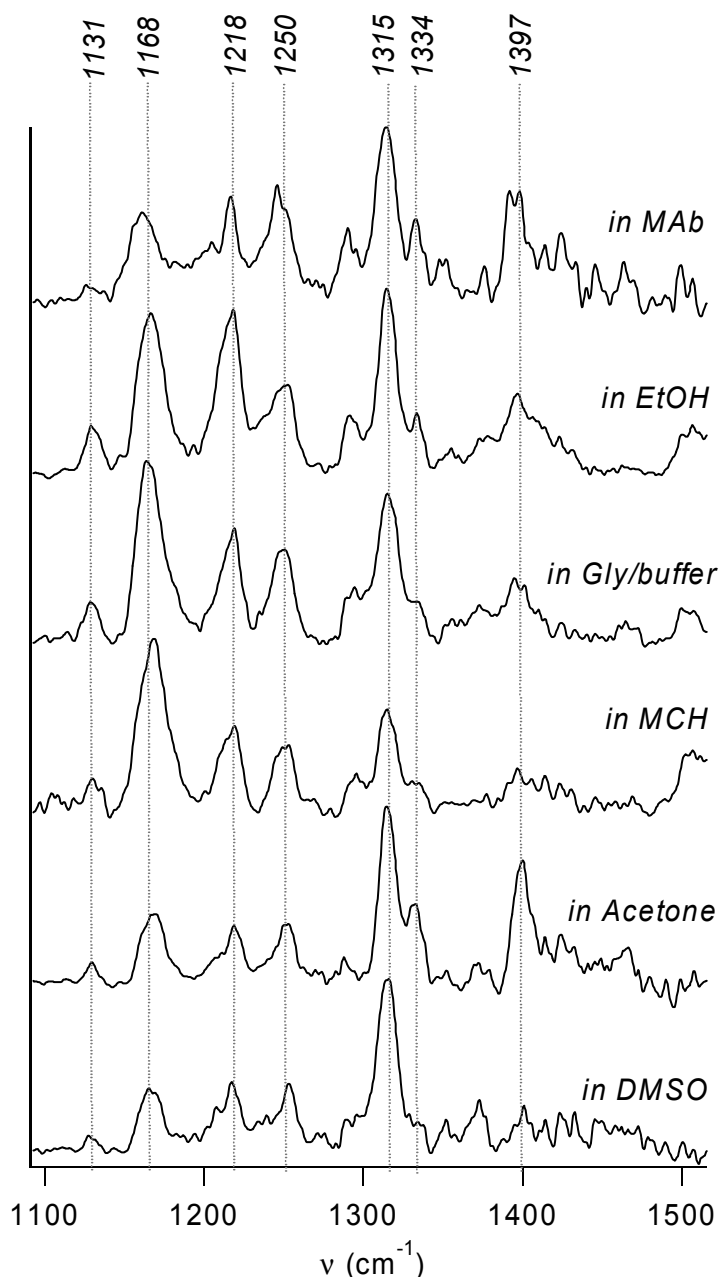
Figure 6: Background subtracted FLN spectra of the multiplet origin band of BP-6-N7Gua in various solvents, excited at 386.0 nm (background: see figure 5). The given wavenumbers are the excited state vibrational energies.

These results show that, unlike the MAb developed for BP-tetrol, the binding site of the MAb for BP-6-N7Gua is not hydrophobic (see the difference with MCH spectrum). On the contrary, the similarity to the spectrum in acetone suggests that π–π interactions (for instance with carbonyl groups) are involved in the binding site of the MAb. Since only minor effects of H-bonding solvents were observed in the spectra of BP-6-N7Gua, no conclusions can be drawn about the extent of hydrogen bonding (for instance to the guanine moiety) in the binding site.

Conclusions

The results presented here show that FLNS can provide qualitative information on the interaction between benzo[a]pyrene derivatives and the monoclonal antibodies developed to selectively bind them. Based on our data BP-tetrol is located at a site not exposed to the solvent, the binding site being of a hydrophobic nature. In contrast, the binding site of BP-6-N7Gua is not hydrophobic and appears to be dominated by the interaction between π-electrons of the B[a]P-moiety and those of the surrounding protein.

We note that the combination of FLNS and solvent dependent studies to investigate the nature of antibody/antigen binding interactions will only be useful for antigens (or ligands in general) that exhibit native fluorescence as well as fluorescence line-narrowing under cryogenic conditions. The latter feature – which fluorescent molecules show FLN and which not – has not been systematically investigated yet. A second prerequisite is that the FLN spectra are solvent dependent, a phenomenon that is hardly described in the literature and needs further exploration.

It should be emphasized that in FLNS sample handling is simple – the only requirement is cooling to temperatures in the vicinity of 4 K – and furthermore that FLNS has a high inherent sensitivity. The information on the type of binding interactions that is obtained can be useful for the development of MAbs and the understanding of which compounds will show cross-reactivity. Currently the applicability of our approach is being extended by a study of binding sites of enzyme receptors (for example the estrogen receptor). Furthermore, FLN spectroscopy is being used to determine the cross-binding activity of various monoclonal antibodies.

Acknowledgment

References

1. D.S. Hage, D.S., *Anal. Chem.*, **1999**, 71 **(1999)**, 294R-304R
2. M.D. Marazuela, M.D.,; M.C. Moreno-Bondi, M.C., *Anal. Bioanal. Chem.*, **2002**, 372 (2002), 664-682
3. T. Vo-Dinh, T.;, B. Cullum, B.,; *Anal. Bioanal. Chem.*, **2000**, 366 (2000), 540-551
4. A.R. Friedman, A.R.,; V.A. Roberts, V.A.,; J.A. Tainer, J.A., *Proteins*, **1994**, 20 (1994), 15-24
5. W.M. Mullett, W.M.,; E.P.C. Lai, E.P.C.,; J.M. Yeung, J.M., *Methods*, **2000**, 22 (2000), 77-91
6. J. Gervay, J.,; K.D. McReynolds, K.D., *Curr. Med. Chem.*, **1999**, 6 (1999), 129-153
7. J.L. Pellequer, J.L.,; B. Zhao, B.,; H.L. Kao, H.L.,; C.W. Bell, C.W.,; K. Li, K.,; Q.X. Li, Q.X.,; A.E. Karu, A.E.,; V.A. Roberts, V.A., *J. Mol. Biol.*, **2000**, 302 (2000),: 691-699
8. N. Grubor, N.M.,; G.J. Small, G.J.,; R. Jankowiak, R. in preparation
9. S.D. Duhachek, S.D.; J.R. Kenseth, J.R.; G.P. Casale, G.P.; G. J. Small, G.J.; M.D. Porter, M.D.; R. Jankowiak, R. *Anal. Chem.*, **2000**, 72, (2000), 3709-3716
10. P.L. Lioy, P.L.; J.M. Waldman, J.M.; R. Harkov, R.; C. Pietarinen, C.; A Greenberg, A. *Arch. Environ. Health*, **1988**, 43 (1988), 304-312
11. F.J. Jongeneelen, F.J.; R.B.M. Anzion, R.B.M.; P.T.J. Scheepers, P.T.J.; R.P. Bos, R.P.; P. Th. Henderson, P. Th.; E.H. Nijenhuis, E.H.; S.J. Veenstra, S.J.; R.M.E. Brouns, R.M.E.; A. Winkes, A. *Ann. Occup. Hyg.*, **1988**, 32 (1988), 35-43
12. E. Cavalieri, E.; E. Rogan, E. *Pharmacol. Ther.*, **1992**, 55(1992), 1083-1099
13. E. Cavalieri, E.; E. Rogan, E. In *"Handbook of Environmental Chemistry"*, A.H. Nielsen, A.H. (Ed.);, Springer-Verlag:, Heidelberg, Germany, 1998, Vol. 3, pp 81-117
14. T.M. Penning, T.M.; M.E. Burcynski, M.E.; C.-F. Hung, C.-F.; K.D. McCoull, K.D.; N.T. Palackal, N.T.; L.S. Tsuruda, L.S. *Chem. Res. Toxicol.*, **1999**, 12 (1999), 1-18
15. G.P. Casale, G.P.; E.G. Rogan, E.G.; D. Stack, D.; P. Devanesan, P.; E. L. Cavalieri, E.L. *Chem. Res. Toxicol.*, **1996**, 9, (1996), 1037-1043
16. F. Ariese, F.; R. Jankowiak, R. In *"Shpol'skii Spectroscopy and Other Site-Selection Methods"*, C. Gooijer, C.; F. Ariese, F.; J.W. Hofstraat, J.W. (Eds.),; Wiley & Sons:, New York, 2000, pp 333-362
17. K. Singh, K.; P.L. Skipper, P.L.; S.R. Tannenbaum, S.R.; R.R. Dasari, R.R. *Photochem. Photobiol.*, **1993**, 58 (1993), 637-642
18. S.J. Kok, S.J.; R. Posthumus, R.; I. Bakker, I.; C. Gooijer, C.; U.A.Th. Brinkman, U.A.Th.; N.H. Velthorst, N.H. *Anal. Chim. Acta*, **1995**, 303 (1995), 3-10
19. K.P. Roberts, K.P.; C.H. Lin, C.H.; M. Singhal, M.; G.P. Casale, G.P.; G.J. Small, G.J.; R. Jankowiak, R. *Electrophoresis*, **2000**, 21 (2000), 799-806
20. R. Jankowiak, R. In *"Shpol'skii Spectroscopy and Other Site-Selection Methods"* C. Gooijer, C.; F. Ariese, F.; J.W. Hofstraat, J.W. (Eds.), .); Wiley & Sons,: New York, 2000, pp 235-271
21. R. Jankowiak, R.; G.J. Small, G.J. *Anal Chem.*, **1989**, 61 (1989), 1023A-1032A
22. M.U. Kumke, M.U.; F.H. Frimmel, F.H.; F. Ariese, F.; C. Gooijer, C. *Environ. Sci. Technol.*, **2000**, 34 (2000), 3818-3823

23. M. Suh, M.; F.Ariese, F.; G.J. Small, G.J.; R. Jankowiak, R.; T.M. Liu, T.M.; N.E Geacintov, N.E. *Biophys. Chem.*, **1995**, 56 (1995), 281-296

24. Hofstraat, J.W.; Gooijer, C.; Velthorst, N.H. In *"Molecular Luminescence Spectroscopy: Methods and Applications, Part 2"* Schulman, S.G. (Ed.); Wiley & Sons: New-York, 1993, 383-397

25. Trevigen Inc. (see http://www.trevigen.com for product information about the *anti*-BPDE 8E11 MAb).

26. J.M. Hayes, J.M.; T. Reinot, T.; N. Dang, N.; G.J. Small,; G.J. *J. Phys. Chem.* 2003 (in press).

CHAPTER 3.2

The chemical interaction between the estrogen receptor and mono-hydroxybenzo[*a*]pyrene derivatives studied by fluorescence line-narrowing spectroscopy

Arjen N. Bader, Maarten M. van Dongen, Marola M.H. van Lipzig,
Jeroen Kool, John H.N. Meerman, Freek Ariese and Cees Gooijer,
Chem. Res. Tox, **2005***, 18(9),* 1405-1412,

Abstract

A novel approach is presented for studying the chemical interaction between receptor binding sites and ligands. Mono-hydroxylated poly-aromatic compounds were found to be environment sensitive ligands when applying a special mode of fluorescence: fluorescence line-narrowing spectroscopy (FLNS). With this technique, solvent dependencies and ligand-receptor interactions can be studied in great detail, due to the high spectral resolution and the fact that at cryogenic temperatures (4K), no solvent reorientation effects are complicating the interpretation. The FLN spectrum of a ligand bound to the receptor is compared to its spectra in solvent mixtures that mimic the functionalities present within the receptor's binding site. It is shown that for the well-known estrogen receptor (ER), the orientations of two xeno-estrogenic ligands 3- and 9-hydroxybenzo[*a*]pyrene (3- and 9-OH-BaP) can be determined. The FLN results clearly indicate that an H-bond accepted by HIS524 plays a major role in the binding of these ligands to the ER. Furthermore, the spectra indicated $\pi-\pi$ stacking aromatic interaction for 9-OH-BaP with PHE404. These results are in line with molecular modelling studies published earlier.

Introduction

Exposure to environmental estrogens or xeno-estrogens has been proposed to be a risk factor, associated with disruption of reproductive development and tumorigenesis in humans and wildlife [1]. Endogenous estrogens play a crucial role in the development, growth and regulation of sexual and reproductive organs and behaviour of mammals [2]. They act via binding to estrogen receptors (ER), members of the nuclear receptor superfamily that function as transcription factors to modulate gene expression in a ligand-dependent manner [3]. In the nucleus, binding of ligands induces a conformational change of the ER, enabling the receptor to dimerise. The dimer binds to the palindrome estrogen response elements (ERE) in DNA, where it enhances gene transcription leading to e.g. protein synthesis and cell proliferation [4]. Two ER isoforms have been identified, ER-α and ER-β, that show different tissue expression and distinct ligand binding properties [5]. In the present study, the attention is confined to ER-α.

Polycyclic aromatic hydrocarbons (PAHs) form a class of well-known environmental pollutants. Many different PAHs are formed during incomplete combustion of organic material: they can be found in e.g. (cigarette) smoke, exhausts, and burned meat. After uptake in the body, PAHs are metabolised in various ways, resulting in a large variety of oxygenated compounds, some of which are known to be potentially toxic or carcinogenic. An example of such a PAH is benzo[*a*]pyrene (BaP). In addition to its carcinogenicity and cytotoxicity, BaP also possesses endocrine activity. The structural resemblance of BaP's with the endogenous estrogen 17β-estradiol (E2) is evident (see Figure 1), and the estrogenic properties have been the objective of several studies [6-8]. BaP was reported to exhibit estrogenic activity in several cellular systems *in vitro*, [9-11], but no ER-affinity of BaP was found in radioligand binding assays. Recently, it was shown that the estrogenic effect of BaP in T47D breast cancer cells is due to the formation of BaP metabolites [12]. For several mono-hydroxylated BaPs (OH-BaPs), including 2-OH-, 3-OH-, 8-OH- and 9-OH-BaP, low-affinity estrogenic activity was reported [12]. Despite these relatively low affinities for the individual OH-BaPs, the estrogenic properties of BaP may still be relevant. It should be realised that *in vivo* always a mixture of various metabolites are formed after exposure to PAHs. It was recently shown that a mixture of OH-BaPs induces significant estrogenic responses, much higher than expected [12].
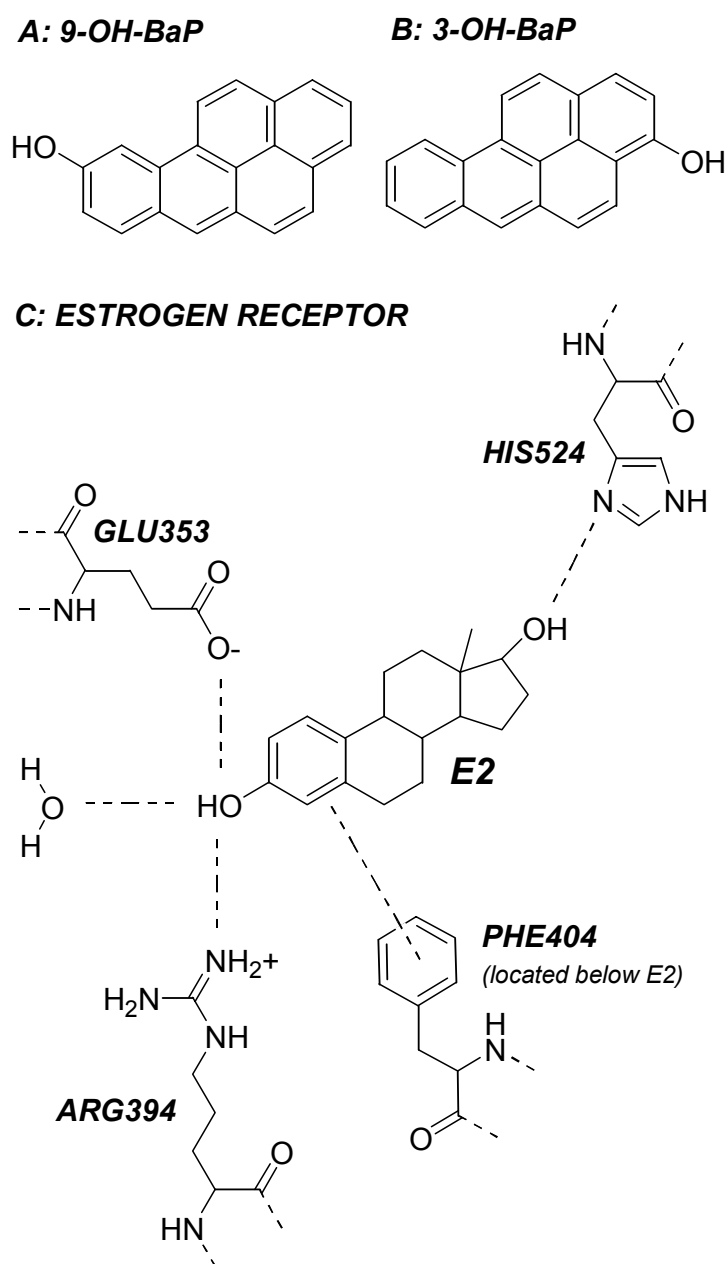
Figure 1: *The molecular structure of 9-OH-BaP (A), 3-OH-BaP (B), and Estradiol (E2) located in the estrogen receptor (ER) binding pocket (C). The amino acids shown are involved in the binding of E2 to the ER.*

Although for E2 (and also for estrogens such as DES and THC) the binding orientation in the ER is known from crystallographic data (see Figure 1 for E2) [4,13-14], it is very hard to predict binding orientations (and binding affinities) of ligands such as the OH-BaPs dealt with in the present study. Recently, a computational model was published, predicting binding orientation and affinity for many (xeno)estrogens, including estrogenic OH-BaP-metabolites [15]. The shape and planarity of an OH-BaP molecule is quite similar to that of E2. The main

difference, however, is that an OH-BaP possesses only one hydroxy-group whereas E2 has two. This implies that the orientation of the hydroxyl group of OH-BaPs in the ER may be either towards GLU353 and ARG394, or towards HIS524 (left hand or right hand side in Figure 1, respectively). Unfortunately, experimental data supporting the one or the other orientation are difficult to obtain. Here, we present a novel methodology that may provide such information, i.e., a special mode of molecular fluorescence known as fluorescence line-narrowing spectroscopy (FLNS). Recently it was shown that FLNS is appropriate for investigating in detail the interaction of adducts and metabolites of BaP with their corresponding antibodies [16].

Briefly, FLNS is a technique in which high-resolution fluorescence spectra are obtained by freezing a liquid sample to below 10 K and applying selective laser excitation [17-18]. FLNS can be successfully applied to (substituted) PAHs, even in solvent systems like aqueous buffers. The only restriction to the solvent is that upon cooling it should form an amorphous rather than a (poly) crystalline matrix. Under such conditions the inhomogeneous broadening of the spectral bands is still significant: each individual analyte molecule is embedded in a particular surrounding of solvent molecules, thus experiencing its own particular interaction. Of course in the rigid, frozen matrix these interactions do not change in time, at least not during the nanosecond fluorescence lifetime. The crucial feature of FLNS is that by using laser excitation, only those analyte molecules with a transition energy between the ground state S_0 and the first electronically excited state S_1 exactly matching the wavelength of the laser will be excited, and as a result only those selected solute molecules will emit fluorescence. This explains why narrow lines in emission are obtained [17-18]. If the laser wavelength is somewhat shorter so that vibrations of the S_1 state are excited, the FLN emission pattern usually becomes more complicated. This is illustrated in Figure 2A, where four S_1 vibrations are simultaneously excited. After excitation, non-radiative relaxation of the molecule to the associated $S_{1,0}$ level takes place, followed by light emission. As a result four line-narrowed bands (also known as zero phonon lines, ZPLs) are observed in the emission spectrum. The photon energy differences between these lines and the laser line correspond to the excited state vibrations.
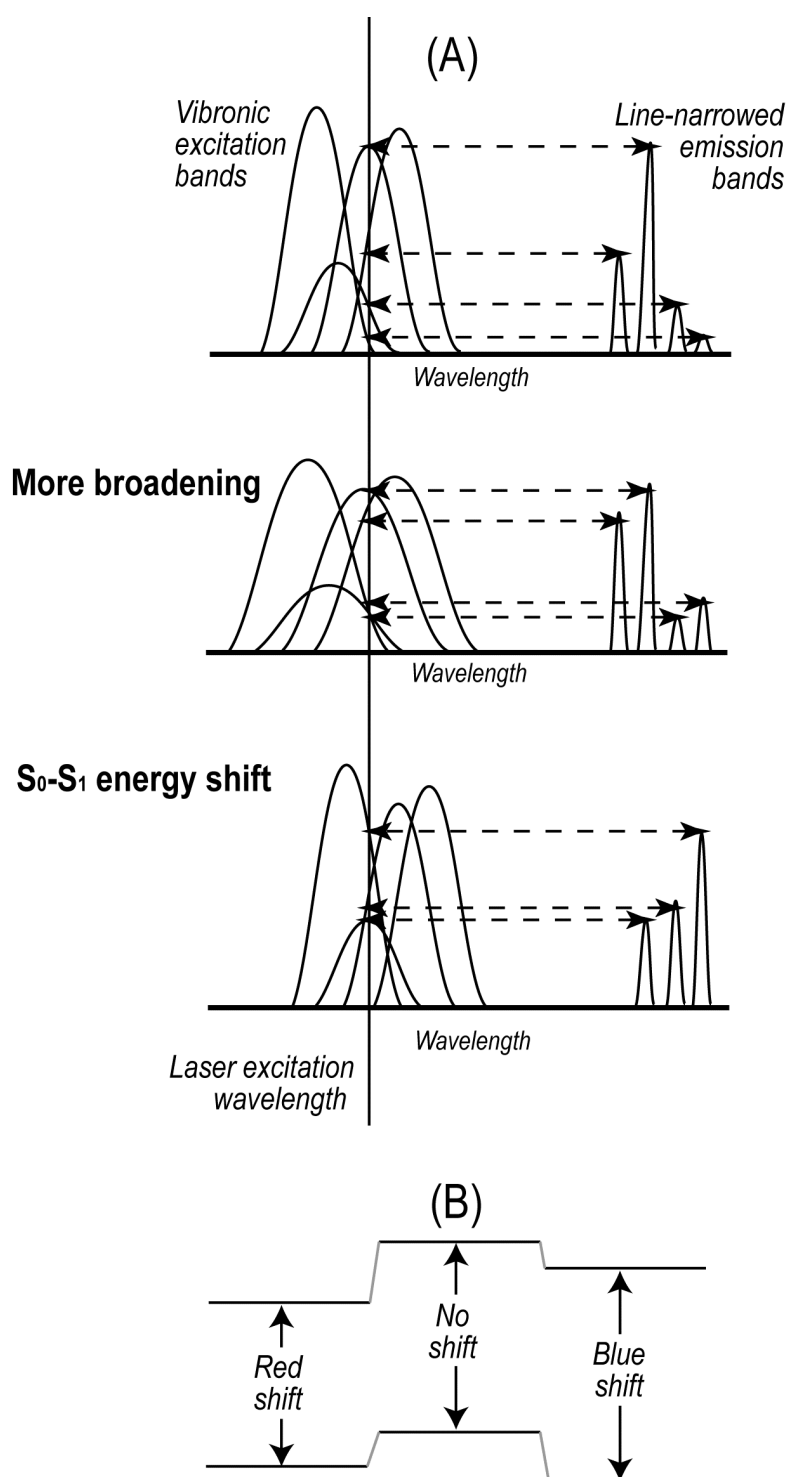
Figure 2: *Solvent dependencies in FLN spectra. (A) Schematic of a limited number of excitation and emission bands in a low temperature amorphous matrix. More broadening of the vibronic bands in excitation or a shift in S_1-S_0 energy results in a change in the relative intensities of the ZPLs in emission. (B) Schematic to show the effect of solute/solvent interaction on the S_0-S_1 energy difference. The S_1 can be less or more stabilised than the S_0 state, resulting in a blue or red shift, respectively.*

For the present purposes it is of main importance to note that the shape of the emission pattern is strongly influenced by solute-solvent interaction. This is schematically illustrated in Figure 2A where four vibrations are considered. For ease of comparison the intensities of the four ZPLs are labelled A/B/C/D and the intensity of the strongest ZPL is arbitrarily set equal to 10. This results in an intensity ratio of 4/10/2/1 in the upper spectrum in this figure. When the vibronic excitation bands are broadened, as in the middle spectrum of Figure 2A, the ratio becomes 8/10/2/3. This means that an enhancement of the relative intensity of the ZPLs at both edges of the multiplet origin band, i.e., band A and D, can be attributed to an increase of the inhomogeneous broadening. In other words, there is a larger variety in interaction energies with the solvent. When the vibronic excitation bands shift to lower energy (to the red), as is the case in the lower spectrum in Figure 2A, the ratio becomes 0/5/6/10. This implies that an increase in the relative intensity of the ZPLs on the right hand side in the multiplet origin band, i.e., bands C and D, is indicative for a red shift in the excitation spectrum. Obviously the opposite is true in case of decreased inhomogeneous broadening and a blue shift, respectively. To summarize, the qualitative analysis of Figure 2 illustrates how minor solvatochromic shifts and minor changes in inhomogeneous broadening that are hardly observable in conventional, broadbanded fluorescence spectroscopy can be sensitively monitored in FLNS using the relative intensities of the ZPLs. Importantly, solvent reorientation effects (Stokes' shifts) will be minor in the 4 K matrix and thus will not complicate the interpretation. In other words, FLNS will be an appropriate technique to probe the local environment of the solute for specific (static) solvent effects (H-bonding, $\pi-\pi$ interaction) [16].

It should be realized that Figure 2A gives only a simplified picture in which exclusively ZPLs are shown in the FLN spectrum while other, complicating, spectral features are ignored. In practice, in most cases a strong broad background is observed, red shifted compared to the ZPLs. This background is composed of phonon side bands (PSBs) [17-18]. PSBs are due to electron phonon coupling, i.e., coupling of electronic transitions with lattice vibrations of the solvent matrix. The relative intensities of the ZPLs compared to the PSBs decreases with the strength of the interaction between solute and matrix; therefore PSBs are not only complicating the spectra but in principle they provide substantial information as well.

In a previous study, devoted to the interaction between antigens and their corresponding antibodies [16], the approach followed was to record the FLN spectra of the fluorophore in a variety of solvent mixtures selected for their different solvation behaviour. By comparing the spectrum of the fluorophore bound to its antibody to this set of reference spectra, the dominating chemical interaction between antigen and antibody could be established. In the present study, a similar approach is chosen to investigate the binding of 3-OH-BaP and 9-OH-BaP to the ER. These two compounds were selected because they show a clear solvent dependency in their FLN spectra. Unlike the antibodies in the previous study, the crystal structure of the ER is known. This makes the selection of the solvent mixtures straightforward: they are chosen such that the functionalities in the binding site are mimicked as much as possible. The ligands, however, have an affinity for the ER that is lower than that of E2. This indicates that in case of OH-BaPs only part of the functionalities in the binding pocket is used. Our main goal is to determine experimentally which functionalities are important for the binding and thus determine the orientations of the two OH-BaPs inside the ER binding pocket. The results can be verified by using the molecular modelling data published recently [15]. Furthermore, such an investigation will help in further exploration of the FLNS approach for studying protein/ligand interactions, a method that may become relevant in determining ligand orientation, especially in situations where protein crystal structures are lacking.

Experimental:

The solvents glycerol and triethylamine were obtained form Aldrich (Seelze, Germany). Acetone, methylcyclohexane, n-butyl alcohol, were obtained from Baker (Deventer, The Netherlands), toluene from Fisher (Loughborough, UK). 3- and 9-hydroxybenzo[a]pyrene were obtained from NCI-MRI (Kansas City, MO, USA) and 17β-estradiol from Sigma Chemical Co. (St. Louis, USA). L(+)-Ascorbic acid (Baker) was added to prevent the monohydroxbenzo[a]pyrene derivatives from further oxidation.

The estrogen receptor-α LBD (ER; a kind gift of Dr Marc Ruff; Laboratoire de Biologie et Génomique Structurales 1, IGBMC, Illkirch, France) was expressed in *e-coli* according to Eiler et al [19], but without estradiol in the medium. The cells were pelleted at 4600 rpm for 60 min. and the pellet was subsequently suspended in 50 ml 10 mM monosodium hydrogen

phosphate buffer (pH 7.4; adjusted by KOH) containing 150 mM NaCl. The cells were again pelleted at 4000 rpm for 15 min. and the pellet was suspended in 50 ml of the same buffer. This washing step was repeated two more times. After the last washing step, the pelleted cells were suspended in 25 ml of the same buffer. Purification of the ER-α was performed by use of three french press cycles (700 bar) and ultrasonic sound (microtip, 30% duty cycle output 7, 10 cycles) to break up the cells and finally ultracentrifugation (100.000 g) for one hour to obtain the soluble receptor in the supernatant. Functional characterization of the LBD and receptor concentration, estimated by determining the B_{max} value, was done by measuring its E2 binding ability in a saturation radioligand binding assay, as described by Gurer-Orhan et al [20] and by Eiler et al [19]. The soluble receptor (concentration of approximately 1 μM) stock solution was stored at -80°C.

1-10 μM solutions of OH-BaP in various solvents were measured. The solutions of ER-bound compound were made by diluting a 100 μM OH-BaP stock solution in ethanol 10 times with 1 μM ER in 10 mM Tris EDTA buffer, followed by incubation for one hour at 4°C. Any unbound OH-BaP fraction was removed by a dextran-coated charcoal (0.01%/0.1%) column in Tris EDTA buffer (pH 7.5). The purified effluent containing the bound fraction was directly cooled on ice to avoid re-establishing of the equilibrium between bound an unbound ligand. As a control experiment, an excess of E2 was added to a solution of ER and OH-BaP. In earlier work, 3-OH-BaP and 9-OH-BaP competed for radiolabeled E2 with EC_{50} values of $1.08*10^{-6}$ and $1.01*10^{-5}$ M [12]. Because of the strong affinity differences (the affinity of E2 is $4.0*10^{-10}$ M [12]), the receptor binding sites will become exclusively occupied by the high-affinity ligand E2 and therefore all OH-BaP molecules will be displaced and subsequently adsorb to the charcoal in the column. For both 3-OH-BaP and 9-OH-BaP no fluorescence emission in the column effluent (ER/E2 complex solution) was observed, indicating that the charcoal purification is fully effective in removing unbound OH-BaP and that in our FLNS study we are exclusively dealing with OH-BaP/ER complexes. Binding of 3-OH-BaP or 9-OH-BaP was further checked by recording FLN spectra in Gly/Buf both in the presence and absence of ER; major spectral differences demonstrated binding to the ER (see below).

Four quartz tubes at a time were placed in a home-made sample holder mounted to the top of the cold head of a closed-cycle 4K liquid helium refrigerator (SRDK-205 Cryocooler, Janis Research Company, Wilmington, MA, USA). The excitation source was a XeCl excimer laser (Lambda Physik LPX 110i, Göttingen, Germany) pumping a dye laser (Lambda Physik, LPD 3002). The excimer laser was operated at 10 Hz, producing 10 ns 50 mJ pulses. Using PBBO as a dye, a tuneable output in the 386 nm - 420 nm range was obtained. The four samples could be measured separately by moving the cold head at an angle of 45° with respect to both the excitation beam and collection optics. Fluorescence emission was collected with a 3-cm F/l.2 quartz lens at a 90° angle to the excitation beam, focused by a 10-cm F/4 quartz lens on the entrance slit of a Spex 1877 0.6-m triple monochromator (Edison, NJ, USA) and detected with an intensified CCD camera (iStar DH720-25U-03, Andor instruments, Belfast, Northern Ireland) operated in the gated mode to reject stray- and scattered light. The spectral resolution of the emission spectrum was 0.1 nm. All samples were analyzed 2-4 times; the resulting spectra showed differences in absolute intensity due to differences in optical alignment and dye laser output, but no differences in relative intensities were observed.

Results

As illustrated in Figure 1, the key amino acids involved in binding to the ER are GLU353, ARG394 (H-bonding interaction), HIS524 (exclusively H-bond accepting) and PHE404 ($\pi-\pi$ interaction). The main aim of this research was to determine the relative importance of these binding modes from the FLN spectra in the ligands in the ER. Separately, a set of FLN spectra of the free ligands was recorded in a number of standard solvents or solvent combinations mimicking these interactions. These solvent combinations are shown in Table 1 and 2. Four categories can be distinguished: (1) reference solvent, (2) H-bonding solvents, (3) $\pi-\pi$ interacting solvents, and (4) combinations of the latter two. The reference solvent, methylcyclohexane (MCH), is nonpolar and nonprotic and will therefore show minimal interactions. MCH was found to yield amorphous matrices under cryogenic conditions, unlike some of the other solvents that we wanted to include in this study. For those solvents, mixtures with MCH were used (solvent/MCH = 10/90 v/v). Such an approach also allowed using combinations of solvents from the different categories (solvent1/solvent2/MCH = 10/10/80 v/v/v). Another selection criterion was that miscibility with MCH should not be a

problem; no phase separation should occur, even under low temperature conditions. Additionally, the solubility of the OH-BaPs concerned was not a problem at the concentrations dealt with.

To study the role of H-bonding, two solvents were added to MCH, i.e., 1-butanol (BuOH) and triethylamine (TEA). The interaction with the H-bonding network of GLU353 and ARG394 (see Figure 1C) is mimicked using BuOH; this solvent can both donate and accept an H-bond (*22*). In view of the miscibility conditions with MCH, alcohols with a shorter alkyl chain could not be used. The interaction with HIS524 is mimicked by TEA, a solvent known to have exclusively H-bond accepting properties similar to the imidazole ring of this amino acid (*22*). To mimic the aromatic interaction due to PHE404, toluene (Tol.) was used. It should, however, be realized that π-electron interaction can also be due to other functionalities present in the ER such as carbonyl groups. Therefore also acetone (Ace.) was used as a solvent. Finally, in the ER, H-bonding and π–π interaction can play a role simultaneously. Therefore, the four possible combinations of these two categories of solvents were included as well.

The estrogen receptor itself was dissolved in 50% Tris EDTA buffer and 50% glycerol (Gly/Buf), the latter solvent being added to ensure the formation of an amorphous matrix under cryogenic conditions, a basic requirement to obtain FLN spectra. Since the affinity of the ER to the two OH-BaPs considered is relatively weak (*12*), a clean-up step was involved to remove the unbound fraction as described in the Experimental Section.

9-OH-BaP

The FLN spectra of 9-OH-BaP bound to the ER (in Gly/Buf; top spectrum) and of the free ligand dissolved in the abovementioned solvent combinations are shown in Figure 3. First, it should be noted that the spectrum of 9-OH-BaP in presence of the ER differs strongly from its spectrum in Gly/Buf alone, confirming complete binding of 9-OH-BaP to the ER. Furthermore, significant differences are observed for the other spectra. Already from the shapes of the baselines some information can be inferred. In the spectrum of 9-OH-BaP bound to the ER, weak ZPLs located on a strong red-shifted and broad baseline are observed. Since the observed background is intense, the electron-phonon coupling will be strong. Similar features are observed for 9-OH-BaP in the presence of TEA (H-bond accepting

interaction), toluene (aromatic π-electron interaction) and acetone (carbonyl π-electron interaction), but the degree of electron phonon coupling is much stronger in the presence of acetone or TEA than in the presence of the other solvents. In order to distinguish the ZPLs from the baseline, the concentration of acetone had to be lowered to 0.1% and the concentration of TEA to 0.01% (these are the concentrations used to record the spectra in Figure 3). It should be noted that the shape of the baseline in the presence of acetone differs from the ones in toluene or TEA. The baselines observed for the latter two are similar to the one of 9-OH-BaP bound to the ER, whereas for acetone it is much less red-shifted. Also the combination of TEA and toluene or acetone yields spectral baselines similar to that of the ER.

Baseline subtraction is an appropriate way to better visualize the relative intensities of the ZPLs (see Figure 4) [16]. Across the 0-0 region, five main bands were selected to monitor solute/solvent interaction: (A) 840 cm^{-1}, (B) 980 cm^{-1}, (C) 1055 cm^{-1}, (D) 1175 cm^{-1} and (E) 1330 cm^{-1}, corresponding to vibrations in the S_1 excited state. The intensity ratios of these bands observed in various solvents are listed in Table 1. In Gly/Buf, the intensity ratio is 10/3/3/0/0. When the ER is present, this ratio changes dramatically to 2/2/7/6/10. MCH (reference spectrum) provides an intensity ratio of 1/2/10/6/2. In the presence of BuOH (both H-bond accepting and donating interaction) it changes to 3/2/10/5/2, i.e., a minor blue shift is observed. Conversely, in the presence of TEA (H-bond accepting interaction only) the intensity ratio becomes 2/1/10/10/8, i.e., a red shift with respect to MCH is observed. Considering π-electron interaction, the intensity ratio in the presence of toluene becomes 1/1/10/7/6 (red shift), whereas in the presence of acetone the ratio becomes 4/6/10/6/4 (more broadening, no significant shift).

When solvent mixtures are measured in which both BuOH and π-electron containing molecules are present, the FLN spectra are rather similar to those recorded in absence of the latter. There is only a minor change in going from BuOH (3/2/10/5/2) to BuOH-toluene (2/2/10/6/2) and BuOH-acetone (2/3/10/6/3). It is, however, not very likely that in such solvent mixtures 9-OH-BaP will exclusively interact with 1-butanol, and not with toluene or acetone at all. Probably, the effect of BuOH on the spectrum is much stronger than the effect of $\pi-\pi$ interaction. As mentioned earlier, both the presence of TEA and toluene results in a red shift. In BuOH-toluene this effect is even stronger: the intensity ratio becomes 2/2/9/9/10.

If TEA and acetone are combined, the ratio becomes 5/2/7/8/10 indicating more broadening and a red-shift as well (note that band A is relatively strong).
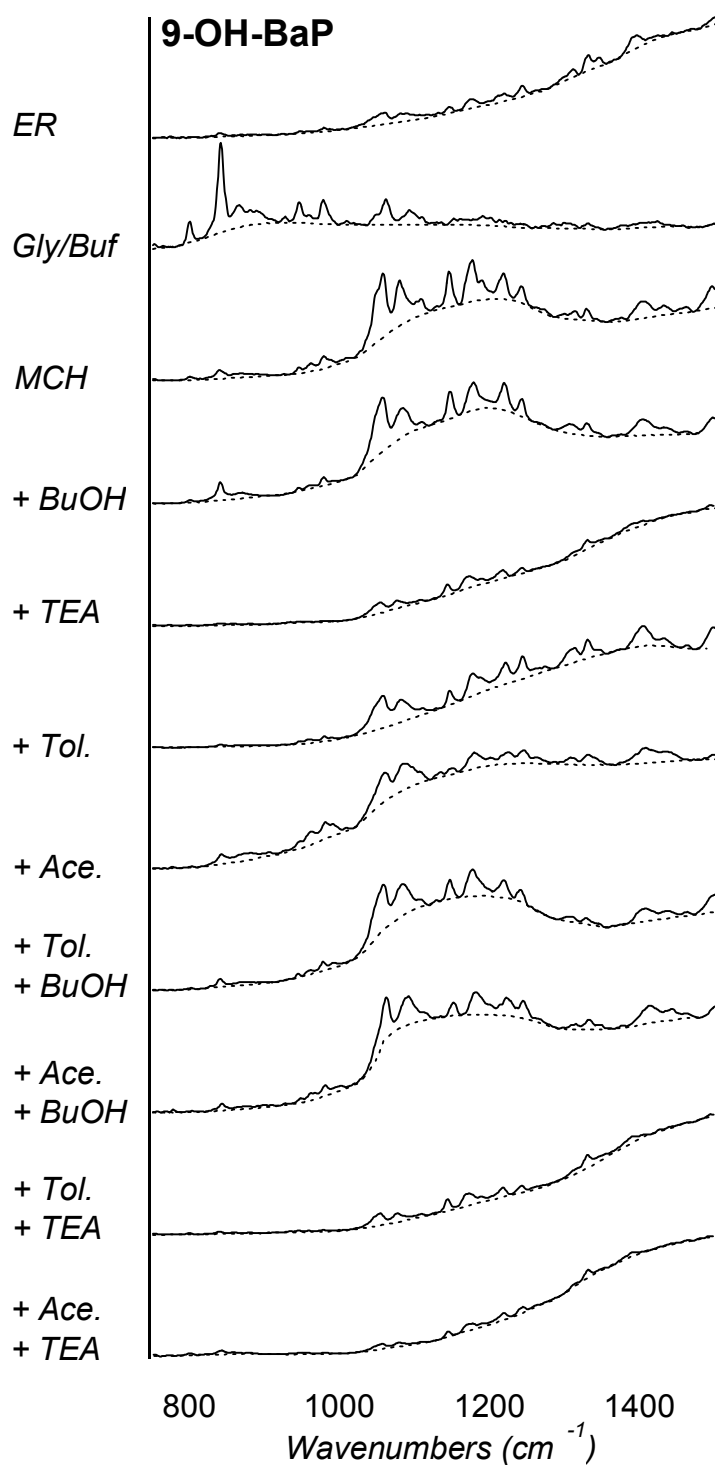
Figure 3: Normalised FLN spectra of 9-hydroxybenzo[a]pyrene in various solvents (or solvent combinations) and bound to the estrogen receptor. On the x-axis the energy difference with respect to the excitation wavelength in wavenumbers is used. The excitation wavelength was 403 nm.
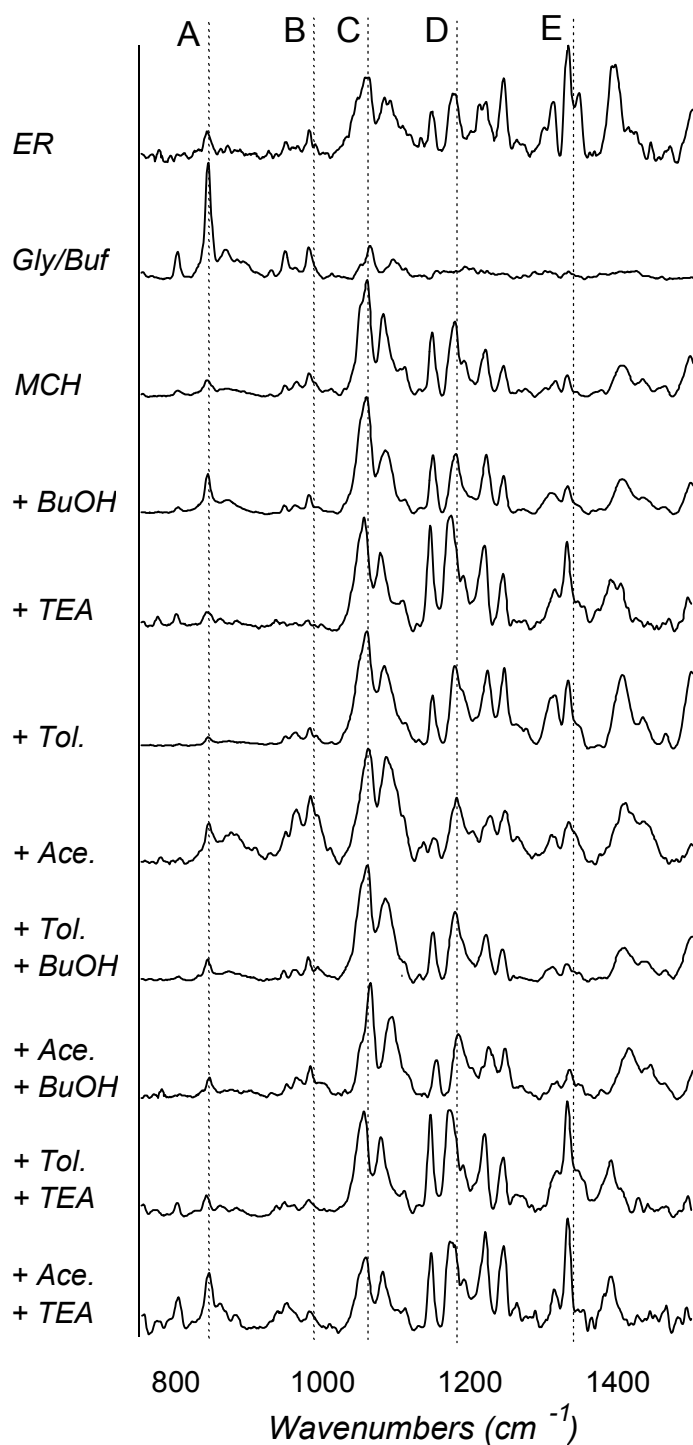
Figure 4: *Normalised FLN spectra of 9-hydroxybenzo[a]pyrene after baseline correction in various solvents (or solvent combinations) and bound to the estrogen receptor (the uncorrected spectra are shown in Figure 3). The relative intensities of bands (A), (B), (C), (D) and (E) are given in Table 1.*

Table 1: *Relative intensities of the multiplet origin ZPLs (A) 840 cm^{-1}, (B) 980 cm^{-1}, (C) 1050 cm^{-1}, (D) 1177 cm^{-1} and (E) 1328 cm^{-1} in the FLN spectrum of 9-OH-BaP (see Figure 4).*

	Solvent	A	B	C	D	E
Estrogen Receptor						
- ER present	*ER in Gly/Buf*	2	2	7	6	10
- ER absent	*Gly/Buf*	10	3	3	0	0
Hydrophobic interaction	*MCH*					
- reference	*MCH*	1	2	10	6	2
H-bonding interaction	*MCH*					
- with GLU&ARG	*+ BuOH*	3	2	10	5	2
- with HIS	*+ TEA*	2	1	10	10	8
π–π interaction	*MCH*					
- with PHE	*+ Tol.*	1	2	10	7	6
- with C=O	*+ Ace.*	4	6	10	6	4
Both H-bonding and						
π–π interaction	*MCH*					
- with PHE and GLU&ARG	*+ Tol. + BuOH*	2	2	10	6	2
- with C=O and GLU&ARG	*+ Ace. + BuOH*	2	3	10	6	3
- with PHE and HIS	*+ Tol. + TEA*	2	2	9	9	10
- with C=O and HIS	*+ Ace. + TEA*	5	2	7	8	10

3-OH-BaP

The FLN spectra of 3-OH-BaP bound to the ER (in Gly/Buf) and of the free ligand dissolved in the abovementioned solvent combinations are shown in Figure 5. Similar to the results obtained for 9-OH-BaP, the ER and the Gly/Buf spectrum are strongly different, indicating complete binding of 3-OH-BaP to the ER. Also for the baselines the trend is similar: in the spectrum of 3-OH-BaP bound to the ER low intensity ZPLs are seen, located on a strong red-shifted broad baseline. For the unbound 3-OH-BaP the degree of electron-phonon coupling is also high in the presence of acetone (carbonyl π-electron interaction) and in the presence of TEA (H-bond accepting interaction); again the concentration had to be lowered to 0.1 % and 0.01% respectively to be able to distinguish the ZPLs above the broad background. In contrast with the results obtained for 9-OH-BaP, in the presence of toluene (aromatic π-electron interaction) no strong red-shifted baseline was observed. Considering the shapes of the baselines, the spectrum of 3-OH-BaP bound to the ER is most similar to the spectra recorded in the presence of TEA (both with and without an additional π-electron containing solvent).

The baseline-subtracted spectra of 3-OH-BaP are shown in Figure 6. Four main bands were monitored: (A) 1075 cm^{-1}, (B) 1175 cm^{-1}, (C) 1325 cm^{-1} and (D) 1395 cm^{-1}; their relative intensities are shown in Table 2. In Gly/Buf, the intensity ratio is 6/10/6/8. Three additional ZPLs were found at the blue edge of the Gly/Buf spectrum at 770, 857 and 960 cm^{-1} (with relative intensities 4, 10 and 6, respectively); since these bands did not show up in the other spectra they are not included in Figures 5 and 6 and Table 2. In the presence of the ER, the ratio becomes 0/1/4/10. In the reference spectrum (MCH) the intensity ratio is 1/10/8/6. In the presence of BuOH (both H-bond donating and accepting interaction) it changes to 1/7/8/10, while in the presence of TEA (H-bond accepting interaction only) it becomes 1/2/7/10. Apparently, both H-bonding solvents cause a red shift (in the presence of TEA this red shift is much more pronounced); conversely, for Gly/Buf the shift is to the blue. Considering π-electron interaction, the intensity ratio in the presence of toluene becomes 2/10/8/10 (red shift), whereas in the presence of acetone the ratio becomes 4/10/7/5 (minor blue shift).

Table 2: *Relative intensities of the multiplet origin ZPLs (A) 1075 cm^{-1}, (B) 1175 cm^{-1}, (C) 1325 cm^{-1} and (D) 1395 cm^{-1} in the FLN spectrum of 3-OH-BaP (see Figure 6). For Gly/Buf, three other strong blue shifted bands are observed (at 770, 857 and 960 cm^{-1}, with relative intensities 4, 10 and 6, respectively).*

	Solvent	A	B	C	D
Estrogen Receptor					
- ER present	*ER in Gly/Buf*	0	1	4	10
- ER absent	*Gly/Buf*	6	10	6	8
Hydrophobic interaction					
- reference	*MCH*	1	10	8	6
H-bonding interaction	*MCH*				
- with GLU&ARG	*+ BuOH*	1	7	8	10
- with HIS	*+ TEA*	1	2	7	10
π–π interaction	*MCH*				
- with PHE	*+ Tol.*	2	10	8	10
- with C=O	*+ Ace.*	4	10	7	5
Both H-bonding and π–π interaction	*MCH*				
- with GLU&ARG and PHE	*+ Tol. + BuOH*	1	4	8	10
- with GLU&ARG and C=O	*+ Ace. + BuOH*	1	5	7	10
- with HIS and PHE	*+ Tol. + TEA*	0	3	10	8
- with HIS and C=O	*+ Ace. + TEA*	0	4	10	8
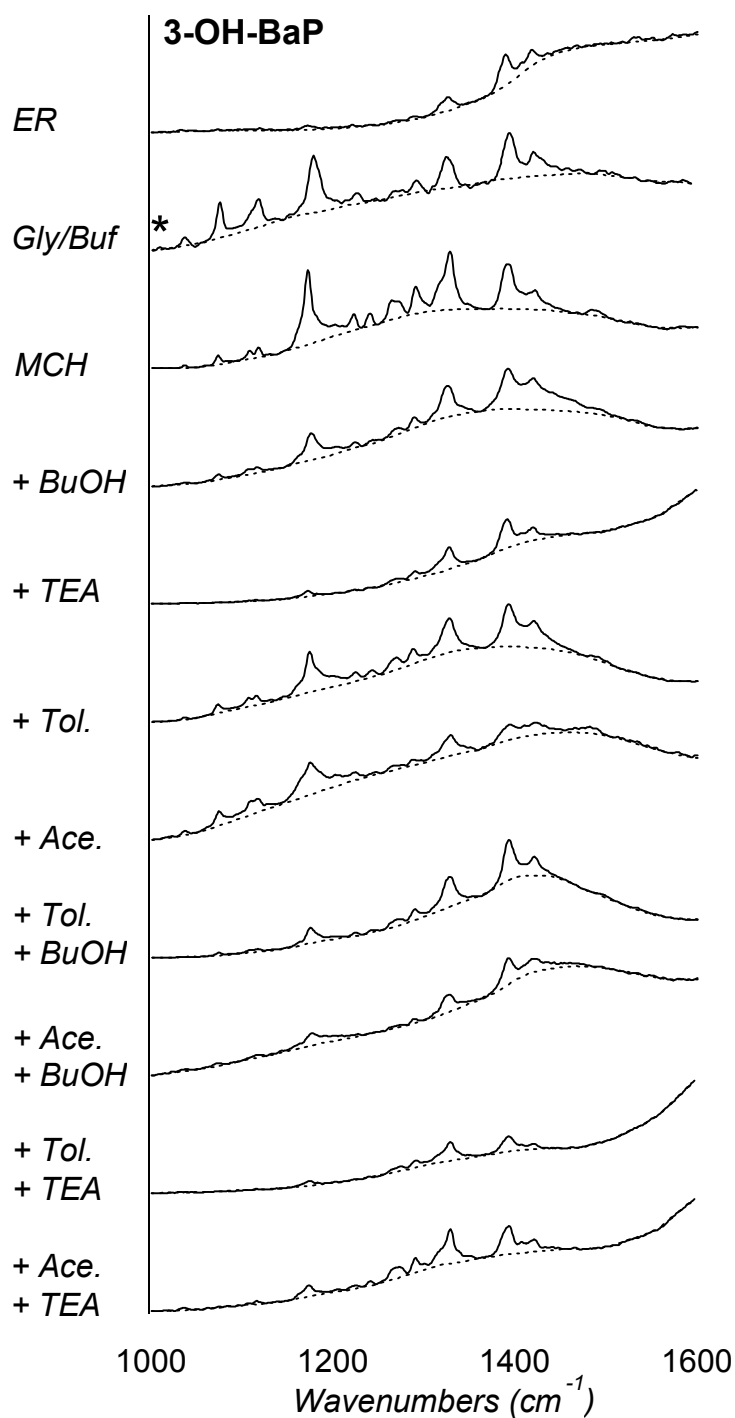
Figure 5: *Normalised FLN spectra of 3-hydroxybenzo[a]pyrene in various solvent (or solvent combinations) and bound to the estrogen receptor. On the x-axis the energy difference with respect to the excitation wavelength in wavenumbers is used. The excitation wavelength was 410 nm. The star indicates that in the 700-1000 cm^{-1} range three additional major bands are observed.*
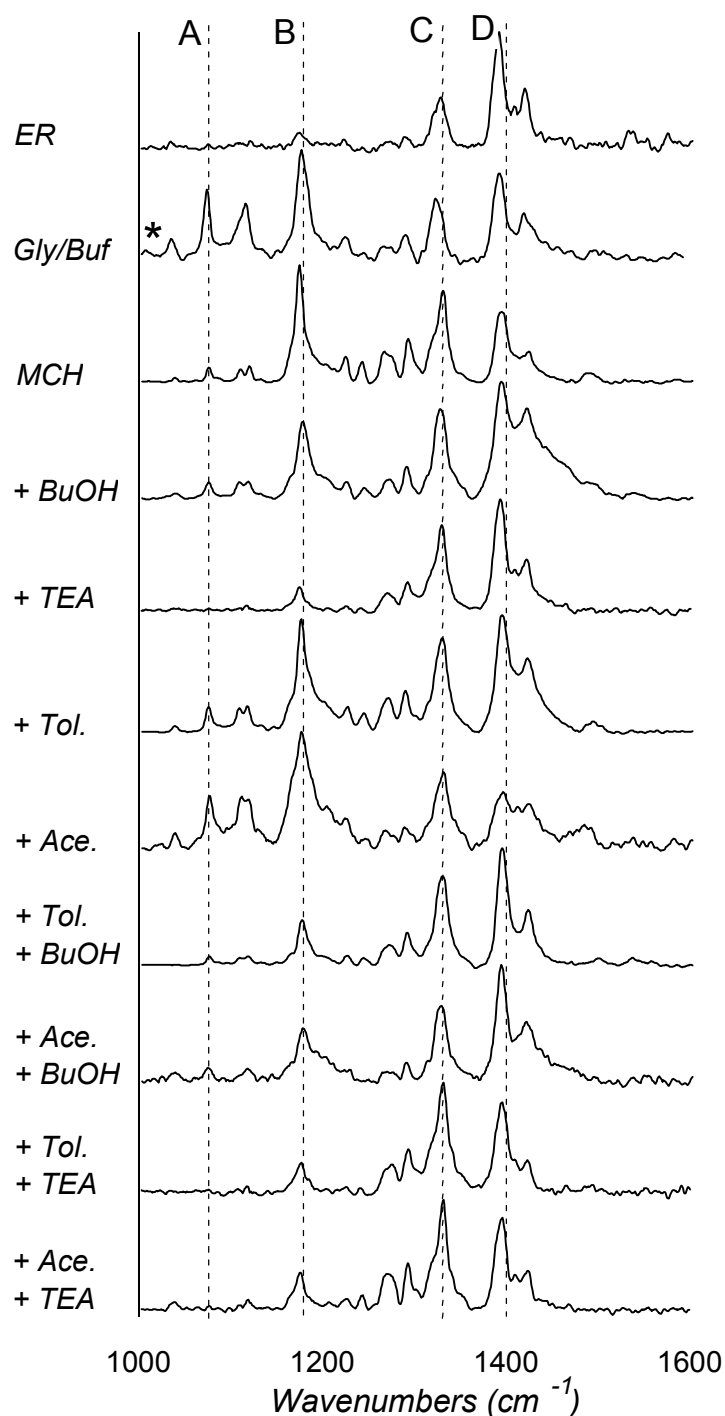
Figure 6: *Normalised FLN spectra of 3-hydroxybenzo[a]pyrene after baseline correction in various solvent (or solvent combinations) and bound to the estrogen receptor (the uncorrected spectra are shown in Figure 5). The relative intensities of bands (A), (B), (C) and (D) are given in Table 2. The star indicates that three other strong blue shifted bands are observed (at 770, 857 and 960 cm^{-1}); these bands are not observed in the other spectra.*

As regards solvent mixtures with both H-bonding and π-electron containing molecules, the combination of BuOH and one of the π-electron containing solvents results in a red shift in the 3-OH-BaP spectrum, i.e., the intensity ratios become 1/4/8/10 (in the presence of BuOH and toluene) and 1/5/7/10 (in the presence of BuOH and acetone). In the presence of TEA and toluene the intensity ratio becomes 0/3/10/8, and in the presence of TEA and acetone 0/4/10/8. Apparently, the latter two solvent combinations cause a less pronounced red shift; for TEA the intensity of red edge band D is higher when π-electron containing solvents are not present.

Discussion:

The results presented above clearly show that the FLN spectra of 3- and 9-OH-BaP are strongly solvent dependent. Considering H-bonding, even a distinction between donating and accepting properties can be made. These solvent characteristics can be quantified using the Kamlet-Taft parameters for solvatochromic properties [21]. According to these parameters, a solvatochromic shift caused by TEA, and similarly by the imidazole moiety of HIS524, is exclusively due to its H-bond accepting capabilities [21]. In the spectra of both 3- and 9-OH-BaP, the presence of TEA resulted in a red shift. Conversely, solvatochromic shifts in aqueous solution and glycerol are predominantly due to the H-bond donating properties of these solvents [21]. In the spectra of both 3- and 9-OH-BaP in Gly/Buf, a blue shift is observed. The influence of BuOH is less easily predictable because it has both H-bond donating and accepting properties [21]. For 9-OH-BaP, BuOH causes a minor blue shift compared to the spectrum in MCH. For 3-OH-BaP, the opposite is observed: the presence of BuOH results in a red shift. These opposite shifts can be conceived as follows. Solute/solvent interaction always causes a stabilisation of the S_0 state. Whether a blue or red shift is observed, depends on the extent of stabilisation in the S_1 state: more stabilisation in the S_1 state than in the S_0 state will result in a red shift, in the opposite case a blue shift is observed (see Figure 2B). The amount of stabilisation in these states not only depends on the solvent dealt with; it is also influenced by changes in the solute's properties upon excitation. For example, a change in acidity will influence the impact of H-bonding interaction. Such changes in acidity might play a role in the solvent dependency in the spectra of 3- and 9-OH-BaP.

As regards π–π interactions, fortunately carbonyl π-electrons and aromatic π-electrons induce significant differences in the FLN spectra so that their influences can be readily established. Strong red-shifted baselines due to electron phonon coupling indicate π-π-stacking interaction [16,22], as observed for 9-OH-BaP in the presence of toluene. For 3-OH-BaP this coupling is only weak. Nonetheless, 3-OH-BaP and toluene do interact significantly since the spectra in MCH + toluene and in pure MCH are different (see Figure 6). Most probably, this solute/solvent combination is not interacting in a π–π stacking manner; a T-shape conformation is more likely. Because the aromatic ring of phenylanaline is similar to toluene (a benzene ring with an alkyl substituent), the PHE404 group in the ER is expected to behave similarly.

A systematic comparison of the FLN spectra (before and after baseline subtraction) in different solvent combinations leads to the following conclusions. For 9-OH-BaP, the spectrum in the presence of TEA and toluene shows the most similarities with that of the ER complex. This suggests that in the ER binding site, 9-OH-BaP interacts with an H-bond acceptor, i.e., the imidazole moiety of HIS524. Furthermore, the spectra indicate that 9-OH-BaP interacts with a toluene-like moiety in the ER, i.e. PHE404, in a π–π stacking manner.

From a similar inspection of the 3-OH-BaP spectra the following conclusions can be drawn. The spectrum in the ER complex is most similar to the one in the presence of TEA, indicating interacting interaction with an H-bond acceptor, i.e., the imidazole moiety of HIS524. If there is some interaction between 3-OH-BaP and the PHE404 side group, it will most likely be in a T-shape conformation.

For both 3- and 9-OH-BaP, the orientation in the ER is remarkably different from what is expected based on the studies with E2. For this estrogen, the contributions of the two H-bonds to the total receptor/ligand binding energy have been estimated, showing that the participation of E2's phenolic OH-group in the H-bonding network with GLU353 and ARG394 contributes to a larger extent than the H-bond donated to the HIS524 does [4,23]. Apparently, this cannot be simply generalized and applied to other ligands. For both mono-hydroxylated BaPs studied here, our results strongly suggest that H-bonding with HIS524 is the predominant interaction.

The observed H-bonding of the two solutes in the ER that occurs with HIS524 is in line with molecular modelling data [15]. Although molecular modelling and forcefield parameters are particularly suitable for the simulations and calculations of protein/ligand interactions, they do not describe π–π interaction very well. However, the molecular modelling data described by Van Lipzig *et al* [15] predicted interaction with PHE404. This is confirmed by the FLNS data. Interestingly, the FLNS data indicate whether π–π stacking (as for 9-OH-BaP) or a T-shape conformation (as for 3-OH-BaP) should be expected.

Thanks to its unique features, FLNS can become a useful tool in ligand/receptor studies. Especially when the functional groups in a receptor binding pocket can be mimicked, as is the case for HIS and PHE, very useful information can be obtained. Further exploration of this technique is needed because still little is known about the solvent dependency in FLN spectra.

References:

1. McLachlan, J. A., Korach, K. S., Newbold, R. R. and Degen, G. H., *Fundam. Appl. Toxicol.,* **1984***, 4*, 686-691
2. Evans, R. M., *Science,* **1988***, 240*, 889-895.
3. Danzo, B. J., *Environ Health Perspect,* **1997***, 105*, 294-301.
4. Brzozowski, A. M., Pike, A. C., Dauter, Z., Hubbard, R. E., Bonn, T., Engstrom, O., Ohman, L., Greene, G. L., Gustafsson, J. A. and Carlquist, M., *Nature,* **1997***, 389*, 753-758.
5. Kuiper, G. G. J. M., Carlsson, B., Grandien, K., Enmark, E., Haggblad, J., Nilsson, S. and Gustafsson, J. A., *Endocrinology,* **1997***, 138*, 863-870.
6. Cook, J. W., Dodds, E., C., Hewett, C. L. and Lawson, W., *Proc. R. Soc. B.,* **1934***, 114*, 272-286.
7. Santodonato, J., *Chemosphere,* **1997***, 34*, 835-48.
8. Yang, N.C., Lewis, M., Wong, T.-W., and Castro, A. J., *Science,* **1961,** *134*, 386-387.
9. Charles, G. D., Bartels, M. J., Zacharewski, T. R., Gollapudi, B. B., Freshour, N. L. and Carney, E. W., *Toxicol. Sci.,* **2000,** *55*, 320-326.
10. Fertuck, K.C., Kumar, S., Sikka, H.C., Matthews, J.B., and Zacharewski, T.R., *Toxicol. Lett.*, **2001,** *121*, 167-177.
11. Hirose, T., Morito, K., Kizu, R., Toriba, A., Hayakawa, K., Ogawa, S., Inoue, S., Muramatsu, M., and Masamune, Y., *J Health Science,* **2001***, 47*, 552-558.
12. Van Lipzig, M.M.H., Vermeulen, N.P.E., Gusinu, R., Legler, J., Frank, H., Seidel, A., Meerman, J.H.N., *Environ. Toxicol. Pharmacol.,* **2005,** *19*, 41-55.
13. Pike, A.C.W., Brzozowski, A.M., Hubbard, R.E., Bonn, T., Thorsell, A.-G., Engström, O., Ljunggren, J., Gustafsson J.-Å., and Carlquist, M., *EMBO J.,* **1999,** *18*, 4608 – 4618.
14. Shiau A.K., Barstad D., Radek J.T., Meyers M.J., Nettles K.W., Katzenellenbogen B.S., Katzenellenbogen J.A., Agard D.A., Greene G.L., *Nat. Struct. Biol.,* **2002,** *9*, 359-364
15. Van Lipzig M.M.H., ter Laak A.M., Jongejan A., Vermeulen N.P.E., Wamelink M., Geerke D., Meerman J.H.N., *J. Med. Chem.,* **2004,** *47*, 1018-1030.
16. Bader, A.N., Grubor, N.M., Ariese, F., Gooijer, C., Jankowiak, R., Small, G.J., *Anal Chem.,* **2004,** *76*, 761-767.

17. Jankowiak, R., in *Shpol'skii Spectroscopy and Other Site-Selection Methods,* Gooijer, C., Ariese, F., and Hofstraat, J.W., Eds., Wiley & Sons: New York, **2000** pp 235-271.
18. Jankowiak, R., and Small, G.J., *Anal Chem.*, **1989,** *61*, 1023A-1032A.
19. Eiler, S., Gangloff, M., Duclaud, S., Moras, D., and Ruff, M., *Protein Exp. Pur.,* **2001**, *22*, 165-173.
20. Guher-Orhan, H., Kool, J., Vermeulen, N.P.E., Meerman, J.H.N., Int. J. Environ. Anal. Chem., **2005**, *85*, 149-161
21. Kamlet, M.J., Abboud, J.-L.M., Abraham, M.H., Taft, R.W., *J. Org. Chem.*, **1983,** *48*, 2877-2887
22. Suh, M., Ariese, F., Small, G.J., Jankowiak, R., Liu, T.M., Geacintov, N.E., *Biophys. Chem.*, **1995**, *56*, 281-296
23. Anstead, G. M., Carlson, K. E., and Katzenellenbogen, J. A., *Steroids*, **1997,** *62*, 268-303.

Summary

In analytical chemistry and several other research fields, fluorescent molecules are being used to 'probe' their microenvironment in order to obtain information on local parameters such as pH, polarity, viscosity, etc.. The spectral and temporal properties of such probes should be significantly influenced by their interaction with the surrounding solvent and/or matrix. A wealth of literature is available on this subject. Special probes have been designed that show distinct (spectral) effects on predominantly one solvent parameter. Unfortunately, these spectral changes are often obscured by the fact that the excitation and emission spectra generally show little detail. Instead of distinct vibronic transitions, usually only broad and featureless bands are obtained, in which detailed vibrational patterns can hardly be discerned. A second problem is that spectral shifts can be the result of both static effects (e.g., hydrogen-bonding) and dynamic effects (e.g. solvent reorientation), thus complicating interpretation. In this thesis we attempt to circumvent these problems by using high-resolution molecular fluorescence spectroscopy at cryogenic temperatures and the objective is to explore 'probing' under such conditions.

The first requirement to reduce the poor resolution in the fluorescence spectra of liquid solutions is to lower the temperature to 10 K or lower. Usually, this is not sufficient – the spectra are still broad-banded – but the interpretation of solvent effects is simplified because to a good approximation the microenvironment does not change during the fluorescence process: reorientation is largely inhibited in the frozen matrix. Therefore, the effects observed are predominantly due to specific static chemical interactions between functionalities of the solvent/matrix and the probe molecule. In this thesis, two techniques are used that yield high resolution spectra under low temperature conditions, i.e., Shpol'skii spectroscopy and fluorescence line-narrowing spectroscopy. Basic aspects of these techniques are discussed in Chapter 1.2 and 1.3, respectively. So far, these techniques had predominantly been used for fingerprint identification and sensitive detection of fluorescent compounds; in this thesis we will explore their potential to study the photophysics of fluorescence probes and obtain more detailed information on the micro-environment of fluorophores.

In Shpol'skii spectroscopy, high resolution is achieved by using a solvent (often *n*-octane) that forms a regular crystal where the solute fits into. At first sight such a technique allows only nonpolar environments to be studied, which would seem rather limited. In Chapter 2,

however, it is shown that Shpol'skii spectroscopy is a very powerful tool to investigate the photophysics and photochemistry of a special class of probes, i.e. the derivatives of 3-hydroxyflavone (3HF), a fluorophore that undergoes an excited state intramolecular proton transfer reaction (ESIPT). The rate of this reaction is strongly solvent dependent. If proton transfer is too slow, so that it cannot be accomplished within the lifetime of the excited state, the compound emits in the blue. However, if it is fast a tautomeric species is formed in the excited state that subsequently emits in the green. Therefore, 3HF compounds are used as ratiometric probes; the ratio in intensity between the blue and green emission band serves to accurately quantify solvent effects.

A number of new approaches in Shpol'skii spectroscopy are described in this chapter. Even though 3HF derivatives have a moderately polar character, good Shpol'skii spectra could be obtained in *n*-octane, and proton transfer reactions still occurred under cryogenic conditions. Researchers from the University of Kiev (Ukraine) and the TUBITAK institute (Turkey) contributed to this work. First, in Chapter 2.1 it is shown that the rates of ESIPT and back proton transfer can be obtained from the spectra since they caused significant broadening of the spectral lines (uncertainty relationship). The extent of broadening could be quantified as follows: The deuterated analogue of 3HF (3DF) is assumed to fit in a Shpol'skii matrix in an identical way, so inhomogeneity effects and instrumental contributions should be the same. On the other hand, in a tunneling mechanism deuteron transfer is expected to be much slower than proton transfer and lifetime broadening in 3DF is negligible. Therefore, the additional broadening in the spectra of 3HF compared to 3DF is due to the very short lifetimes caused by fast proton transfer in 3HF. In excitation, the lifetime reduction is due to ESIPT, whereas in emission it is due to back proton transfer. It is shown that for 3HF and derivatives ESIPT time constants on a femtosecond timescale can be determined, whereas picosecond and slower processes do not produce measurable changes in line widths. The technique is therefore especially suitable for fast processes that are difficult to measure accurately in the time domain.

Several studies have demonstrated the effects of the electron donating ability of the substituent at the 2-position of the chromone ring on the rate of ESIPT: in the case of furan derivatives (Chapter 2.2) the ESIPT process was slowed down significantly. A systematic study (Chapter 2.3) was carried out to directly compare the ESIPT and BPT rates of 3HF, its 2-furan and 2-paramethoxyphenyl derivatives. No change in bandwidth was observed over the temperature range 4-20 K, in agreement with a tunneling mechanism. Estimates for the

barrier heights and proton-transfer distances could be given. In addition, a change in O-H bond strengths between ground and excited states could be calculated from the isotope effect, observed as the shifts of the 0-0 bands in the excitation and emission spectra upon deuteration. The substantial effect of electron donating substituents on the rates of ESIPT and BPT reactions is in agreement with these changes.

Chapter 2 also describes the interesting possibility of incorporating a hydroxyl group in the Shpol'skii matrix. By adding minor fractions of one of the octanol isomers to *n*-octane, spectra can be obtained of 3HF (or one of its derivatives) interacting intermolecularly with a hydroxyl group. Consequently, information about the mechanism how hydroxyl groups influence or even block the ESIPT reaction could be obtained. In conclusion, the results from these photophysical Shpol'skii studies provide additional insight into the mechanisms of ESIPT and BPT and the effects of electron-donating substituents in this class of molecules, and will be very useful for the further development of ratiometric probes.

In the last part of this thesis (Chapter 3), fluorescence line-narrowing spectroscopy (FLNS) is used; this technique can be applied in a variety of amorphous matrices, including aqueous buffers with biological macromolecules. Unlike in a Shpol'skii matrix, all fluorophores in FLNS experience a different solvent environment, i.e., inhomogeneous broadening is still present. By using a laser, a selected group of iso-energetic fluorophores is excited and their interactions with the local environment remain constant during the lifetime of the excited state because of the cryogenic conditions. This results in line-narrowed emission, in which the vibronic transitions in ground and excited state are clearly visible. Furthermore, the relative intensities of the line-narrowed bands in emission are strongly dependent on the exact position of the broadened absorption bands relative to the laser excitation wavelength. The FLN spectrum is therefore a sensitive probe of the local environment; even minor shifts or changes in the amount of broadening can be clearly observed by using FLNS. As mentioned, because of the absence of solvent reorientation under cryogenic conditions, the dominant solvent induced changes are caused by specific, static solvent-solute interactions.

To test the applicability of this approach, some important protein-ligand complexes were studied. Crucial was the recording of the FLN spectrum of the ligand bound to the protein. Next, this spectrum was compared to the spectra of the unbound ligand in a variety of solvents or solvent combinations that mimic the possible interactions with the protein as

closely as possible. When the spectrum of the protein-bound ligand matches its spectrum in a certain solvent, apparently similar solvent-solute interactions play a role. In Chapter 3.1 this approach was successfully applied to study the antibody-antigen interaction with one metabolite and one adduct of benzo[*a*]pyrene (BaP). BaP is a well-known carcinogen, and the presence of the metabolite (+)-*trans-anti*-7,8,9,10-benzo[*a*]pyrenetetrol (BaP-tetrol) or the depurinating DNA adduct 7-(benzo[*a*]pyren-6-yl)guanine (BaP-6-N7Gua) in urine is an indicator of recent uptake of BaP or DNA damage from BaP, respectively. For both compounds monoclonal antibodies had been developed, and in a collaborative study with Iowa State University (Ames, IA, USA) the binding mode to their respective antibodies was studied by FLNS. From the spectra we could conclude that the antibody for BaP tetrol has an internal binding site and that the interaction is of a hydrophobic character. For BaP-6-N7Gua, however, $\pi-\pi$ interactions play an important role in the binding with its antibody.

Chapter 3.2 describes a similar approach aimed at studying the interaction of the estrogen receptor and monohydroxy-BaPs. These compounds have pseudo-estrogenic properties, and in a collaborative study with the Molecular Toxicology department (VU) the FLN spectra of 9-OH BaP and 3-OH BaP bound to the estrogen receptor were recorded and compared with the FLN spectra recorded in a series of solvents and solvent combinations. A clear distinction could be made between hydrogen bond donating and accepting interactions. Also, $\pi-\pi$ interaction could be observed in the spectra. The FLN results clearly indicate that H-bond accepting by the histidine group HIS524 plays a major role in the binding of these ligands to the estrogen receptor. Furthermore, the spectra indicated $\pi-\pi$ stacking aromatic interaction for 9-OH-BaP with the phenyl group of PHE404. These results add important information to earlier molecular modelling studies and demonstrate the relevance of FLNS probing for studying the interactions between fluorescent molecules and their environment.

Samenvatting

Fluorescerende moleculen worden vaak gebruikt om informatie te verkrijgen over hun directe omgeving in een complex monster. Afhankelijk van de gekozen fluorescerende "probe", kan bijvoorbeeld de pH, de viscositeit of de polariteit van de omgeving bepaald worden. Veelal worden deze probes speciaal ontwikkeld voor één omgevingsparameter, die een meetbare invloed heeft op het spectrum dan wel op de levensduur van de fluorescentie. Bij de meeste fluorescerende verbindingen is de afhankelijkheid van de omgeving slechts gering. Kleine veranderingen in een doorgaans breed en structuurloos spectrum zijn lastig te bepalen. Daarom worden zulke verbindingen zelden als omgevings-probe gebruikt. Ook zijn spectrale veranderingen niet altijd gemakkelijk te interpreteren. Ze kunnen namelijk zowel door statische (bijv. waterstofbrug vorming) als door dynamische (bijv. oplosmiddel herorientatie) effecten veroorzaakt worden. In dit proefschrift wordt beschreven hoe deze problemen verholpen kunnen worden door de probe bij lage temperaturen, onder hoge-resolutie condities, te bestuderen.

De resolutie in fluorescentie spectra kan aanzienlijk verbeterd worden door bij extreem lage temperaturen te meten, doorgaans lager dan 10K. Temperatuurverlaging op zich is vaak echter onvoldoende; de spectra zijn nog steeds tamelijk breedbanding. De afhankelijkheid van het oplosmiddel wordt in ieder geval aanmerkelijk simpeler, doordat de directe omgeving nauwelijks kan veranderen tijdens het fluorescentie proces. De omgevingseffecten bij 10K worden derhalve overwegend veroorzaakt door statische chemische interacties tussen functionaliteiten van de oplosmiddelmoleculen en de fluorescerende stof. In dit proefschrift zijn twee technieken gebruikt waarmee cryogene meetcondities ook leiden tot hoge-resolutie spectra: Shpol'skii spectroscopie en fluorescence line-narrowing spectroscopie (FLNS). De basis van deze technieken wordt uitgelegd in Hoofdstukken 1.2 en 1.3. Ze werden tot op heden in de analytische chemie voornamelijk gebruikt om de fluorescerende stoffen te identificeren dan wel bij lage concentraties selectief te detecteren. In dit proefschrift wordt de mogelijkheid onderzocht om de toepasbaarheid van Shpol'skii en FLN spectroscopie te vergroten; er wordt beschreven hoe de fotofysica van fluorescerende probes bestudeerd kan worden en op welke wijze zeer gedetailleerde informatie over de directe omgeving van fluorescerende moleculen kan worden verkregen.

In het geval van Shpol'skii spectroscopie wordt de hoge-resolutie verkregen doordat bij lage temperaturen het oplosmiddel (vaak wordt *n*-octaan gebruikt) een regelmatig kristal vormt, waar de opgeloste stof heel goed past, als een sleutel in een slot. Op het eerste gezicht lijkt dit geen nuttige benadering voor het bestuderen van oplosmiddelafhankelijkheid; er kunnen namelijk alleen maar niet-polaire omgevingen mee bestudeerd worden. Hoofdstuk 2 laat echter zien dat voor derivaten van 3-hydroxyflavon (3HF) zeer nuttige informatie verkregen kan worden over de fotofysica en fotochemie van de intramoleculaire protonoverdracht die in de aangeslagen toestand van dit molecuul kan plaatsvinden. Omdat deze reactie sterk afhankelijk is van de directe omgeving, kan deze klasse verbindingen gebruikt worden als omgevingsprobe. Als de reactie traag verloopt, kan deze niet plaatsvinden binnen de levensduur van de aangeslagen toestand; de emissie is in dit geval blauw. Is de reactiesnelheid daarentegen hoog, dan wordt voordat licht wordt uitgezonden een tautomeer gevormd en het uitgezonden licht is groen. 3HF en de derivaten daarvan kunnen dus gebruikt worden als ratiometrische probe; de intensiteitsverhouding tussen de blauwe en de groene emissie geeft nauwkeurige en te kwantifiseren informatie over de oplosmiddelomgeving.

In Hoofdstuk 2 wordt een aantal nieuwe manieren beschreven waarop Shpol'skii spectroscopie gebruikt kan worden. Ondanks het feit dat 3HF enigzins polair is, bleek het mogelijk te zijn Shpol'skii spectra op te nemen van deze verbinding in *n*-octaan. Onder Shpol'skii condities werd de groene emissie van de tautomere vorm van 3HF gemeten; de proton overdracht vindt dus nog steeds plaats bij dergelijke temperaturen. Ook derivaten van 3HF pasten in een Shpol'skii matrix. Het bestuderen van deze derivaten kwam voort uit een samenwerking met onderzoekers van de Universiteit van Kiev (Oekraine) en het TUBITAK instituut (Turkije). In hoofdstuk 2 wordt beschreven hoe de snelheden van de proton overdacht in de aangeslagen- en grondtoestand afgeschat kunnen worden uit de verbreding in het spectrum (levensduur verbreding). De verbreding kon worden bepaald door het spectrum van 3HF met dat van de gedeutereerde verbinding 3DF te vergelijken, een verbinding die op dezelfde wijze in de matrix past. De extra verbreding wordt daarom veroorzaakt door het verschil in snelheid tussen proton overdracht in 3HF en de vele malen tragere deuteron overdracht in 3DF. In het excitatiespectrum wordt de levensduur beperkt door de reactie in de aangeslagen toestand, terwijl in het emissiespectrum de snelheid van de teruggaande reactie zichtbaar wordt. Voor tragere reacties is de extra levensduur verbreding niet goed meetbaar,

maar reactietijden op een femtoseconde tijdschaal kunnen op deze manier goed bepaald worden. Juist zulke snelle reacties zijn experimenteel lastig te bepalen in het tijdsdomein.

Verschillende literatuur studies laten zien dat de intramoleculaire proton overdracht langzamer verloopt als de substituent aan de 2-positie een sterkere electron donor is. Dit geldt bijvoorbeeld voor furaanderivaten (Hoofdstuk 2.2). In een vergelijkende studie van 3HF en de 2-furaan en 2-paramethoxyfenyl derivaten worden de reactiesnelheden direct vergeleken (Hoofdstuk 2.3). Hieruit werd een inschatting van de hoogte en breedte van de reactiebarrières gemaakt. Uit het isotoopeffect kon de verandering in de sterkte van de OH binding bij de overgang van de grond naar de aangeslagen toestand bepaald worden voor deze drie verbindingen. De resultaten laten inderdaad een sterk effect van electron donerende zijgroepen zien.

Hoofdstuk 2 beschrijft ook de invloed van de hydroxyl-substituent in het oplosmiddel. Door kleine fracties van een octanol isomeer aan *n*-octaan toe te voegen, kan het Shpol'skii spectrum verkregen worden van 3HF dat intermoleculaire interactie heeft met deze hydroxyl groep. Dit levert informatie op over de manier waarop zo'n groep de reactie beïnvloedt of zelfs blokkeert. De conclusie luidt dat met behulp van Shpol'skii spectroscopie nieuwe inzichten verkregen worden in het mechanisme van de proton overdrachtsreacties in deze klasse verbindingen. Dit is zeer nuttige informatie in het kader van de ontwikkeling van deze omgevingsprobes.

In het laatste deel van dit proefschrift (Hoofdstuk 3) wordt FLNS gebruikt. Bij deze techniek moet de matrix niet kristallijn maar amorf zijn, zoals dat het geval is bij biologische macromoleculen in gebufferd water. In tegenstelling tot de kristallijne matrix bij Shpol'skii spectroscopie, ervaren de individuele fluorescerende moleculen in een amorfe matrix elk een andere omgeving. Omdat je heel veel moleculen tegelijkertijd meet zie je brede banden in de spectra. Door echter met een (smalbandige) laser te exciteren, vinden er selecties plaats van moleculen met een bepaalde iso-energetische omgeving. Wanneer deze moleculen licht uit gaan zenden hebben ze vanwege de cryogene omstandigheden nog steeds dezelfde omgeving en dus zal het emissielicht ook smalbandig zijn. In het FLN spectrum zijn per emissieovergang meerdere banden te zien, die overeenkomen met de excitatie van verschillende vibronische niveaus. De relatieve intensiteiten van deze banden hangen sterk af van de exacte positie van de verbrede absorptieband ten opzichte van de laser golflengte. Het spectrum is derhalve erg gevoelig voor invloeden van de omgeving. Zelfs een kleine

verschuiving of verbreding van de absorptieband door de omgeving kan nauwkeurig bestudeerd worden met FLNS. Zoals reeds opgemerkt is heroriëntatie van het oplosmiddel niet mogelijk bij lage temperaturen en zodat vooral de statische omgevingseffecten het spectrum bepalen.

De bruikbaarheid van FLNS voor het bestuderen van de omgeving van fluorescerende verbindingen werd onderzocht voor een aantal eiwit-ligand complexen. De eerste stap was het opnemen van het FLN spectrum van zo'n ligand gebonden aan het eiwit. Vervolgens werd dit spectrum vergeleken met de spectra van het ongebonden ligand in een aantal verschillende oplosmiddelen of mengsels daarvan. Met deze oplosmiddelcombinaties werd geprobeerd het spectrum van het ligand gebonden aan het eiwit te benaderen. In dat geval zijn vergelijkbare interacties aanwezig en kunnen deze bepaald worden aan de hand van de karakteristieken van het oplosmiddel. In Hoofdstuk 3.1 wordt deze benadering succesvol toegepast voor antilichaam/antigen interactie met een adduct en een metaboliet van benzo[*a*]pyreen (BaP). BaP is een bekende carcinogene verbinding en de aanwezigheid van het metaboliet (+)-*trans-anti*-7,8,9,10-benzo[*a*]pyreentetrol (BaP-tetrol) of het depurinerende DNA adduct 7-(benzo[*a*]pyren-6-yl)guanine (BaP-6-N7Gua) in urine, is een indicatie voor recente blootstelling aan BaP, respectievelijk DNA schade door BaP. Tegen deze verbindingen waren reeds antilichamen ontwikkeld en in samenwerking met de Iowa State University (Ames, IA, USA) is de binding met de bijbehorende antilichamen onderzocht. De spectra laten zien dat de bindingsplaats van het antilichaam tegen BaP-tetrol vooral een hydrofoob karakter heeft. In het geval van BP-6-N7Gua is echter $\pi-\pi$ interactie veel belangrijker voor de binding.

Hoofdstuk 3.2 beschrijft een vergelijkbare benadering met als onderwerp van studie de oestrogeen receptor die interactie aan kan gaan met monohydroxy-BaPs. Van deze verbindingen is bekend dat ze pseudo-oestrogene eigenschappen hebben. In samenwerking met de Afdeling Moleculaire Toxicologie (VU) zijn de FLN spectra opgenomen van 9-OH-BaP en 3-OH-BaP, gebonden aan de oestrogeen receptor. In deze studie was bekend welke zijgroepen van aminozuren mogelijk interactie aan konden gaan. Er zijn derhalve oplosmiddelen gekozen die deze interacties nabootsen. Zo kon een duidelijk onderscheid worden gemaakt tussen waterstofbrug donerende en accepterende omgevingen. Verder kon de invloed van $\pi-\pi$ interactie bestudeerd worden. De FLN spectra laten zien dat waterstofbrugacceptatie door HIS524 een belangrijke rol speelt bij de binding van deze liganden aan de receptor. Verder is er zogenaamde $\pi-\pi$ stacking interactie van 9-OH-BaP

met de fenyl group van PHE404. Deze resultaten bevestigen de bevindigen van moleculaire modelling studies en laten zien dat FLNS zeer relevante informatie op kan leveren over interacties fluorescerende moleculen en hun omgeving.

List of publications

Chapter 2.1:

Bader, A.N., Ariese, F., Gooijer, C.
Proton transfer in 3-hydroxyflavone studied by high-resolution 10 K laser-excited Shpol'skii spectroscopy
JOURNAL OF PHYSICAL CHEMISTRY A 106 (12): 2844-2849, 2002

Chapter 2.2:

Bader, A.N., Pivovarenko, V., Demchenko, A.P., Ariese, F., Gooijer, C.
Solvent influence on excited-state intramolecular proton transfer in 3-hydroxychromone derivatives studied by cryogenic high-resolution fluorescence spectroscopy
SPECTROCHIMICA ACTA PART A-MOLECULAR AND BIOMOLECULAR SPECTROSCOPY 59 (7): 1593-1603, 2003

Chapter 2.3:

Bader, A.N., Pivovarenko, V.G., Demchenko, A.P., Ariese, F., Gooijer, C.
Excited state and ground state proton transfer rates of 3-hydroxyflavone and its derivatives studied by shpol'skii spectroscopy: The influence of redistribution of electron density
JOURNAL OF PHYSICAL CHEMISTRY B 108 (29): 10589-10595, 2004

Chapter 3.1:

Bader, A.N., Grubor, N.M., Ariese, F., Gooijer, C., Jankowiak, R., Small, G.J.
Probing the interaction of benzo[a]pyrene adducts and metabolites with monoclonal antibodies using fluorescence line-narrowing spectroscopy
ANALYTICAL CHEMISTRY 76 (3): 761-766, 2004

Chapter 3.2:

Bader, A.N., Van Dongen, M.M., Van Lipzig, M.M.H., Kool, J., Meerman, J.H.N., Ariese, F., Gooijer, C.,
The chemical interaction between the estrogen receptor and mono-hydroxybenzo[a]pyrene derivatives studied by fluorescence line-narrowing spectroscopy
CHEMICAL RESEARSH IN TOXICOLOGY, 18 (9): 1405 – 1412, 2005

Other publications:

Dosche, C., Kumke, M.U., Lohmannsroben, H.G., Ariese, F., Bader, A.N., Gooijer, C., Miljanic, O.S., Iwamoto, M., Vollhardt, K.P.C., Puchta, R., Hommes, N.J.R.V.
Deuteration effects on the vibronic structure of the fluorescence spectra and the internal conversion rates of triangular[4]phenylene
PHYSICAL CHEMISTRY CHEMICAL PHYSICS 6 (24): 5476-5483, 2004

Dosche, C., Kumke, M.U., Ariese, F., Bader, A.N., Gooijer, C., Dosa, P.I., Han, S., Miljanic, O.S., Vollhardt, K.P.C., Puchta, R., Hommes, N.J.R.V.
Shpol'skii spectroscopy and vibrational analysis of [N]phenylenes
PHYSICAL CHEMISTRY CHEMICAL PHYSICS 5 (20): 4563-4569, 2003

De Serio, M., Bader, A.N., Heule, M., Zenobi, R., Deckert, V.
A near-field optical method for probing liquid-liquid interfaces
CHEMICAL PHYSICS LETTERS 380 (1-2): 47-53, 2003

Dijkstra, R.J., Bader, A.N., Hoornweg, G.P., Brinkman, U.A.T., Gooijer, C.
On-line coupling of column liquid chromatography and raman spectroscopy using a liquid core waveguide
ANALYTICAL CHEMISTRY 71 (20): 4575-4579, 1999

Gooijer, C., Hoornweg, G.P., de Beer, T., Bader, A., van Iperen, D.J., Brinkman, U.A.T.
Detector cell based on plastic liquid-core waveguides suitable for aqueous solutions: one-to-two decades improved detection limits in conventional-size column liquid chromatography with absorption detection
JOURNAL OF CHROMATOGRAPHY A 824 (1): 1-5, 1998

Dankwoord

Als eerste wil ik mijn promotor, *Cees Gooijer*, bedanken. Tijdens mijn hoofdvakstage leerde ik hem al kennen als een enthousiaste 'leermeester'; een doorslaggevende reden om bij hem te solliciteren voor een AiO-plaats. 'Ver-ceesingen' als "consequently", "can be readily concieved", "interestingly, " en "as regards", hebben de leesbaarheid van dit proefschrift aanmerkelijk vergroot. Ook de verbale correctie - "het antwoord is dus nee" - bleek "reproduceerbaar" te zijn. Zijn zorgzaamheid en goed-werkgeversschap heeft mij erg geholpen toen ik tijdelijk fysiek gelimiteerd was en niet "in vier-punt-nul jaar" kon promoveren. Mijn dank is groot.

Daarnaast wil ik mijn copromotor *Freek Ariese* bedanken. Freek, die altijd uitgebreid de tijd nam om goed na te denken over zijn antwoorden op mijn onmogelijke vragen, maar deze tijd compenseerde door met een onnavolgbare snelheid naar huis te fietsen. Onze gewoonte om rond vijf uur 's middags mijn onderzoeksresultaten te bespreken, draaide er regelmatig op uit dat ik vele uren later thuis kwam met een aantal uitstekende reistips. Tijdens zo'n sessie is ook het idee ontstaan om een paar maanden van mijn onderzoek aan de Iowa State University (Ames, Iowa) te verrichten. Dit was voor Freek een uitstekend excuus om daar weer eens een weekje rond te kijken. Ruim een jaar later bezochten wij opnieuw de VS voor een congres in Florida. Reisgenoot Arjan Mank wilde gebruik maken van de gelegenheid om wilde dieren te gaan bekijken in Nationaal Park de Everglades. Deze waren er ook in grote getalen, helaas allemaal van het type mug. Freek en ondergekende hebben nog dagen met honderden muggenbulten rondgelopen op het FACSS congres (Arjan Mank had zelf uiteraard nergens last van). De royale hoeveelheden Ben & Jerry's ijs maakten echter veel goed.

Voor het beoordelen van dit proefschrift wil ik de leden van de leescommissie bedanken: *Prof. Uwe Karst, Dr. Steven Kok, Dr. Michael Kumke, Prof. Ton Visser en Prof. Silvia Völker*.

A large part of this work is done in collaboration with other research groups. I would like to thank *Ryszard Jankowiak* (Iowa State University), for giving me the opportunity to work for four months in Ames; it resulted in a very nice paper (Chapter 3.1). The (other) members of the group of Prof. Gerry Small, for letting me use the low temperature equipment in the

humid summer heat of Iowa; it is very sad that Gerry Small died last year. Additional thanks to *Nenad Grubor*, for guiding me around Ames and taking me on a wild Iowan canoe trip (fortunately the local optician had a one-hour service for new glasses). Also, I am very grateful to *Alexander Demchenko* (TUBITAK research institute, Turkey) and *Vasyl Pivovarenko* (Kiev National Taras Shevchenko Univ., Ukraine), the experts on 3-hydroxyflavone derivatives. The measurements on their compounds (packed in a piece of tape attached to a letter that was posted by regular mail) gave very nice results, as can be seen in Chapters 2.2 and 2.3. The collaboration with *Michael Kumke* and *Carsten Dosche* (Univ. of Potsdam, Germany) was also both enjoyable and very successful (two papers). Ook *Marola van Lipzig, Jeroen Kool, John Meerman* en *Joran Beckman*, van moleculaire toxicologie (VU) wil ik bedanken voor de oestrogeen receptor, een goede testcase voor onze FLN benadering (hoofdstuk 3.2).

Verder wil ik de studenten die een bijdrage hebben geleverd aan dit proefschrift bedanken: *Maarten van Dongen*, die een groot deel van hoofdstuk 3.2 bij elkaar heeft gemeten. Na een schijnbaar simpele verplaatsing van de gehele opstelling over een afstand van slechts tien centimeter, kon hij eindelijk gaan meten. Hij heeft vervolgens een pakket FLN spectra weten te produceren van veel hydroxy-PAKs in nog veel meer (steeds merkwaardiger wordende) combinaties van oplosmiddelen. Verder leerden wij als analytisch chemici van de toxicologen wat de beste monstervoorbewerking was (een kolommetje). Het voorwerk voor deze metingen is gedaan door de andere *Maarten (Scholtes)*. Het nieuwe stuk linoleum voor de lift op de begane grond bij ingang 1083A is een blijvende herinnering van het heugelijke feit dat we dankzij hem een nieuwe vloeibare stikstof dewar moesten kopen. *Bas Teunissen* was de enige HBO stagiair die bij Henk Lingeman had aangegeven dat hij niet perse LC of GC wilde doen. Dus kwam hij in het laserlab terecht, waar ze een of andere exotische fluorescentie techniek gebruikten; niet alleen met een laser maar ook nog bij hele lage temperaturen. De timing van zijn begeleiders om reeds na anderhalve maand voor drie weken naar Florida te gaan, had dus beter gekund. Dat hij het in die periode desondanks voor elkaar heeft gekregen om een ongekende hoeveelheid spectra op te nemen, mag een hele prestatie genoemd worden.

Verder wil ik al mijn collega's in het laserlab bedanken, die het tikken van de laser (10 Hz) en de stoomboot-geluiden van de cryostaat jarenlang aan hebben moeten horen. Hout-,

touw- en dubbelzijdig-plakband-liefhebber *Reyer Dijkstra*, die als Raman-man bleef volhouden dat fluorescentie "de vijand" is. *Aike Stortelder*, met een wetenschappelijke carrière die vooral sinds het derdejaars AAF practicum opvallend veel overlap met de mijne vertoond. *Joost Buijs*, die om een of andere reden altijd in vakantietijd het lab ging opruimen. *Eva de Rijke*, van al haar flavonoiden bleek er slechts één een hoge-resolutie fluorescentie spectrum te geven. Voor haar was het niet echt een interessant stofje, maar ondergetekende kon er een half proefschrift mee te vullen (zie hoofdstuk 2). *Koos Kuijt*, wiens koffiedrink activiteiten regelmatig negatief interfereerde met mijn metingen. *Joost de Klerk*, in tegenstelling tot zijn voorganger wel iemand die hard loopt. *Junko Hirata*, met wie ik het legendarische doch eenmalige praticum onderdeel "Analyse van PAKs in verbrand voedsel met behulp van Shpol'skii spectroscopie" heb opgezet. Vooral de synthese van de PAKs in het oude broodrooster van Freek zal ik niet snel vergeten. Ook de Zuid- en Oost-Europese collega's wil ik bedanken, die dit dankzij hun Nederlandse les moeiteloos kunnen lezen: *Evtim Efremov* (kritisch volger van de Bulgaarse politiek: "stupid @#$*&$#s"), *Alois Bonifacio* en *Diego Millo* (de Italiaanse heem-eiwitten maffia) en *Mirka Smoluch* (die vaak stampvoette van plezier). Verder *Gregor Luthe, Lineke van der Sneppen, Carmen Garcia Ruiz, Reza Seifar, Arjan Wiskerke* en de vele studenten die de afgelopen jaren in het laserlab rondgelopen hebben.

Verder wil ik de andere vaste-staf leden van ACAS bedanken: *Gert van der Zwan*, voor alle theoretische ondersteuning en zijn pogingen de geheimen van de wiskunde achter de spectroscopie uit te leggen aan mensen-die-wel-weten-hoe-je-een-laser-aanzet. Eén vraag heeft hij echter nooit kunnen beantwoorden: wat is nou eigenlijk écht de beste film ooit? *Pim Voogt*, de electrochemicus die met veel plezier oplosmiddelen voor mij destilleerde. *René Vreuls*, de GC-man, die er samen met *Mohamed Adahchour* en *Leo van Stee* achterkwam wat voor verontreinigingen er in mijn oplosmiddelen bleken te zitten (voor het antwoord, zie hoofdstuk 2.1 en 2.2). Verder *Hubertus Irth, Henk Lingeman, Gisèle Cassee* en alle AiO's, postdoc's, studenten en anderen die "boven" werkten. En natuurlijk *Nel Velthorst*, die mij ook tijdens mijn kortstondige verblijf in Nijmegen kwam bezoeken.

Uiteraard de mannen van de werkplaats: met name *Dick van Iperen* en *Klaas van Altena*. Zij zorgen niet alleen voor de goede ideeën (bijvoorbeeld een nieuwe cryostaat

ondersteboven met een verschuifbare metalen plaat in een gat in de tafel hangen), maar ook nog eens voor de uitvoering ervan!

Ook dank aan mijn nieuwe 'baas' *Hans Gerritsen* en collega's van de Universiteit Utrecht, waar ik al ruim een jaar als "post-doc, maar eigenlijk nog geen doc" werk. Dankzij jullie heb ik nauwelijks een cultuurschok van chemie naar fysica ervaren. Ik heb echter wel herhaaldelijk moeten uitleggen waarom dit proefschrift nog niet af was en waarom sommige (VU-) chemici daar wel 200 pagina's voor nodig hebben.

Joost van Stralen en *Janneke Hulshof* voor alle "12.15h M1 lunch"-sessies.

Tot slot wil ik *Gerdy, Lennart, Suzanne* (scheikunde is wèl leuk) en *Nico* (die dat wel begreep) bedanken. Ook dank aan de andere familie, schoonfamilie en vrienden die interesse hebben getoond in mijn promotieonderzoek ("iets met lasers").

Als laatste wil ik natuurlijk *Nienke* bedanken. Voor de combinatie van je oprechte geïnteresseerdheid en totale onbegrip van beta-wetenschappen in zijn algemeenheid. Jij bent gelukkig veel beter in andere dingen, zoals dit soort teksten schrijven. Maar om je te vragen om het voor jouw bedoelde deel van het dankwoord te schrijven, dat vind zelfs ik te ver gaan.

Ta-daa!